Communication-Based Load Allocation and Restoration to Improve Efficiency and Resilience in Smart Grids Integrated with Renewables and Electric Vehicles

By

Pouya Jamborsalamati

A thesis submitted to Macquarie University

for the degree of Doctor of Philosophy

Department of Engineering

March 2020

MACQUARIE
University
SYDNEY·AUSTRALIA

Except where acknowledged in the customary manner, the material presented in this thesis is, to the best of my knowledge, original and has not been submitted in whole or part for a degree in any university.

Pouya Jamborsalamati

Acknowledgements

I would like to express my sincere gratitude to my principal supervisor Associate Professor Jahangir Hossain for his guidance, unconditional support, understanding, patience, wisdom, and encouragements during this PhD.

I am fully grateful to Assistant Professor Payman Dehghanian from George Washington University, USA. A truly humble and knowledgeable scientist who shed light on my research directions. I am thankful to Dr. Georgios Konstantinou from University of New South Wales (UNSW), who provided me with knowledge and permission to use Real-time laboratory at UNSW. I would also like to thank the nominated thesis reviewers for their agreement to examine this thesis despite their busy schedules.

There are people in everyone's life who make the path to success smooth and rewarded. My appreciation goes to my friends and colleagues, specifically Dr. Seyedfoad Taghizadeh, Dr. Mojtaba Moghimi, Dr. Milad Momayyezan, and Dr. Abhinav Sadu.

I would like to dedicate my thesis to my beloved grandmother, who passed away while I was writing this thesis, and most of all, I am heavily and forever indebted to my parents for their love and support, without which, pursuit of this advanced degree would never have been started and accomplished.. . .

Abstract

Recent developments in the area of advanced information and communication technologies offer provisions to power utilities to run an elegant load allocation and restoration in smart grids. Communication-enhanced platforms enable higher situational awareness with more grid components getting actively involved in load allocation and restoration, which results in higher network flexibilities and lower grid demand. For instance, multi-functional Electric Vehicle (EV) chargers, in aggregated level, can enable new ancillary services for operators to use (e.g. EV-assisted Volt-Var Control (VVC)). In addition, service restoration after a High-Impact Low-Probability (HILP) event in the grid could be improved by modern grid components, such as EVs and Distributed Energy Resources (DERs), to be dispatched during the restoration. This results in higher restoration rapidity and robustness in future grids.

Communication-based load allocation and restoration can improve various phases of the power system behavior from planning (preventive activities in pre-event period) to operation (corrective activities in post-event time interval). This Ph.D. study encompasses chapters on both planning and operation stages. A resilience-oriented multi-objective decision-making framework has been designed in this work to plan for higher structural resilience in the grid subject to HILP events.

Unlike the widely accepted standard metrics for reliability assessment in power distribution systems (e.g. system average interruption duration index (SAIDI), system average interruption frequency index (SAIFI), energy not supplied (ENS) etc.), a resilience index which

quantifies resilience features such as preparedness, robustness, and restorative/disruptive rapidity is missing. A novel multi-dimensional resilience metric is proposed in this Ph.D. study to be adopted by power utilities to evaluate resilience of the grid and optimize the aforementioned characteristics of power system behavior.

For operational resilience, a communication-based EV-assisted load restoration system is designed and implemented in this Ph.D. work. Unlike the past studies, the proposed solution harnesses (a) the imported power and flexibility from the neighboring networks, (b) Distributed Energy Resources (DERs), and (c) aggregated vehicle to grid (V2G) capacity in all steps of restoration when facing an extreme HILP incident with multiple faults. The proposed real-time SR mechanism is implemented using the RTDS Hardware In the Loop (HIL) platform and the contribution of each SR resource was numerically quantified by the developed resilience metric in previous chapter. The proposed solution ensures an enhanced feeder-level resourcefulness that can contribute to agile response and efficient recovery. This is primarily achieved by a strategic deployment of major modern resources (with focus on EVs contribution) during a sequence of multiple faults.

Keywords: Smart Distribution Grids, Resilience, Electric Vehicle (EV), IEC 61850, Hardware-in-the-Loop Platform, multi-objective optimization; high impact low probability (HILP) event, reconfiguration, state estimation, Cloud-based Communication, Demand Reduction, Smart Neighborhood Appliance Management, MQTT.

Contents

List of Figures

List of Tables

List of Publications

Refereed Journal Papers

- P. Jamborsalamati, M. J. Hossain, S. Taghizadeh, G. Konstantinou, M. Manbachi and P. Dehghanian, "Enhancing Power Grid Resilience through an IEC61850-based EV-assisted Load Restoration," published in IEEE Transactions on Industrial Informatics, 2019. **Impact Factor: 7.37 (Chapter 5)**

- M. Moghimi, J. Liu, P. Jamborsalamati, F.H.M. Rafi, S. Rahman, M. J. Hossain, S. Stegen, J. Lu, "Internet of Things Platform for Energy Management in Multi-Microgrid System to Improve Neutral Current Compensation," published in Energies 2018, Vol. 11, issue 11, 3102. **Impact Factor: 2.70 (Chapter 3 Extension)**

- P. Jamborsalamati, E. Fernandez, M. Moghimi, M. J. Hossain, A. Heidari and J. Lu, "MQTT-Based Resource Allocation of Smart Buildings for Grid Demand Reduction Considering Unreliable Communication Links," published in IEEE Systems Journal, vol. 13, no. 3, Sept. 2019. **Impact Factor: 4.46 (Chapter 3)**

- P. Jamborsalamati, R. Garmabdari, M. J. Hossain, A. Sadu, J. Lu, and P. Dehghanian, "Planning for Resilience in Power Distribution Networks: A Multi-Objective Decision Support," submitted to IEEE Systems Journal, 2019. **Impact Factor: 4.46 (Chapter 4)**

Refereed Conference Papers

- P. Jamborsalamati, M. Moghimi, M. J. Hossain, J. Lu, "Design and Implementation of a Hierarchical Hybrid Communication Platform for Multi-Microgrid Applications," in Sustainability in Energy and Buildings, KES-SEB 2018, Smart Innovation, Systems and Technologies, vol 131. Springer, Cham.

- M. Moghimi, P. Jamborsalamati, J. Hossain, S. Stegen and J. Lu, "A Hybrid Communication Platform for Multi-Microgrid Energy Management System Optimization," in IEEE 27th International Symposium on Industrial Electronics (ISIE), Cairns, QLD, 2018.

- S. Taghizadeh, P. Jamborsalamati, M. J. Hossain and J. Lu, "Design and Implementation of an Advanced Vehicle-to-Vehicle (V2V) Power Transfer Operation Using Communications," in IEEE International Conference on Environment and Electrical Engineering and 2018 IEEE Industrial and Commercial Power Systems Europe (EEEIC / ICPS Europe), Palermo, 2018.

- M. Moghimi, F. HasanMd Rafi, P. Jamborsalamati, J. Liu, M. J. Hossain and J. Lu, "Improved Unbalance Compensation for Energy Management in Multi-Microgrid System with Internet of Things Platform," in IEEE International Conference on Environment and Electrical Engineering and 2018 IEEE Industrial and Commercial Power Systems Europe (EEEIC / ICPS Europe), Palermo, 2018.

- P. Jamborsalamati, M. Moghimi, M. J. Hossain, S. Taghizadeh, J. Lu and G. Konstantinou, "A Framework for Evaluation of Power Grid Resilience Case Study: 2016 South Australian Blackout," in IEEE International Conference on Environment and Electrical Engineering and 2018 IEEE Industrial and Commercial Power Systems Europe (EEEIC / ICPS Europe), Palermo, 2018.

- P. Jamborsalamati, A. Sadu, F. Ponci, A. Monti and M. J. Hossain, "Improvement of supply restoration in multi-spare-feeder active distribution grids using IEC 61850," in IEEE Innovative Smart Grid Technologies - Asia (ISGT-Asia), Auckland, 2017.

- E. Fernandez, P. Jamborsalamati, M. J. Hossain and U. Amin, "A communication-enhanced price-based control scheme for HVAC systems," in IEEE Innovative Smart Grid Technologies - Asia (ISGT-Asia), Auckland, 2017.

- P. Jamborsalamati, E. Fernandez, M. J. Hossain and F. H. M. Rafi, "Design and implementation of a cloud-based IoT platform for data acquisition and device supply management in smart buildings," in Australasian Universities Power Engineering Conference (AUPEC), Melbourne, VIC, 2017.

Chapter 1

Introduction

1.1 Background and Research Motivation

Recent improvements in information technology and Internet of Things (IoT) platforms bring new challenges and at the same time new opportunities to smart grids [1, 2].

Communication-enhanced components of smart grids can actively participate in modern control and protection schemes to improve efficiency and resilience in power grids [3]. One of the major components of the modern grids are smart neighborhoods. Grid demand could be reduced by deploying communication-based load allocation algorithms in the smart community of buildings. Energy sharing among the community members can make benefits for all players of the energy market [3].

Higher penetration of renewbales and Electric Vehicles (EVs) in future grids provides grid operators with new ancillary services [4]. Multi-functional EV chargers in aggregated level can be dispatched during extreme conditions in the network to improve system behavior and feeder-level resilience of the grid. Resilience could be improved within different phases of the power system behavior subject to a High Impact Low Probability (HILP) event. Prior to HILP even, there are preventive actions which could be done in system planning phase [5]. Furthermore, after HILP event occurrence, there are corrective actions to be taken in operation phase [6]. In other words, power system resilience can be divided in two major categories: 1) structural resilience and 2) operational resilience [7]. The research motivation of this Ph.D thesis is to tackle both operational and structural resilience in the grid providing solutions for improvements in both domains.

Unlike widely accepted reliability indices, such as System Average Interruption Duration

Index (SAIDI), Customer Average Interruption Duration Index (CAIDI), System Average Interruption Frequency Index (SAIFI), etc., there is no standard metric to evaluate resilience of a power grid [8].

This Ph.D. thesis proposes a novel multi-dimensional resilience metric, which aims to quantify resilience in terms of disruptive and restorative parameters. This metric could be adopted by power utilities to evaluate resilience of a grid. Furthermore, it could be used as objective function to run resilience-oriented optimization in the network.

1.1.1 On the Concept of Resilience

A generic behavior of a power system subject to perturbations is indicated in Figure 1.1. This figure illustrates different phases of a power system performance from fundamental operation to faulty operation and step(s) to full restoration.

P(t) is the time-variant system behavior function representing the load level served in the grid under study. From t_0 to t_{N_0} is the Normal Operation (NO) duration related to pre-event period.

t_{N_0} to t_{PD} is Performance Degradation (PD) period due to a disruptive event occurred at t_{N_0}. t_{PD} to t_{OU} is the down time of the system with minimum performance level P_{OU} and minimum loads served.

At t_{OU} the load restoration process starts with F steps to full recovery. After each step of the partial recovery, system performance level is named P_{PR_i} and the time-variant system function assigned to that partial recovery step is denoted as $R_i(t)$. This function is called $R_{FR}(t)$ for the final recovery step.

Figure 1.1. shows the first recovery step between t_{OU} and t_{ER_1} with P_{PR_1} as a temporary stable performance level between t_{ER_1} and t_{PR_1}. Similar transition is demonstrated for the i^{th} partial recovery step accomplished. The final recovery step begins at t_{PR_1} and after t_{FR} the system is fully restored with the performance level back to NO state. Associated to each phase of the system behavior, depicted in Figure 1.1, there would be a metric to evaluate resilience as follows:

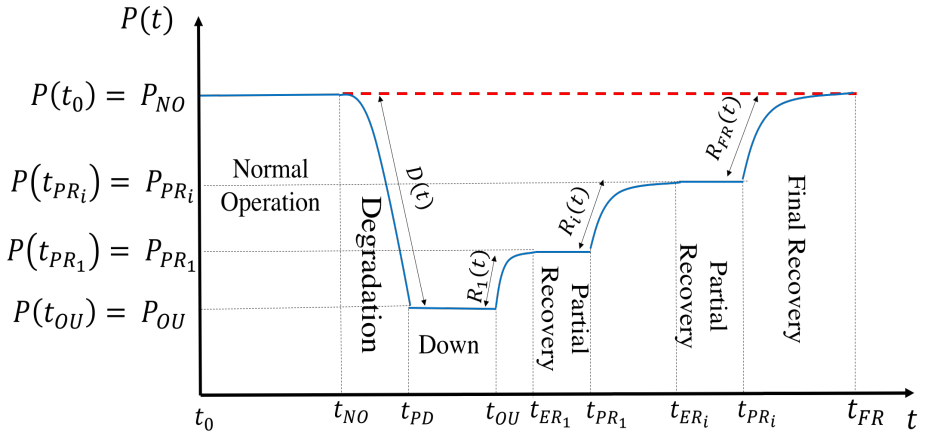

FIGURE 1.1: Generic system behavior subject to perturbation [9].

- **Performance Degradation (PD)**: PD is an energy-related metric assigned to the degradation period. This metric reflects the infrastructural robustness of the system and represents the system performance degradation by the catastrophic event from the original operational state. Lower PD value indicates a more resilient system with higher infrastructural robustness.

- **Outage Loss (OL)**: OL is an energy-related index allocated to the down time of the system. This index exhibits the performance loss of the system due to the disastrous event. Lower OL value shows more resilience in the system.

- **Energy-used-in-Recovery (ER)**: ER is another energy-related element defined over the recovery period. ER aims to highlight the effectiveness of the system restoration mechanism from the start of the recovery period until the full restoration.

  Interpretation of the ER index is the energy used by the system to bounce back to the normal operation (pre-event point). Therefore, higher ER values mean less resilience in the system.

- **Total Energy Loss (TEL)**: TEL is a broader energy-related metric, which reflects the entire energy losses in the system from the moment that catastrophic event, occurs to the end of the recovery process. TEL is the total energy not served due to a natural disaster. Hence, lower TEL represents higher resilience level in the system under study.

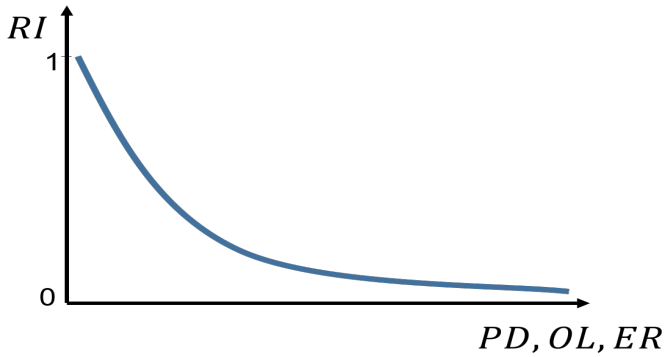

FIGURE 1.2: Changes in Resilience as a result of variation in resilience elements [9].

- **Degradation Rate (DR)**: DR is a time-related factor assigned to the degradation period. This factor represents the degradation rapidity in the system. Higher DR values indicate less resilience in the system.
- **Recovery Rate (RR)**: Similarly to DR, recovery rate could be defined over the recovery period as a time-related measure. *RR* calculated for each restoration transition and is averaged over the entire recovery period as a recovery rate indicator of the entire recovery duration. The higher RR means more resilience in the system.

Figure 1.2 indicates the trend of changes in resilience (RI) subject to the changes in the quantified elements of resilience such as PD, OL, and ER. It could be observed from this figure that resilience has a reverse relationship with PD, OL, and ER. This means that increase in the aforementioned elements results in less resilience in the grid and utilities need to minimize them in order to achieve maximized resilience in the network.

1.2 Problem Statement

Based on the above-mentioned constraints and the literature review which is presented in detail in Chapter 2, the below problem statements can be listed as follows:

- The majority of the existing communication-based load allocation systems in smart neighborhood do not break down to appliance-level allocation algorithms.
- There is a gap between appliance-level resource allocation algorithms and real-world implementation of such algorithms with realistic communications. This study does

not intend to alter the consumption pattern of the appliances with load shifting but to achieve reduction of the total grid demand of the smart neighborhood by strategic allocation of the available energy resources in the community including Community Storage Facility, Distributed Energy Resources, and Grid.

- Communications used by the LA algorithms in the existing literature are mostly assumed to be ideal. However, efficiency of the existing LA algorithms in case of losing a communication node or high latency in the network needs to be verified.

- Unlike the widely accepted standard metrics for reliability assessment in power distribution systems such as system average interruption duration index (SAIDI), system average interruption frequency index (SAIFI), energy not supplied (ENS) etc., a comprehensive evaluation framework which quantifies the *resilience* features such as preparedness, robustness, and restorative rapidity (among the others) is missing

- There are several research efforts that can be found in the literature on enhancing the resilience of power distribution grids to HILP events. However, a multi-objective decision making platform to support planning for resilience and run resilience-orientation optimization needs more investigation.

- Past research on outage management solutions mostly (a) are not resilience-driven, (b) are reactive solutions to local single-fault events, and (c) do not address both network built-in flexibilities and flexible resources for restoration.

1.3 Research Objectives and Contributions

In order to address the above-mentioned problems, the following objectives are targeted for this research:

- design and implementation of a communication-based load allocation system.

Contributions:

1) The proposed platform considers unreliable communication nodes in the smart neighborhood and has test cases for extreme latency in the network. The results present that the proposed system is efficient under high latency conditions in the network where there is a huge number of smart devices sending various information types to the controllers.

2) The proposed algorithm breaks down to appliance-level allocation of resources in the smart neighborhood such as community storage facility, distributed energy resources, and grid.

3) The proposed system is implemented with message queue telemetry transport (MQTT) protocol with proposed topics to be subscribed within a cloud-based platform.

4) The algorithm is deployed using a real-world residential load data and a virtual Wide Area Network emulator (WANem machine) to mimic characteristics of a realistic network (with delays).

- Design of a multi-objective resilience-oriented decision making platform (Planning)

Contributions:

1) Nodal-level resilience measures and metrics are proposed to quantify several resilience features that could be adopted by utilities for resilience-oriented planning and operation decision optimization. The proposed resilience indices are employed in this paper in a multi-objective optimization engine to optimally allocate the Tie switches in radial distribution networks.

2) A modular framework for dynamic evaluation of distribution network reconfiguration practices to maximize the resilience metrics is proposed. The developed framework utilizes a WLS-based state estimator, which considers dynamic admittance matrix to evaluate the network operating condition at each reconfiguration plan.

3) A diverse set of HILP scenarios is generated, followed by a detailed analysis of the results to demonstrate the efficacy of the proposed framework in boosting the network resilience against HILP disasters.

- design and implementation of a communication-based EV-assisted load restoration to improve resilience (Operational)

Contributions:

1) The proposed load Restoration scheme in this study offers provisions to effectively respond to disastrous events with subsequent impacts on the grid (multiple faults).

2) In addition to the imported flexibility from external and adjacent networks, the proposed autonomous load restoration in this Ph.D. study dispatches all modern resources including DERs, and especially the aggregated non-faulty V2G capacity in a faulty feeder as a new restoration resource. The developed solution continues dispatching these modern load restoration services even during the successive events, which in turn, relaxes the stress on the external resources and enhances feeder-level resourcefulness and resilience.

3) A new feeder-level resilience metric for load restoration is proposed which allows quantifying the performance of the solutions and the impacts on the grid resilience.

4) The real-time performance and scalability of the proposed SR approach are verified on a real-world Medium Voltage (MV) distribution grid, managed by A2A Unareti in a practical setting. This includes Hardware-in-the-Loop (HIL) simulations using specialized output boards of Real Time Digital Simulator (RTDS), which are capable of standardized publisher/subscriber IEC 61850-8-1 GOOSE communication

1.4 Thesis Outline

In order to address the objectives of this research and verify the contributions, this thesis encompasses six chapters which are organised as follows:

Chapter 2 provides an overview of the literature, focusing on communication based load allocation and load restoration in the past studies. To provide better understanding of this thesis an overview of smart grid communication protocols, technologies, and standards is provided in the first subsection of this chapter. This is followed by literature review on load allocation algorithms in smart neighborhoods. Finally, load restoration algorithms in past studies are reviewed in the last subsection of this chapter,

Chapter 3 presents an MQTT-based load allocation for grid demand reduction in smart grids considering unreliable communication links. The first part of the chapter focuses on algorithm development for appliance-level load allocation in smart neighborhoods. The next part presents the details of implementation of the proposed algorithm in real-world scenarios with realistic communication networks,

Chapter 4 proposes a load restoration platform to improve resilience in power distribution networks. This chapter focuses on structural resilience and planning phase to optimally locate tie switches in distribution grids to maximize resilience in the grid. A multi-objective decision making platform is presented in details in this chapter,

Chapter 5 presents an IEC61850-based EV-assisted load restoration system to improve resilience in power distribution networks. The first subsection of the chapter introduces the proposed functional units in the network. The next subsection discusses details of the hardware in the loop and implementation of the proposed communication-based load restoration,

Chapter 6 concludes the thesis and suggests future work for this research. A summary of all chapters and future research objectives are presented in this section.

Chapter 2

Literature Review

This chapter presents a literature review of the past studies relevant to communication-based load allocation (LA) and restoration to improve efficiency and resilience of the smart grids utilizing Electric Vehicles (EVs) and Distributed Energy Resources (DERs).

As a major part of this Ph.D. thesis is involved with implementation of load allocation and load restoration algorithms in smart grids using communication platforms, the first subsection of this chapter presents a review of technologies, protocols, and standards used in smart grid communications. Multiple communication protocols and cloud-based platforms are employed in this Ph.D. work. The aim of this literature review is to provide the reader with cons and pros of commercial smart grid protocols and the reason behind choosing those which are adopted in this Ph.D. thesis.

The second subsection focuses on a general overview of the communication-based load allocation schemes in smart grids. This includes studies on how to improve demand-side efficiency to reduce grid demand utilizing remotely controllable components of smart neighborhoods.

The next subsection of this chapter, provides the readers with a background of resilience-oriented load restoration algorithms in smart grids. This encompasses literature review on 1) structural resilience in planning phase for maximizing preparedness of smart grids against High Impact Low Probability (HILP) events, 2) operational resilience in post-event phase to optimize corrective actions in smart grids after occurrence of a HILP event. This sebsuction is followed by a brief review of resilience evaluation frameworks to be adopted by power utilities to quantify resilience in the networka for potential HILP events such as the one on September of 2016 in South Australian network (which is used as an example of HILP event

in this chapter). Finally, role of modern components such as Electric Vehicles (EVs) in aggregated level in communication-based load restoration algorithms is introduced.

2.1 Review of Smart Grid Communications: Technologies, Protocols, and Standards

The current electricity grid was designed to deliver electricity from large power generators to customers and the control of the network was solely dependent on the customers. Their energy usage behaviour was analysed, and the production could easily be adapted to balance demand and supply in the grid. Because of the shift towards a more decentralized power grid in which consumers can also act as power generators, grid failures and blackouts have become more frequent. Thus, ways to improve reliability, efficiency and security need to be developed [10]. The idea of a Smart Grid (SG) promises great improvements in all three of these disciplines by modernizing the current power supply system to allow monitoring, protection and automatic optimization of every connected element in the network.

These modernizations include generators, transmission and distribution systems as well as industrial and private customers [11]. Therefore, SGs will be complex setups of power and communication networks that need to be planned thoroughly [12]. The communication layer is necessary to allow utilities to manage the so-called intelligent electronic devices (IEDs) from central controlling points. To design a communication network that fulfils every requirement in every application, many different technologies need to be used. Requirements may involve reliability, latency, bandwidth and security [13].

2.1.1 Communication Network Architecture in Smart Grid

The SG communications infrastructure is expected to incorporate a hybrid mesh of different communication technologies to provide efficient and consistent access to grid components in diverse environments [14].

Similar to existing data and voice telecommunication networks, the SG communications

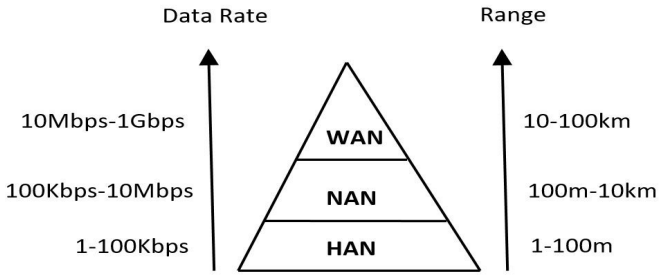

FIGURE 2.1: SG communication hierarchy [13].

infrastructure is expected to be a multi-level network that extends across multiple grid operation tiers. The SG communication networks need to spread over large geographical areas including generation, transmission, and distribution to the consumer premises [15]. Various types of communication networks in SGs are demonstrated in Figure 2.1 [16, 17].

They differ mainly in in terms of data rate and coverage range [18]. Therefore, different technologies will fit better or worse to the requirements of each of these network scales.

The power distribution grid along with the corresponding NAN constitute the heart of the new power systems. Furthermore, two fundamental grid applications, the distribution automation and advanced metering infrastructure systems are within the neighborhood area network domain. To provide security, distribution automation information between substation Local Area Networks (LANs) and aggregated metering data from spatially dispersed home area networks, need to be transmitted through a reliable communication infrastructure [19].

It is noteworthy that the topological/hierarchical differentiation described in this section can be used to define the microgrid concept as a network using home and neighbourhood calibre technologies with the possibility of operation in an autonomous island mode.

2.1.2 Comparison of Technologies for SG communication

The task of converting power grid to smart grid is not possible without the incorporation of suitable wired or wireless technology for enabling communication across the grid. Table 2.1 summarizes a comparison between communication technologies utilized in smart grids [12, 20–27].

TABLE 2.1: Comparison of communication technologies

Technology	Standard/ Protocol	Theoretical Data Rate	Coverage Range	Network		
				HAN	NAN	WAN
		Wireless				
ZigBee	ZigBee/ZigBee Pro	250kbps	Up to 100m	X	X	
WLAN	802.11x	2-600Mbps	Up to 100m	X	X	
Wireless	Various (e.g., RF mesh)	Depending on selected protocols	Depending on deployment	X	X	
Z-Wave	Z-Wave	40kbps	Up to 30m	X		
WiMAX	802.16	75 Mbps	Up to 50km		X	X
Cellular	4G/5G	>100Mbps			X	X
Satellite	Satellite Internet	1Mbps	100-6000km			X
		Wired				
Fiber Optic	PON	155Mbps-2.5Gbps	Up to 60km			X
	WDM	40Gbps	Up to 100km			
	SONET/SDH	10Gbps	Up to 100km			
DSL	ADSL	1-8Mbps	Up to 3.6km		X	
	HDSL	2Mbps	Up to 1.5km			
	VDSL	15-100Mbps	Up to 28km			
Coaxial Cable	DOCSIS	172Mbps	Up to 28km		X	
PLC	HomePlug	14-200Mbps	Up to 200m	X		
	Narrowband	10-500kbps	Up to 3km		X	
Ethernet	802.3x	10Mbps-10Gbps	Up to 100m	X	X	

2.1.3 Comparison of Industrial Protocols for SG Communications

This subsection provides a brief review of the common protocols used in the automation process. The predominant protocols used in the power industry communication, i.e., the internet protocol suite, Modbus, DNP3 and IEC61850 are shortly discussed in the following [28]:

- **The internet protocol suite**: The Internet protocol suite is the conceptual model and set of communications protocols used on the internet and similar computer networks.This model has been developed by the United States Department of Defense and provides end-to-end data communication specifying how data should be packetized, addressed, transmitted, routed, and received [29]. This functionality is organized into four abstraction layers, i.e., the application, transport, internet and link layers. The

most important protocols for the application in SG communication are Network Timing Protocol (NTP), Internet Protocol (IP), Transmission Control Protocol (TCP), User Datagram Protocol (UDP), File Transfer Protocol (FTP) and Simple Mail Transfer Protocol (SMTP).

- **DNP3**: As of today, the Distributed Network Protocol version 3.3 (DNP3) is the dominant Master/Slave communication protocol in electrical utility SCADA systems [30]. Contrary to Modbus, DNP3 is not limited to just sending one single data point. Many different data types (i.e. Boolean, floating point) can be wrapped to single messages. This results in a reduction of data traffic. DNP3 also allows the communication of timestamps and data quality information. In addition, slave devices can independently send update messages with value changes as a trigger. In Modbus for a comparable update, the master would have to poll the slave for this kind of information. Just as Modbus, DNP3 is deployed on different technologies like serial communication, optic fiber, radio, satellite as well as TCP/IP protocols on Ethernet networks [31].

- **IEC 61850**: IEC 61850 presents a two-bus Ethernet architecture as initially developed for substation automation purpose [2]. Over the process bus, IEDs used for time-critical applications (e.g. protection) exchange messages within less than 3ms delay range in networks without congestion [32]. Over the station bus, messages for non-time-critical purposes such as SCADA are transmitted. There are 3 main protocols presented in IEC 61850 standard series: 1) IEC 61850-8-1 Generic Object-Oriented Substation Event (GOOSE) message, 2) IEC 61850-9-2 Sampled Values (SV), 3) Manufacturing Message Specification (MMS). Peer-to-peer publisher-subscriber GOOSE and SV messaging occur over the process bus among time-critical IEDs [33, 33–35].

  Client-server MMS messaging takes place over the station bus for SCADA applications.There is a hierarchical object model introduced by IEC 61850 standard series, which facilitates interoperability among the IEDs from different vendors. The hierarchy starts from a logical device which could consist various logical nodes (which represents

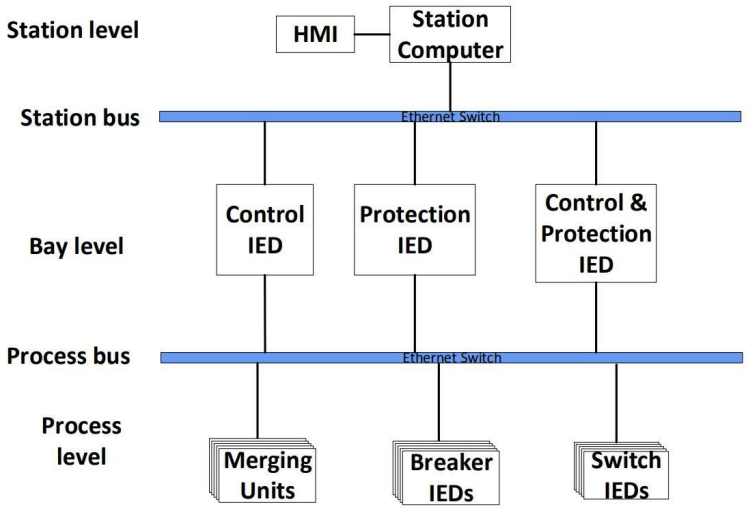

FIGURE 2.2: IEC 61850 SG architecture and IED levels [34].

functions that an IED should perform). Each logical node can hold various data objects and for each data object multiple data attributes could be assigned. This hierarchical naming structure is shown in Figure 2.3. Configuration of the IEDs are standardized by utilizing the standard extensible markup language based (XML) Substation Configuration Language (SCL) file and System Configuration Description (SCD) file. This offers flexibilities for real-world deployments. The flexibilities of using IEC 61850 includes: 1) user-defined data set within GOOSE messages, 2) flexible configuration of SCL files for MMS, and 3) flexibility in defining customizable data objects.

2.1.4 Comparison of IOT-based Protocols for SG Communications

There are various application-layer protocols which could be utilized to implement IoT platforms with applications in SGs. Protocols which are used in past studies include Message Queuing Telemetry Transport (MQTT), Constrained Application Protocol (CoAP), Advanced Message Queuing Protocol (AMQP), Extensible Messaging and Presence Protocol (XMPP),

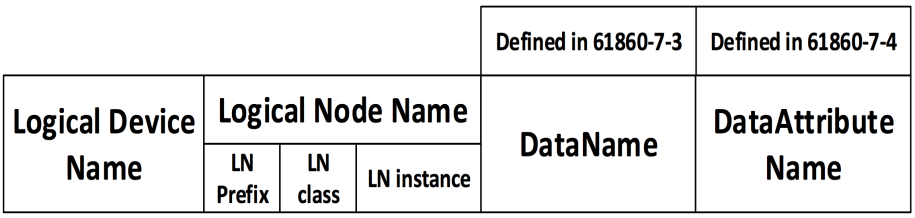

FIGURE 2.3: IEC 61850 hierarchical naming structure [34].

and Hypertext Transfer Protocol (HTTP) REST. These protocols could be clustered and compared from different aspects. The aspects to be considered for comparison of the IoT protocols include latency, bandwidth utilization, energy consumption, and security [35].

- **Message Transmission Mechanisms**: One of the main factors to be used in clustering the application-layer protocols in SGs is message transmission mechanism. There are two basic models in IoT protocols, named publisher-subscriber model and request-reply model [36].

  The main difference between the two mechanisms is that in request-reply model, the two parties must know each other by IP and they run simultaneously. However, in publisher-subscriber model, there is a third party, called message broker, which is in charge of filtering and distribution of the published messages to the subscribers. Hence, the publisher and the subscriber does not necessarily run at the same time and they do not know each other by IP. Furthermore, in publisher-subscriber mechanism, messages are published to customizable topics which are subscribed by the subscribers. Therefore, each subscriber can subscribe to multiple publishers at the same time. Among the popular SG protocols, HTTP REST and CoAP are operated by request-reply mechanism [37, 38]. Examples of popular publisher-subscriber protocols in SGS are MQTT, AMQP, and XMPP [39, 40].

- **Integration with Cloud-based Platforms**: Multiple research works tend to fill the gap between industrial communication protocols such as Modbus, DNP3, and IEC 61850-based protocols and the IoT protocols introduced in this section. In these architectures, a hardware or software entity works as a middleware to receive data from the lower layer (industrial layer) protocols and to pass the collected data to a cloud database by utilizing the higher-layer (application-layer) protocols. Therefore, compatibility and interoperability of the IoT protocols with cloud-based platforms are required to be considered. According to the previous studies, the most popular protocol to be used for cloud interactions is the improved version of REST HTTP [41, 42].

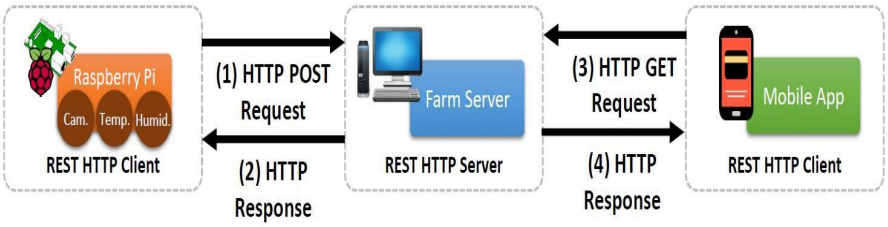

FIGURE 2.4: Client-Server interaction model in HIL platforms using HTTP Requests [43].

TABLE 2.2: Comparison of commercial cloud services

	IBM Bluemix	SiteWhere	ThingSpeak
MATLAB Analysis?	No	No	Yes
REST Provided?	Node-Red Needed	Yes	Yes
Communication with Hardware (e.g. Raspberry Pi)?	Node-Red Needed	Protocol Buffers Needed	Direct HTTP Services
Installation needed?	No	Yes	No
Device Configuration needed?	Yes	Yes	No

The REST HTTP works based on request-reply mechanism. In most of the implementations in previous studies, HTTP POST and GET requests are utilized to develop an interface between cloud-based platforms and IoT protocols. In these studies, hardware products such as Raspberry Pi and software products such as mobile applications are employed as HTTP clients to interact with the cloud server. Overview of the client-server interaction model is indicated in Figure 2.4. There are popular cloud services used in the past studies for implementation of IoT platforms with applications in energy systems. The commercial cloud services include IBM Bluemix, SiteWhere, and ThingSpeak which are compared with each other in Table 2.2 [44]. This table highlights advantages and disadvantages of the popular cloud services. ThingSpeak has favored features for developers such as (1) built-in interface with MATLAB, (2) easy-to-use REST Services, (3) easy integration with Raspberry pi, Arduino, and ESP8266 Wi-Fi module, and (4) provisions for high-resolution real-time data collection (up to seconds sampling time interval).

- **Latency in various conditions**: Latency is another major parameter to evaluate performance of communication protocols in SGs, especially in time-critical applications such as protection of the grid in faulty situations. Previous studies have used hardware-in-the-loop (HIL) simulations to implement machine-to-machine messaging in SGs and to measure latency [45]. Round Trip Time (RTT) has been used as the main index to represent efficiency of a protocol in terms of latency. The best performance in SGs with minimum latency is achieved by two protocols, which are MQTT and CoAP [46].

  There are comparative studies on performance of the two protocols in different Quality of Service (QoS) levels with no network congestion [47, 48]. The outcomes of the studies prove that in QoS0, MQTT has a lower RTT compared with CoAP, while in QoS1 MQTT has longer RTT. In a nutshell, RTT for MQTT is measured in range of milliseconds and for CoAP is recorded in range of hundreds of microseconds. Furthermore, MQTT shows a lower delay range in comparison with AMQP especially for transmission of messages with huge payloads. Delay measurements in an experimental study is shown in Figure 2.5 to compare AMQP and MQTT.

  In popular HIL architectures, cellular network is utilized to transmit CoAP and HTTP messages using Arduino and Raspberry Pi GPRS shields. Delay measurements indicate that response time for HTTP is relatively longer than CoAP [49].

  Hybrid communication architectures switch between centralized and decentralized

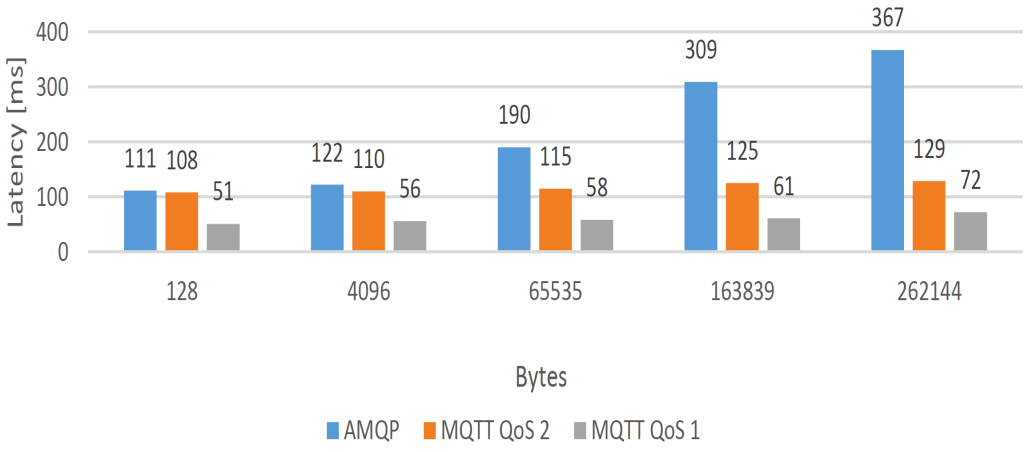

FIGURE 2.5: Client-Server Comparison of MQTT and AMQP in terms of latency [46].

TABLE 2.3: RTT range and communication operation mode

RTT	Communication operation mode
RTT <250 ms	Centralised
250 ms <RTT <350 ms	Decentralised/global
350 ms <RTT <500 ms	Distributed
RTT >500 ms	No communication mode

operational modes depending on the RTT of the MQTT communications. Table 2.3 shows the scenarios with RTT range and communication operational modes [50].

Security of IoT platforms built on the introduced protocols is a major issue to be considered. REST HTTP for cloud interactions utilizes the well-known Transport Layer Security (TLS) for data encryption and security of the channel communications. In this mechanism, a shared secret key is exchanged between the client and server within a TLS hand-shaking process. Similar security management has been adopted for XMPP as a built-in feature.

In MQTT protocol, authentication is realized by the MQTT broker, where a three-step hand shaking process occurs. When an MQTT client attempts to connect to an MQTT broker, there is an initialization process to establish the connection by exchanging control packets such as CONNECT and CONNAC (response) [51]. These control packets include information about QoS level of transmission, topic, payload, etc.

CoAP protocol uses Datagram TLS (DTLS) for enabling secure communication on top of the UDP transport mechanism. The handshaking process to exchange 'hello' message between the client and the server in DTLS is very similar to TLS but with additional possibility for the server to check for an authentic source of 'hello' message [52, 53].

Security layer for AMQP protocol is an external authentication and encryption process which depends on the host framing protocol for AMQP. This protocol supports Simple Authentication and Security Layer (SASL) authentication as a security framework.

Table 2.4 provides a comparison of application layer protocols based on the transmission mechanism, latency, and the security level.

TABLE 2.4: Comparison of application layer protocols

Protocol	Transmission Mechanism	Latency (RTT)	Security
REST HTTP	Request-Response	Hundreds of milliseconds	TLS
MQTT	Publish-Subscribe	Couple of Milliseconds with best performance in QoS0	CONNECT packet authentication
CoAP	Request-Response	Hundreds of microseconds with best performance in QoS1	DTLS
XMPP	Publish-Subscribe	Couple of seconds	TLS
AMQP	Publish-Subscribe	Hundreds of milliseconds with best performance in QoS1	SASL

2.1.5 Standards for Smart Grid Communications

The introduction of the SG concept and the shift towards advanced communication platforms have led to a number of competing standards being introduced around the world. This section provides a brief overview of some of the most popular standards for SG communication [54].

The most popular and most recognized standard is the IEEE-based IEEE 1901. IEEE 1901 was developed in early 2005 and was initially meant for power line networks and at its conception it replaced a hand full of other standards. It is now widely regarded as the predominant standard for SG communication. IEEE 1901is used for high speed communication over broadband power lines (BPLs). It can achieve up to 500Mbit/s and work on frequencies under 100 MHz. In addition to being used in SG applications, the IEEE 1901can also be used in home network applications, Vehicular applications and many other applications.

IEEE 1901has two basic modes of operation. It supports both time division multiple access (TDMA) and carrier-sense multiple access with collision avoidance (CSMA/CA), which makes it compatible with many legacy and new technologies. It also supports two modulation modes in the physical layer, i.e. Orthogonal Frequency Division Multiplexing (OFDM) and wavelet OFDM. OFDM is the primary multiplexing technique used in LTE and forms the basis for what is anticipated to be implemented in 5G networks. Wavelet OFDM is derived from high definition-PLC technology and has been proposed as the basis for multi-carrier modulation systems [55, 56]

Another standard closely linked with the IEEE 1901is the ITU-T G.9972, which was developed by the International Telecommunications Union (ITU) [57], it supports a home networking standard called the G.hn. This standard is the main competing standard for the IEEE1901 which uses the HomePlug technology developed by the HomePlug Alliance [58].

HomePlug uses 2 to 28MHz whereas G.hn uses 1.8 to 80MHz. They both use OFDM for modulation. However, G.hn allows for multiple input multiple output. Table 2.5 provides a comparison between IEEE 1901and ITU-T G.9972.

Another important standard used in SG communications is IEEE 2030 [59]. The IEEE 2030 standard was developed in 2011 by the IEEE and was part of the SG initiative. It provides guidance in applying SG interoperability reference model of IEEE STD 2030 in the development a of control and automation components [60]. Unlike the IEEE 1901, the IEEE 2030 can be thought of as an official guide on SG interoperability. Its main focus is on ensuring that there is a set of rules that governs how the electrical power system, information coming from devices and the end use applications interact in a safe and efficient manner. It discusses the best practices and approaches to minimize risk, decrease lag and increase accuracy. One of the primary goals of this standard is to ensure safe communication in SGs and avoid possible vulnerabilities. This standard is especially effective when there are multiple technologies being used to provide a variety of services to the consumers.

Throughout the early 2000s, IEC released a set of standards to define exchange of information for electricity metering data exchange. IEC 62056 was defined in this context as an extensive set of standards to govern communication from the meters. It can be seen as the nitration standard version of the Device Language Message Specification. The set of specifications defines the object identification system, the interface classes, how data is exchanged between the meter readings, the tariff and the load control. It also defines how different networks interact with each other to optimize communications. This standard was designed to operate over any medium. It is a key standard in establishing the SG for the simple reason that reliable information exchange between the meters and the central nodes is paramount in ensuring efficiency and accuracy. If the data exchange is breached or inefficient, it could have serious implications on the rest of the system [61].

TABLE 2.5: Comparison of IEEE 1901and ITU-T G.9972

	IEEE 1901	ITU-T G.9972
Technology	HomePlug	G.hn
Modulation Type	OFDM/wavelet OFDM	OFDM
Frequency Range	2-28 MHz	1.8-80 MHz
Channel Access	CSMA/CA	TDMA, CSMA/CD
Security	DSNA/PSNA/CCMP	AKM
Burst Mode	Uni/bi directional	Bi-directional

IEC 62351 is another recent standard which is used predominantly for security in communications networks [62]. With the dawn of the digital age and the introduction of SGs, IEC 62351 aims at defining the authentication methods, encryption algorithms and general security procedures and protocols. The different security objectives of this standard include authentication of data transfer through digital signatures, ensuring only authenticated access, prevention of eavesdropping, prevention of playback, and intrusion detection. IEC 62351 has been identified by some to have only partial backward-compatibility which has led to significant problems with legacy systems and products [63].

However, it is a highly regarded standard and continues to play a significant role in ensuring that SG communication is effective, efficient and safe [64].

2.2 Review of Communication-Based LA in SGs

Recent developments in the area of the advanced Information and Communication Technologies (ICTs) enable real-time monitoring and control of the smart-grid components such as smart buildings[1]. Higher penetration of Internet of Things (IoT) platforms and cyber-physical systems (CPS) in distribution grids has turned the previously passive components into active ones. This means that by incorporating Home and Distribution Automation Systems (DAS), Advanced Metering Infrastructure (AMI), and Demand Side Management Systems (DSM), end-users in smart homes do not play a passive role and become active participants in the grid [65].

In near future, smart homes will accommodate Distributed Energy Resources (DERs) along with devices capable of communication in real time. Home appliances in modern

buildings are able to connect to a local network for exchanging information including measurements (Float data type) and device statuses (Boolean data type) with each other and with the Home Management Unit (HMU) [66]. The purpose of implementing such communication platforms in residential sector is to offer provisions for monitoring, automation, and active coordination of home appliances in order to achieve a better utilization of building resources and to improve the energy efficiency of the neighborhoods via energy sharing among buildings [67]. Maximizing the DER utilization in smart buildings, which host local generation and smart devices, can lead into a significant peak-to-average ratio (PAR) reduction and eventually can smoothen the load curves of the traditional grids in order to reduce greenhouse emissions. As the number of Intelligent Electronic Devices (IEDs) with communication capability increases in the buildings, massive amount of data needs to be stored, processed, and exchanged. Hence, cloud-based communication architectures, which enable extensive data sharing, become vital [67].

2.2.1 LA Architectures in Previous Studies

Appliance-level load allocation schemes in residential communities could be implemented in centralized or decentralized fashions [68].

In centralized method, a central neighborhood controller receives information from all of the community members and makes decision for each building inside the neighborhood. Centralized coordination algorithms are effective but they need to deal with heavy computation burdens and they heavily rely on information from each member. For instance, if there are missing data from a single building due to a communication failure, the algorithm cannot achieve results for the whole community [69].

Alternatively, in decentralized decision making, each smart building coordinates its IEDs and communicates with neighboring buildings for energy sharing if possible. Decentralized algorithms could be carried out in different levels: 1) with a central unit 2) without a central unit.

In the proposed LA architecture in this Ph.D. work, decentralized method which uses a

central unit with a two-way communication mechanism is adopted. This method fits the community appliance coordination scheme proposed in this paper and resolves the aforementioned problems of centralized algorithms. In this decentralized scheme, smart home appliances communicate with a central unit in the building bi-directionally. This home central unit aggregates the desired information from appliances (e.g. load profiles) and communicates with the same units in neighboring buildings.

There are various protocols for data sharing via internet which could be used to implement the communications required for home coordination schemes. Message Queuing Telemetry Transport (MQTT), which is a message-oriented information exchange protocol and works on TCP, is utilized in this work to realize the bi-directional communication between appliances and the building controllers and also the messaging among building controllers. The main advantage of using this protocol is that it is a light weight transport protocol and uses the network bandwidth efficiently. MQTT is a publisher-subscriber communication mechanism in which subscribers need to know the topics of published data. The MQTT topics are defined by the publishers and could be customized desirably depending on the goals of the application. In this paper, MQTT topic management for home appliance coordination scheme is presented and topics are proposed accordingly.

Previous studies have considered decentralized energy management Systems (EMS) and Demand Response (DR) in residential sector.

In [1], a day-ahead energy management algorithm for coordination of smart neighborhoods in presence of renewables is developed and presented. However, the developed algorithm in [1] remains at theory level and no solution on practical implementation of such EMS is provided to address challenges such as resilience of the system against communication failures (missing appliance data).

In [65], a home energy management system for a single building based on ZigBee and appliances coordination is conducted but realistic case scenarios with network latency and integration of multiple buildings are not addressed.

An IoT platform is proposed in [66] for energy management systems in production level but is not mapped to appliance-level management in buildings.

References [67, 70–73] show the huge potential in domestic load management which could result in cost benefits for end-users and grid demand reduction by utilizing flexibilities in residential buildings. These studies show that goals of the EMS could be achieved by frequency-sensitive relays triggering the circuit breakers (ripple control), by time clocks in Renewable-energy-integrated platforms in real-time, or by using special tariffs to influence consumer behavior. These studies focus on developing Resource Allocation Systems (RAS) to match residential demands with available resources in a cluster of household prosumers. Although these studies consider optimized utilization of resources for multiple buildings, non of these studies present detailed implementation of appliance-level RAS and investigation on the effects of real communication network characteristics, such as packet delay and packet drop, on the proposed systems.

There are studies focused on communication platforms to implement decentralized decision making in energy systems. In [2, 74], communication protocols presented in IEC 61850 standard series are utilized to implement Multi-agent protection systems for distribution grids but not mapped to residential sector for appliance management.

MQTT protocol is used to design building automation system in [75–77]. These studies have provided solutions to implement building management systems using MQTT, inclduing MQTT topic management. However, these studies have not integrated multiple devices from multiple buildings with traffic in the Local Area Network (LAN).

Cloud-based Machine-to-Machine communication platforms with the aim of effective scheduling of the building resources in presence of distributed energy resources are presented in [78, 79, 79–81]. These articles have not discussed the reliability of the platform to have a backup plan in case of losing the connection to the cloud. The cloud-based RAS and EMS proposed in these studies collapse if the connection to the cloud server is lost.

Linkage of the home appliance coordination algorithms to the communication platforms for real-world implementation in residential communities (more than one building) has yet space to work. Most of the residential energy management algorithms in previous studies remain in design level and challenges that arise when pairing these algorithms with communication protocols stay unanswered.

The authors in [82, 83] have solved optimization problems to minimize the transmission power of information signals for multiple users considering outages and reliability issues. The outage-constrainted robust design of the energy harvesting scheme in these papers minimizes the power consumption of the network components but does not consider optimal allocation of power supply to the building appliances considering the DERs and storage systems based on the users comfort level.

The main contribution of this Ph.D. work is to provide a detailed practical solution for implementation of a novel decentralized appliances coordination scheme in a renewables-integrated community of smart buildings.

2.3 Review of Communication-Based Resilience-Oriented Load Restoration in SGs

Power grid resilience is defined as the ability of the system to avert possible event-driven damages, tolerate accidents, and engender a swift response and recovery following extreme disasters [5, 8]. Power system resilience can be studied in two main categories: 1) structural resilience 2) operational resilience [7].

2.3.1 Structural Resilience and Load Restoration in Smart Grids

Structural resilience focuses on pre-event phase of the power system behavior to boost robustness and infrastructure of the grid to maximize preparedness of the power system subject to a HILP event [6, 84]. The reliable supply of electricity upon which modern society depends is at risk due to the unforeseen effects of a myriad of converging factors: elevated incidences and severity of outage-inducing high-impact low-probability (HILP) events including, most notably, severe weather patterns and cyber attacks, sudden changes and proliferation of renewable resources, and many more. Examples of such HILP incidents in recent years are South Australian blackout in 2016 with 900 MW power outage due to extreme weather [85], major blackout in Brazilian grid in 2018 with 18,000 MW curtailed power in cascaded fault condition, outage in India in 2012 with 1423 TWh outage, severe

power cut in the USA in 2015 with 180,000 customers affected due to abnormal weather condition, among many others [86, 87].

Unlike the widely accepted standard metrics for reliability assessment in power distribution systems, such as system average interruption duration index (SAIDI), system average interruption frequency index (SAIFI), energy not supplied (ENS) etc. A comprehensive evaluation framework which quantifies the *resilience* features such as preparedness, robustness, and restorative rapidity (among the others) is missing [85]. Resilience assessment could be focused on a load point (node level) or the entire system (feeder-level) [88]. An effective resilience metric could be utilized as an objective function in a wide variety of power grid long-term planning and short-term operation decisions to boost its capacity in dealing with the HILP incidents. Such a resilience metric needs to capture various aspects of the power grid behavior ranging from the pre-event (infrastructural resilience) to the post-event (operational resilience) time frames and its evaluation framework has to contain different quantitative and qualitative terms such as measures on energy capacity, rapidity, and economy [85].

There are several research efforts that can be found in the literature on enhancing the resilience of power distribution grids to HILP events. In [89–92], resilience-oriented outage management systems, which utilize microgrids and renewable energy resources to re-energize the critical loads following a natural disaster, are proposed where the focus has been primarily on enhancing the grid operational resilience. In [88, 93–95], novel evaluation frameworks with new metrics to quantify various resilience features are presented. Some of these efforts are founded based on the principle concept of graph theory for single-node level resilience evaluation in the network where parameters such as path redundancy, node connectivity, and resourcefullness are taken into account. Furthermore, parameters such as disruptive and restorative rapidity are suggested in [85, 96, 97] focusing on the system-level (feeder-level) resilience evaluation. While such efforts offer provisions for characterizing the distribution grid resilience and its swift operational response and recovery following a HILP incident, the flexible resources are assumed already planned and readily available to be utilized in practice.

In [6, 98, 99], preparedness against extreme events is pursued by optimal allocation of the grid-scale flexible resources (e.g., battery storage units, renewable resources, and electric

vehicles) during extreme scenarios. Research outcome presented in [84] shows analytical results of a risk assessment framework for weather-resilient power grid operation and control, where predictive measures for minimizing the risk against forecasted weather-driven outages are suggested through effective utilization of network topology control. Enhancing the grid operational resilience through changing the network topology requires additional switches that should be planned to be placed in strategic locations in the network, thereby facilitating rerouting the way electricity flows for swift response and recovery in dealing with the aftermath of HILP events.

2.3.2 Operational Resilience and Load Restoration in SGs

Enhancing the ability of power grids to avert possible event-driven damages, tolerate accidents within the system, and swiftly bounce back to a normal operating condition following a disruption can manifest a well-resilient power system [8]. High Impact Low Probability (HILP) events, such as natural disasters and cyber attacks, can result in remarkable technical and economic losses in the entire energy landscape. Therefore, it is of great importance for power utilities to increase awareness against HILP events and to reduce the outage of the end customers by effective strategies that best harness the integration of modern grid resources and flexible services before, during, and following a HILP disaster [7, 100].

Research on power distribution network resilience and the corresponding solutions could be categorized by single-node improvements or collective (feeder) level enhancements [101]. In another classification, actions for escalation of grid-scale resilience could be taken at three different timescales[102]:

1) Pre-event System Planning: which includes preventive actions before the event happens, such as grid hardening and reinforcement of the infrastructure by installation of new devices. These actions increase infrastructural resilience [103].

2) System Operation During the Event: where corrective actions are triggered to avoid the system blackout. Corrective actions aim to stop a possible cascade scenario through swift response and fast isolation of the predicted fault tree in the network connectivity map[100].

3) Post-Event Service Restoration (SR): which points out to the system operational resilience, where grid services, including traditional and modernized network flexible resources, are deployed for time-critical restoration of the healthy segments of the affected feeder [104, 105].

In [104, 106–112], automated feeder reconfiguration schemes for load restoration are presented and the impact of Distributed Energy Resources (DERs) on reliability of power systems is investigated. In these studies, microgrids are employed to contribute to the restoration of critical loads by prioritizing the restorable demand. However, SRs demonstrated in the aforementioned articles are aimed to heal the credible contingencies and are not focused to the extreme HILP incidents.

Agent-based frameworks for SR are designed and implemented for active distribution grids in [34, 113–115]. Although DER agents and storage components are proposed within the multi-agent outage management systems, the contribution of other modernized grid services, such as Electric Vehicles (EVs), for resilience is not properly addressed, where EV aggregators could be an additional agent in a multi-agent SR scheme. In [116, 117], restoration algorithms in passive distribution grids with unidirectional current flows are suggested which rely solely on the extra capacity available from the adjacent feeders and, therefore, comes at a higher cost compared to using the local generations. Effective utilization of the internal resources, located in healthy segments of a faulty feeder, for service restoration is not studied in most of the past literature.

Higher penetration of EVs in smart grids along with large-scale utilization of multi-functional EV chargers in the near future enables new potentials to be harnessed in service restoration [118, 119]. References [119–126] have investigated integration of EVs in distribution grids and the potential ancillary services such as Volt-VAR optimization and outage management by Vehicle-to-Grid (V2G) services. Nevertheless, these studies (a) do not consider and coordinate both network built-in flexibilities and other flexible resources, (b) are not primarily designed for resilience services to be able to capture the subsequent events and sequential restoration steps, and (c) are limited to local single-fault events.

Different from the past research, the proposed SR solution in this Ph.D. work focuses on

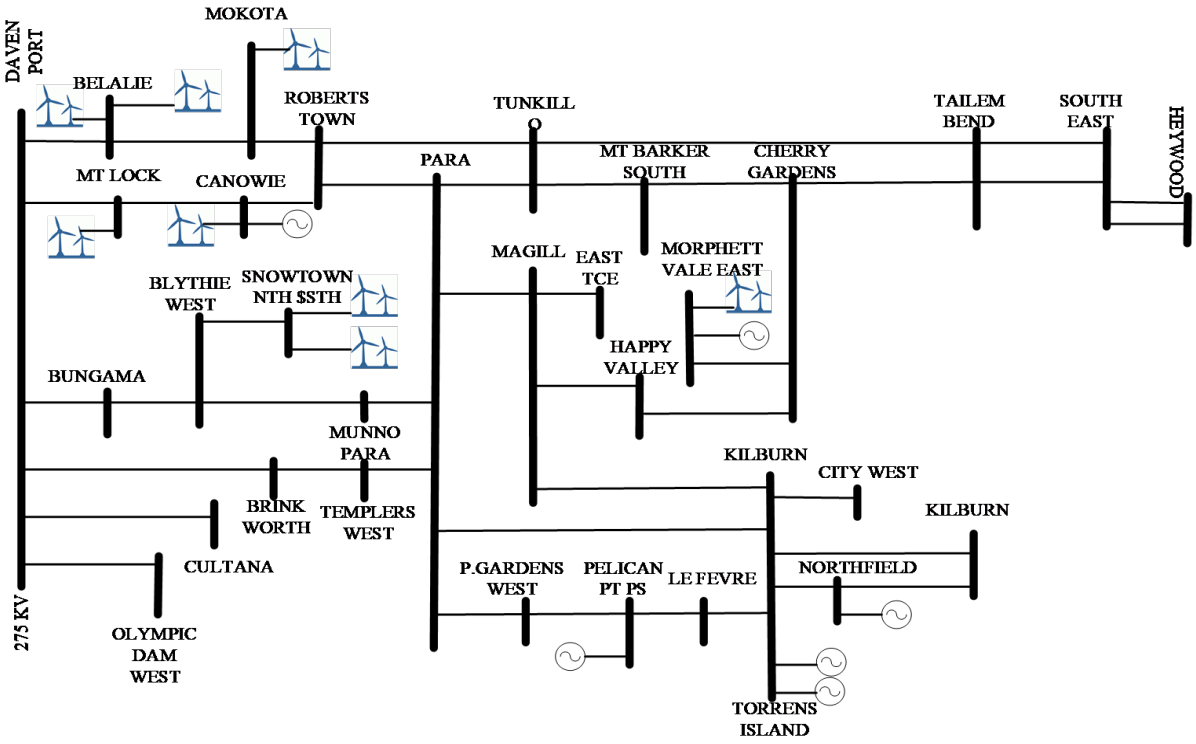

FIGURE 2.6: South Australian 275 kV network subject to blackout [9].

HILP events (e.g., extreme weather conditions) and harnesses network flexibilities, including external and internal resources with quantified contribution factors. Furthermore, real-time evaluation of the designed SR, implemented with real communications, is presented by online evaluation of the proposed collective-level resilience metrics.

2.3.3 Review of Evaluation Frameworks for Power Grid Resilience

On 28th of September 2016, fierce storms and lightning strikes caused multiple faults on the South Australian transmission system and 456 MW of wind generation tripped off-line as a result of Low Voltage Ride Through (LVRT) protection feature of wind turbines. This loss of generation and lack of load shedding activities led to a significant blackout in the area. The SA 275 kV transmission network is indicated in Figure 2.6.

The real demand data related to SA grid is visualized in Figure 2.7. It could be observed from this figure that prior to the event, 1826 MW demand is measured by the SCADA for SA's customers. The distribution of the supply is as follows: 883 MW wind generation, 330 MW gas generation, 613 MW imported power from Heywood interconnection to Victoria.

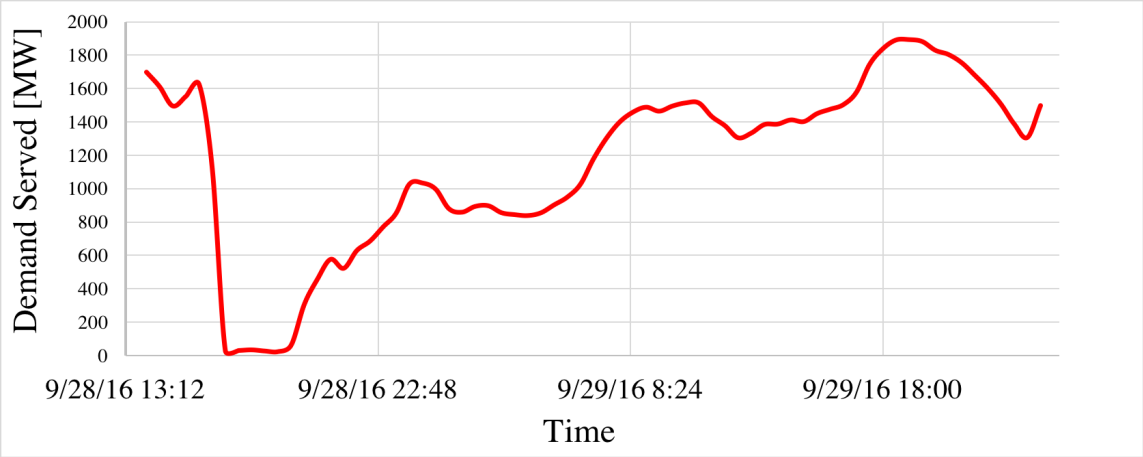

FIGURE 2.7: Generic SA system behavior subject to perturbation [9].

At around 4:16pm on 28th of September, tornados with wind speeds in the range of 190-260 km/h occurred and caused five system faults within 87 s and finally brought three transmission lines down in the SA grid. Consequently, as a response of riding through the fault (LVRT protection features) for wind farms, wind generation of SA grid reduced by 456 MW and the imported power from Heywood interconnection increased significantly. This increase in power flow of the Heywood interconnector made the protection system of the South East Substation trip (disconnect) the transmission circuits of the Heywood interconnector. Hence, 900 MW supply from this interconnection was lost and destroyed the demand-generation balance in the SA grid and finally led to the system frequency collapse and a huge blackout.

ElectraNet and AEMO started the restoration process at 4:30pm with a decision-making algorithm displayed in Figure 2.8. The restoration phase could be divided into three steps: 1) securing the power system, 2) auxiliary power supply to power stations, and 3) load restoration. Restoration strategies exhibited in Figure 2.8 include energizing the sections of the transmission network assessed as safe segments and utilizing contracted generation units in the neighboring networks (Heywood interconnector in Figure 2.6) for the ancillary services. The main action is switching in order to energize the two parallel 275 kV transmission lines between Heywood substation and South East substation in SA grid. This switching began at 5:20pm and by 6:40pm the connections were established [9]. The first customers were restored by 7:00pm on 28th of September. About 40 percent of the restorable loads in SA grid had been restored by 8:30pm (4 hours after the event). At around 8:40pm restoration

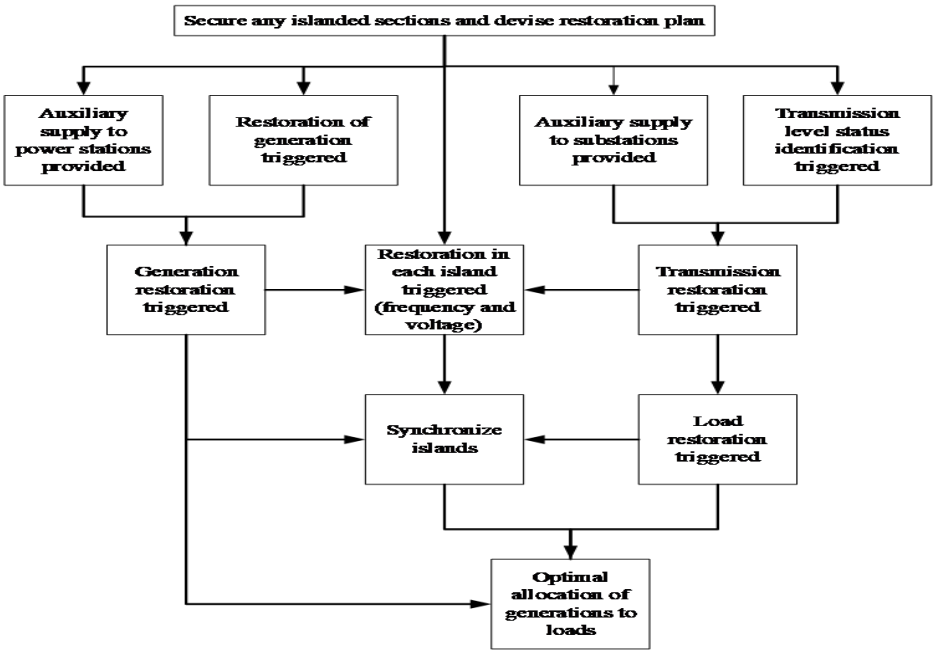

FIGURE 2.8: Overview of the restoration algorithm for SA grid [9].

was stopped temporarily due to overflow of power in the tie-lines but the restoration was continued again at 9:15pm. 80-90% of them were restored by the early morning of 29th of September, 2016 (around 7.5 hours after the event).

This sort of HILP events indicates importance of a comprehensive resilience evaluation framework for power utilities to plan for structural and operational resilience.

Resilience evaluation in power distribution grids contains diverse qualitative and quantitative components related to infrastructural and operational aspects of the system behavior [127]. Measure of the system performance is the key element in resilience evaluation which includes energy-based, rapidity-based, and economy-based dimensions [128].

Reliability assessment and resilience analysis of a system require standardized metrics and measures. The main difference between reliability and resilience is the extensive scale of the disruptive event considered in resilience analysis [9, 101].

Reliability analysis focuses on high-probability low-consequence events (e.g. a single unit failure) while resilience concentrates on low-probability high-consequence happenings (e.g. hurricane). In resilience analysis of power grids, multiple faults occur at the same time (e.g. due to extreme weather situation) and a huge portion of the grid goes down (unlike reliability assessment).

There are widely acceptable reliability indices used by the utilities such as SAIDI, SAIFI, ENS, etc. However, no standard resilience metric exists to quantify dynamics of the entire restoration process from pre-event to post-event stage. Previous studies have investigated resilience analysis frameworks.

In [129], a metric based on the vulnerability time in the grid is developed and applied to real-data related to Hurricane Ike. In [130], a study on real data received from four utilities in Upstate New York on power interruptions of the end customers due to hurricane Sandy is conducted. To evaluate resilience in this paper, authors have defined two metrics: infrastructure resilience and service resilience.

Infrastructure resilience is measured by the failure rate of the nodes in the system. Failure rate is defined by the number of times a node changes status from normal to failure in a specific duration. Service resilience is characterized by the cost due to delays in restoring a failure and the corresponding outages.

In [131–134], resilience in interdependent systems has been conceptualized from various aspects. Evaluation frameworks presented in these papers consider various parameters related to power grid resilience such as robustness, redundancy, rapidity, and resourcefulness. The resilience index of [134] is too generic and does not evaluate different stages of the system. The evaluation frameworks presented by the above-mentioned papers do not quantify the system behavior considering each phase of the load restoration individually. Hence, a complete resilience evaluation framework, which considers disruptive and restorative stages of the system separately and enables stage-wise comparison of system resilience between different power grids, needs further developments.

2.3.4 Electric Vehicles (EVs) in Load Restoration

The global electric car stock evolution from 2010 to 2016 is depicted in Figure 2.9 [135]. As can be observed, electric car stock exceeded two million units in 2016, and the highest electric car market belongs to Norway (29%) in 2016. Such developments in the field of EVs with over 750 thousand sales worldwide in 2016 have led to the transition to electric road transport technologies.It is becoming increasingly difficult to ignore the role of smart-grids in the future

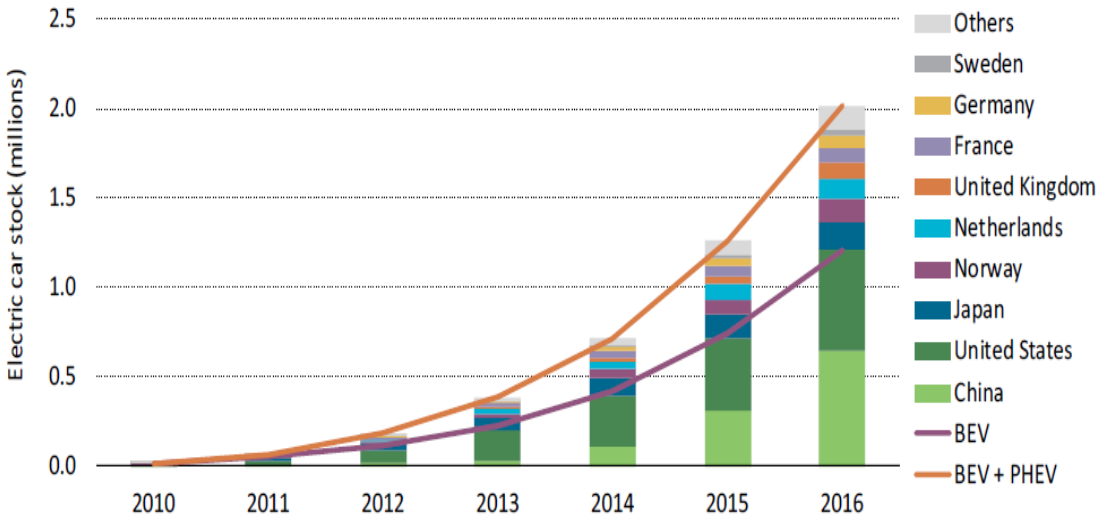

FIGURE 2.9: The global electric car stock evolution from 2010 to 2016 [135].

of the modern electric power system systems. As mentioned before, V2G technologies allow power exchange between vehicle and utility grid. V2Gs are the link between smart-grids as the future of conventional power systems and EVs as the future of vehicles.

V2Gs can provide numerous services to the power grid such as ancillary services, peak load shaving and demand-side management. However, more research needs to be undertaken on optimization techniques, objectives and constraints for the V2G implementation for the future V2G deployment. Power and urban air quality, noise mitigation and greenhouse gas (GHG) reductions are also the main environmental benefits of using V2Gs in the power system. The accomplishment of the V2G technology requires the active participation and collaboration of government, power utilities and EV owners

Over recent decades, because of expanded utilization of power, exhausting petroleum reserves, the need to utilize sustainable sources has been turned into one of the worries of the global society. The past decade has seen the rapid development of EVs in many industrialized countries, as they have the ability to provide low-emission future and high-power quality for power distribution systems. EVs are also appropriate to support synergies with different renewables. Furthermore, the automotive industries have been building up a close association with power utility issues.

Modern EV chargers for medium/large EV charging stations, depicted in Figure 2.10, are capable of detecting the order of the harmonic current, that exceeds the standards and

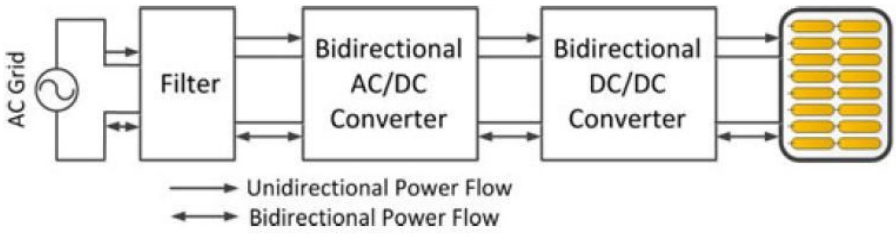

FIGURE 2.10: General unidirectional and bi-directional power flow topology [136].

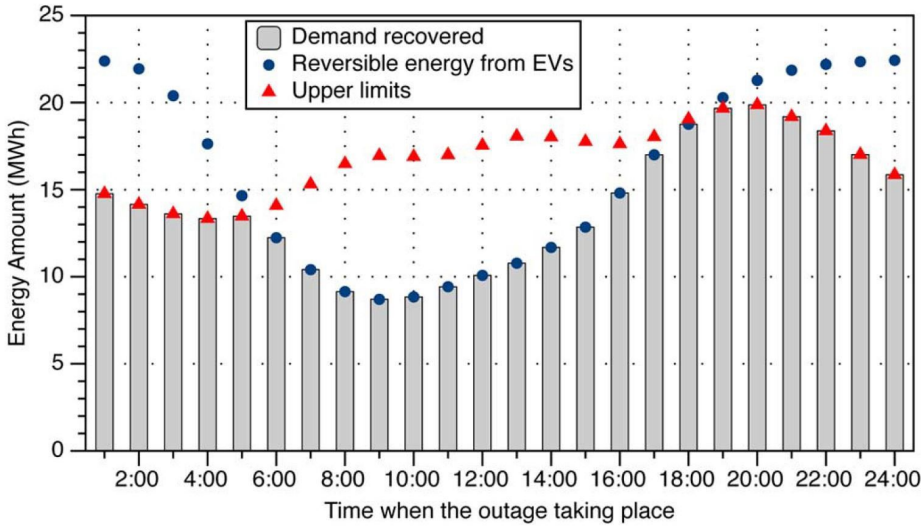

FIGURE 2.11: Demand recovered by local V2G with centralized EV charging [138].

filters them out to avoid EV harmonic effects [136]. Harmonic detection and reactive power compensation are considered additional functionalities in new generation of multi-functional EV chargers.

There are research activities focus on the role of EVs in V2G mode to enhance the power system operation in terms of reliability and demand recovery. In this context, dispatchable EVs are considered the reserve capacity to be used in case of outages in the system. In [137, 138], Results show the scenario when outage occurs in the system and local EVs are utilized to recover the demand during the outage as illustrated in Figure 2.11. This can lead to a significant enhancement in the reliability of the grid and is showed by calculating the widely acceptable reliability indices such as System Average Interruption Duration Index (SAIDI) and Average Energy Not Supplied (AENS).

Figure 2.11 indicates that the reserve capacity (reversible energy) by EVs reaches its maximum at night (around 24:00) when most of the EVs are connected and have enough

SoC, while the minimum reserve capacity occurs in the morning (around 9:00 AM) where the majority of EVs are on the road. This modern network flexibility brings new opportunities to network operators to enhance power system resilience and reliability.

2.3.5 Chapter Summary

This chapter presents a thorough literature review of communication-based load allocation and load restoration schemes to improve efficiency and resilience in smart grids. Various technologies, protocols, and standards utilized in smart grid communications are presented in the first subsection of this chapter.

The first subsection of this chapter aims to compare popular industrial and Iot protocols in smart grids. The reason behind selecting communication protocols such as MQTT and IEC 61850-presented protocols in this Ph.D. work (e.g. GOOSE communication) is provided. Commercial cloud-based platforms (such as ThingSpeak), used in smart grids and smart neighborhoods, are briefly presented with introduction of advantages/disadvantages in a tabular format.

The next subsection of the chapter reviews various communication-based load allocation schemes in smart grids. According to the literature review, the below constraints are identified:

- Most of the communication-based load allocation algorithms do not investigate impacts of network latency or unreliable communication networks on the proposed LA scheme.

  Previous studies do not provide test scenarios for cases where there is an extreme network latency in the communications between smart neighborhood components and the controller (Extreme RTT values). Efficiency of the past LA schemes subject to unreliable communication nodes in the network needs to be verified.

- Many of the previous research works on communication-based load allocation in smart grids do not map to the appliance-level load allocation in smart neighborhood. Appliance-level LA in smart neighborhood needs yet to be further investigated.

- Implementation of communication-based LA schemes in smart grids utilizing efficient platform with popular smart grid protocols and cloud-based platforms are not

sufficiently presented with details .

The following subsection of this chapter focuses on resilience-oriented load restoration platforms. The below constraints are identified:

- Lack of a comprehensive multi-dimensional resilience metric, which quantifies resilience of the power systems in terms of disruptive rapiditi, restorative rapidity, robustness, etc.

- lack of test case scenarios to verify proper functionality of a load restoration algorithm in case of resilience-driven extreme events such as multiple faults in the network. Many of the load restoration algorithms are reactive solutions to local single-fault events.

- Past studies do not address both network built-in flexibilities and flexible resources in all restoration steps. In many of the past studies, modern network flexibilities such as EVs in aggregated level are not harnessed. There is a huge potential in modern grid components such as Distributed Energy Resources (DERs) and EV aggregators to be used in all load restoration steps of a power system subject to an HILP event.

- Lack of a framework for structural resilience. This requires a multi-objective decision support framework for power utilities to arrange preventive activities prior to a HILP event.

Chapter 3

MQTT-Based Load Allocation for Grid Demand Reduction in Smart Neighborhoods Considering Unreliable Communication Links

The research objective in this chapter is to design and implement an appliance level load allocation system with realistic communication networks to reduce the grid demand of a smart residential community. Unlike many previous studies, this chapter considers unreliable communication nodes in the smart neighborhood and the load allocation algorithm switches from centralized to decentralized operational modes depending on the network latency. Selection of Message Queuing Telemetry Transport (MQTT) protocol over many other IoT protocols is justified in in Section 2.1.4. In a nutshell, easy-to-integrate and easy-to-implement features of this protocol in conjunction with interoperability with cloud-based services are the main reasons of adopting this protocol in this chapter.

3.1 Proposed Communication Architecture

In order to provide the reader of this chapter with a better understanding of the proposed communication architecture, components of the designed communication platform along with the communication protocol are presented in details as follows:

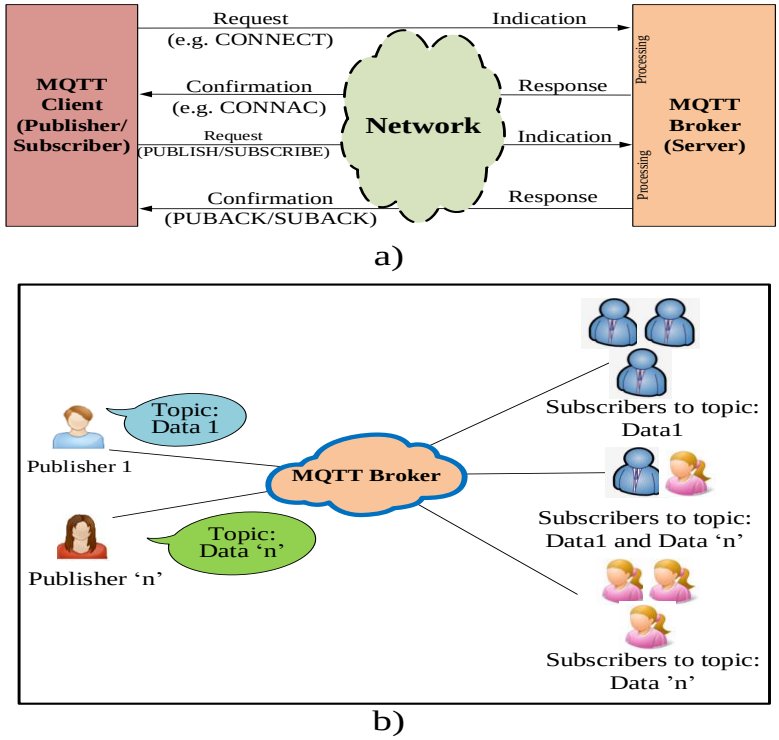

FIGURE 3.1: MQTT protocol:a) Hand-shaking procedure, b) components and topic.

3.1.1 Required knowledge on MQTT Protocol

There are three key players in MQTT messaging: 1) MQTT publisher, 2) MQTT subscriber, and 3) MQTT broker. MQTT publisher and subscriber are not connected to each other by IP address directly and they do not necessarily run at the same time [3]. MQTT broker which performs as a network hub and receives the messages from publishers, filters, prioritizes, and distributes them among up to thousands of concurrently connected MQTT subscribers. MQTT broker is responsible for client authorization and a hand-shaking procedure for initialization of the communication [77].

MQTT publishers use customizable topics for publishing data which must be subscribed by the clients. MQTT protocol does not support labeling messages with Metadata [3]. Hence, MQTT topic management in order to attach meaningful attributes to the topic could present metadata of the message payload and becomes substantial. MQTT Topic is a string which has a hierarchical structure with multiple levels and attributes [77]. Each level is separated by a forward slash in the topic tree. These topics could be modified to represent routing information.

Figure 3.1 (a) shows the initialization of the connection by exchanging control packets between clients and the broker. These control packets such as CONNECT, CONNAC, PUBLISH, PUBACK, SUBSCRIBE, SUBACK, etc. contain details about the Quality of Service (QoS) level of transmission, topic, and payload [3]. Figure 3.1 (b) indicates the components of the MQTT communication.

3.1.2 Design Specifications of the Proposed Architecture

The overview of the proposed hierarchical platform for smart buildings with physical layer, cyber layer, and control layer is indicated in Figure 3.2. There are two communication layers in the proposed hybrid platform. In the first layer (local layer), the smart building appliances (a) publish MQTT messages to the Building MQTT Client (BMC) for reporting events/measurements and (b) subscribe to MQTT messages published by the BMC for control/protection purposes. The second layer (global layer) is the interactions between the BMC and the cloud via HTTP POST/GET requests.

In the proposed architecture, each appliance is equipped with a Wi-Fi module, connected to a local gateway, and publishes measurements to a dedicated pre-defined topic periodically. The BMC subscribes to all of the topics and posts the received measurements to a cloud channel. The aggregated data in the cloud is accessible via the cloud MATLAB interface that runs a designed appliance resource allocation algorithm. The results of the algorithm are transferred from the cloud to the appliances via the BMC to be actuated by them.

The proposed architecture offers resilience in case of partial communication failure in each layer (local or global). In other words, the BMC is designed in such a way that in case of high latency in the network or communication link failure, it operates as a local controller (back-up controller) for the building appliances. This functionality of the BMC is indicated in a case scenario in the results section of this chapter.

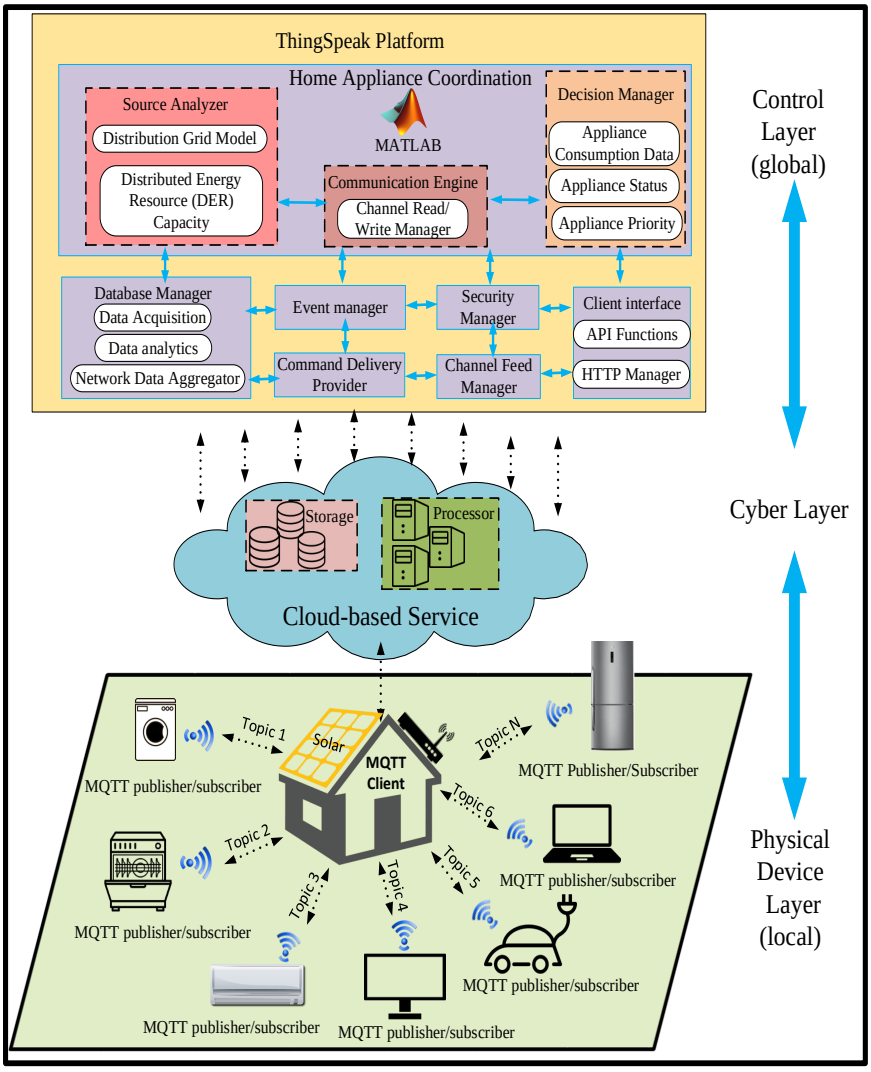

FIGURE 3.2: Proposed communication architecture for smart buildings.

3.2 Proposed Appliance-level Resource Allocation Algorithm

The algorithm developed in this work aims to coordinate the supply of the building appliances utilizing available resources. The algorithm schedules the supply of the appliances in the buildings according to the user defined operational modes.

Resource allocation algorithm in this paper is designed for two operational modes with different purposes. The user has the freedom to decide on the desired operational mode. These modes are: 1) maximizing DER-utilization, and 2) priority-based. In both modes, the algorithm maps appliances to resources in each individual building and shares the extra energy of DER units of the building with the community. The first mode allocates the supply

of the building appliances with the aim of maximizing the utilization of the installed DER capacity for that particular building. Hence, in this selfish mode, amount of the building DER capacity which is shared with the community is minimized.

The second mode (Priority-based) is suitable for places where the end user comfort zone comes at a higher priority than optimal utilization of the DER. This could refer to the locations where the number of minutes of interruptions in case of using the grid supply is higher than the number of minutes of interruptions in case of using the DER for sensitive appliances.

3.2.1 Maximizing DER-utilization mode

For a set of all appliances (I) in the building, the inputs to the algorithm are: appliances' consumption levels (Pl_i), statuses (on / off) of the appliances (Sw_i), and the available DER capacity $S_{available}$.

Building appliances publish their consumption levels periodically, if and only if, they are switched on, i.e., they are an element of ON_i. Depending on the availability of the DER units, the algorithm finds the optimal set of appliances (ON_s) that could be supplied by the building DER units. The algorithm in this mode solves the following mixed-integer optimization problem for the current time interval once the input values published by the appliances are received in the cloud:

$$\min \left[S_{available} - \sum_{i=1}^{I} J_i \times Pl_{ON_i} \right] \tag{3.1}$$

$$S.t.\ S_{available} \geq \sum_{i=1}^{I} J_i \times Pl_{ON_i} \tag{3.2}$$

where J_i is a binary variable determining whether the appliance must be in the optimal set (assigned to 1) or not (assigned to 0) and Pl_{ON_i} are the power levels of the switched-on appliances which are taken as fixed values for each time interval.

The remaining appliances ON_r which are elements of ON_i and not elements of ON_s are connected to the grid. Finally, a Common Storage Facility (CSF) located in the community, owned and maintained by a separate entity, will be charged by the remaining capacity of the installed DER ($S_{remaining}$). It must be noted that $S_{remaining}$ is the remaining DER capacity after

connecting the algorithm-determined appliances to the DER. $S_{available}$ is the available DER capacity and is considered to be fixed for the next time slot. $S_{available}$ is published frequently by the DER unit in the building and updates the corresponding value in the cloud using MQTT protocol and $S_{remaining}$ is calculated as an algorithm output and is used for charging the CSF in the community.

The power from the CSF may be utilized for GDR of the community at peak hours. The cost of electricity that is delivered to or taken from the CSF also could be an encouragement for the community members to charge the CSF.

Algorithm 1 : *Maximizing DER-utilization mode*

1: Read the available DER capacity $S_{available}$.
2: $\forall i \in I$: read the switch status of all appliances Sw_i.
3: $\forall ON_i \in I$: read the power levels of appliances Pl_i.
4: $\forall ON_i \in I$: find the possible combinations of ON_r that can be supplied by $S_{available}$ and that minimizes $S_{remaining}$.
5: $\forall ON_s \in ON_i$: connect to the DER.
6: $\forall ON_i \notin ON_s$: connect to the grid.
7: Charge the common storage facility by $S_{remaining}$.
8: Wait for the new data to be received for the next time slot and go to step 1.

3.2.2 Priority-based mode

The additional input to the algorithm in this mode is the user-defined priorities for the building appliances (P_i). The users can prioritize their appliances to suit their comfort level. This algorithm reads the appliances' priorities and sorts them in ascending order. In the next step, it finds the appliance with the highest priority which could be supplied by the DER unit in the building and connects it to the DER unit. The available DER capacity is updated by subtracting the power level of the connected appliances from the previous available capacity. This step is repeated for the subsequent appliances until the available DER units cannot feed any appliance in the building. Finally, the CSF of the community is charged by the remaining capacity of the building DER units. This algorithm runs separately for each building every time that a new set of data is published to the cloud by that building's MQTT client.

Algorithm 2 : *Priority-based Mode*

1: Read the available DER capacity $S_{available}$.
2: $\forall i \in I$: read the switch status of all appliances Sw_i.
3: $\forall i \in I$: read the priorities of the appliances P_i.
4: $\forall ON_i \in I$: read the power levels of appliances Pl_i.
5: Sort the priorities in ascending order.
6: $\forall ON_i \in I$: find the highest-priority appliance such that $Pl_{ON_i} \leq S_{available}$ and connect it to the DER and update $S_{available} = S_{available} - Pl_{ON_i}$.
7: Repeat step 6 until $Pl_{ON_i} \geq S_{available}$.
8: $\forall ON_i \notin ON_s$: connect to the grid.
9: Charge the common storage facility by $S_{remaining}$.
10: Wait for the new data to be received for the next time slot and go to step 1.

3.2.3 Market design for discharging CSF

A simplified bidding mechanism, initiated by the BMC, is designed to showcase the functionality of the CSF to achieve higher grid demand reduction. The calculations are quite simplified and do not account for a lot of financial factors, which can vary from case to case. The stored energy in the CSF during the day is sold and delivered back to the members in a pay-as-bid market clearing process in the cloud during the very-low-solar-generation period. Members have the freedom whether or not to participate in the bid and for which appliances the bid can be placed in the cloud. Members bid in proportion to the power they have shared with the community to charge the CSF.

The BMC in each building can send a bid to the cloud to receive energy from the CSF as per the equations below

$$C = \begin{cases} C_1 & \text{for } P_R \leq 70\% \text{ of } P_S \quad (3.3) \\ \gamma \left[\dfrac{P_R}{P_S} \times \alpha + \tau C_2 \right] & \text{for } 70\% < P_R \leq 90\% \text{ of } P_S \quad (3.4) \end{cases}$$

where P_R is the requested power from the CSF (the amount that BMC bids for) and P_S is the power shared with the community by that member. If the user decides to receive less than 70% of P_S, (3.3) is applied to the member (a fixed cost), where C_1 represents the fixed cost value. This fixed cost is the minimum cost that can yield profit to the CSF over the life time of the CSF. If the member decides to receive between 70% to 90% of P_R, (3.4) is applied to

the member and bidding is processed by the BMC where γ and τ are binary integers to be set by the members. In case of participation in the bidding mechanism, γ must be set to 1, else it is 0. The bid price may be increased by the member by setting τ to 1 and C_2 to a value that secures the bid. But at any instant the maximum bid is kept less than the cost of power from the grid. α is a constant determined by the size of the battery, the expected life cycle, and the power of the grid that it can displace over its life-cycle. The aforementioned thresholds (70% and 90%) are designed in such a way that all members can receive a fair amount of energy from the CSF.

3.3 Real-world Neighborhood Appliances Data Models and MQTT Topic Management

To showcase effectiveness of the proposed RAS, real data representing a residential sector in Australia has been taken from Energex Co. This data includes total consumption of 3 residential buildings in kW during peak hours from 1:00 pm to 8:00 pm with 15-minute resolution. In this work, the total-consumption data of the buildings are broken down to the appliance-level consumption data using equations below:

$$P_{(t)}^{Aij} = P_{(t)}^{j_{(tot)}} \times \beta^i \tag{3.5}$$

$$\sum_{i=1}^{n} P_{(t)}^{Aij} = P_{(t)}^{j_{(tot)}} \tag{3.6}$$

$$P_{(t)}^{min} \leq P_{(t)}^{tot} \leq P_{(t)}^{max} \tag{3.7}$$

where β^i is the appliance consumption ratio defined for each individual appliance in each building. $P_{(t)}^{j_{(tot)}}$ is the time-variant total power consumption of building j and $P_{(t)}^{Aij}$ is the power consumption of appliance i in building j. The appliances in this work are assumed to be non-shiftable and the algorithm does not aim to alter the consumption patterns but to allocate resources to the appliances strategically. There are 3, 4, and 5 appliances considered

TABLE 3.1: Neighborhood Solar Generation Parameters

Building	V (W)	Installed Cap. (W)	Panel Cap. (W)	$\gamma \times l_{coeff.}$
1	Low	3025	335	0.170
2	Medium	4550	325	0.175
3	High	7370	275	0.156

for resource allocation in building 1, 2, and 3 respectively.

Neighborhood appliance data including location, consumption ratios, and priority settings are reported in Table 3.2, where VH, H, M, L, and VL stand for Very High, High, Medium, Low, and Very Low priorities respectively. As the neighborhood under study is located in Australia, the appliance consumption ratios are capped by data from [139].

The DER considered for each building in this study is roof top solar panels. The neighborhood under study is located in Australia and buildings are considered to be oriented at 3 different directions and the irradiations parameters are considered for a sunny day in Australia. The main equation used to generate building solar profiles is:

$$E_t = A \times \lambda^e_{(t)} \times \gamma \times l_{coeff.} \tag{3.8}$$

where A is the area of the panel, $\lambda^e_{(t)}$ is the irradiation value including the forecast error, γ is the solar panel efficiency and $l_{coeff.}$ is the coefficient for losses. γ is calculated at standard test conditions (STC) : radiation = 1000 W/m^2, cell temperature = 25 ^0C, Wind speed = 1 m/s. The losses considered in this work are inverter losses (4% to 10%), temperature losses (5% to 20%), DC & AC cable losses (1% to 3%) and shadings (0% to 80%). The irradiation values for Sydney are predicted using the $SolarPro$ simulation software [140].

The PV parameters are reported in table below. The buildings are categorized on the ratio of the installed capacity to the loads. To cater to the fluctuations in irradiance value, a white noise ϵ is added to the predicted irradiance as follows:

$$\lambda^e_{(t)} = \lambda_{(t)} + \epsilon \tag{3.9}$$

The appliance-level consumption data for the buildings are depicted in Figure 3.3 and the solar generation profiles are visualized in Figure 3.4. In the CSF discharging market

TABLE 3.2: Neighborhood Appliances Data : Location, Consumption, and Priority Settings

Appliance	Consumption Rate (kW)	Location	β			Priority Settings		
			B1	B2	B3	B1	B2	B3
Electric Vehicle (EV)	8.2	B1, B2, B3	71%	58%	45%	H	H	M
Air Conditioner	1.5	B1, B2, B3	23%	21%	25%	M	M	H
Chillers	1.432	B1, B2, B3	6%	5%	4%	VH	VH	VH
ELV Lighting Converter	1.5	B3	N/A	N/A	11%	N/A	N/A	L
Commercial Refrigerator	1.296	B2, B3	N/A	16%	15%	N/A	L	VL

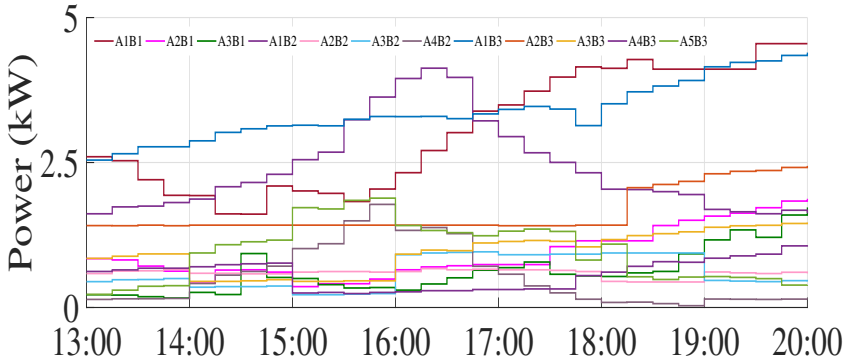

FIGURE 3.3: Appliance-level power consumption of a residential community (legend 'AnBm' shows Appliance 'n' in Building 'm').

presented in this work, α is assumed to be 0.45 which is derived from [141] for a typical storage topology and could be modified depending on the installation in each community.

The inputs to the designed algorithm which are sent to the cloud periodically and retrieved in MATLAB®are appliance power levels, solar generations, and appliances statuses. To implement the algorithm described in Section III for a community of 3 buildings, a set of private cloud channels are configured and dedicated to each building. For each appliance in

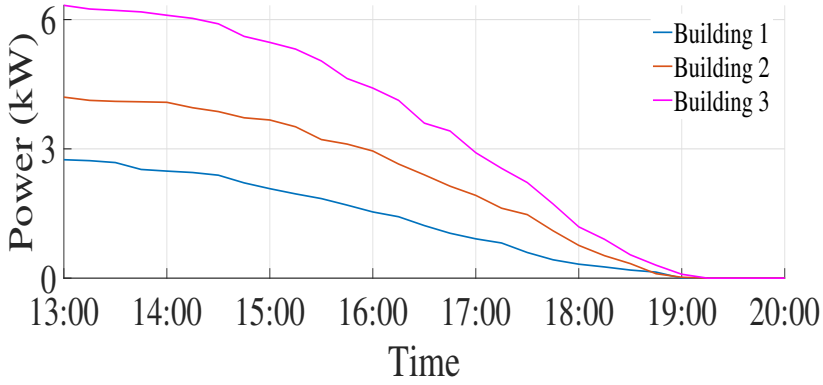

FIGURE 3.4: Solar generation profiles.

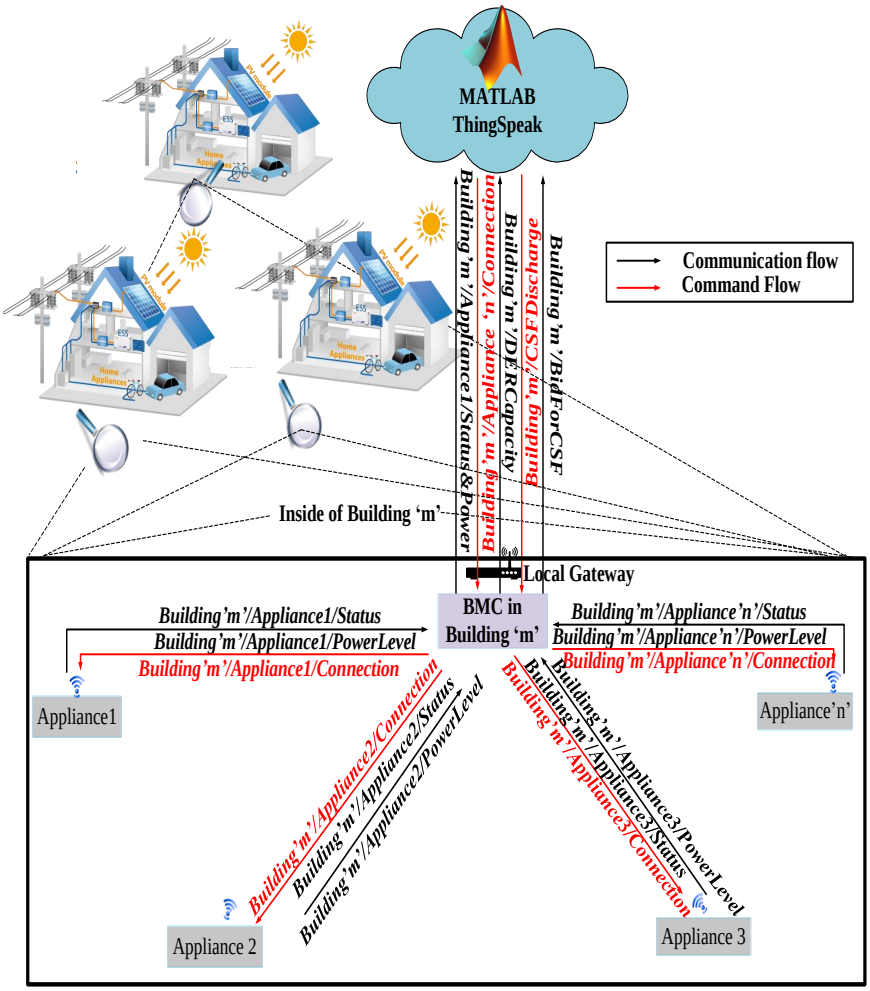

FIGURE 3.5: Proposed MQTT Topic management in a residential community.

each building, 2 fields of the corresponding channel are enabled to store appliance statuses (0 representing off and 1 representing on) and real-time appliance consumption (in W) from appliance MQTT publishers. Another set of channels are created and allocated to store algorithm results. MATLAB®runs RAS for each building separately and writes the results for each building in a separate private channel using MATLAB ThingSpeak®toolbox. These results are frequently published by the BMC to the topics which are subscribed by the appliance subscribers.

There is another channel created to manage the DER capacity of the buildings to enable energy sharing among the buildings in the community. The rooftop solar panels installed on the buildings publish the available capacity to this channel periodically via the BMC similar to the other building appliances. Based on the solar capacities received from each building,

the algorithm calculates the spare capacity of that building and generates a command for the CSF to be charged. These calculations to schedule CSF are shown below:

$$SOC_{(t)} = SOC_{(t-1)} + \left(CSF_{disc.(t)}.\Delta t\right)/CSF_{power} \tag{3.10}$$

$CSF_{disc.}$ is the CSF charging/discharging power and CSF_{power} is the total installed capacity of the CSF.

$$SOC_{(t)} = SOC_{(t-1)} + \theta \times batt_{power} \tag{3.11}$$

$$SOC_{(t)} = SOC_{(t-1)} + \frac{batt_{power}}{\Theta} \tag{3.12}$$

θ is the charging efficiency and Θ is the discharging efficiency. If the solar generation level in the community is insufficient to supply appliances in the buildings, the bidding process described in Section III-C to receive energy from the CSF will be triggered by the BMCs in the buildings. Bids from the BMCs are collected in a separate channel of the cloud designed for the market operation and the market clearance occurs in the MATLAB®interface of the cloud. Customized MQTT topics are proposed in this work to represent the source of the messages (source appliances) and the type of the data within the message. The proposed multi-attribute hierarchical topic strings used to implement the designed algorithm are shown in Figure3.5. Topics have 3 elements: 1) Building name, 2) Appliance Name, 3) DataType Name. The generic format of the topics used in this work is: BuildingName/ApplianceName/DataType. Datatype could be either appliance consumption level, appliance status, or DER capacity.

3.4 Case Scenarios and Results

There are four case scenarios designed and tested in this chapter to showcase effectiveness of the proposed RAS under various conditions. The following cases highlight functionality of the proposed RAS in (a) decentralized mode with only local communication layer, (b) centralized mode with both local and global communication layers, (c) communication failure in local layer, and (d) communication failure in global layer. The time resolution for appliances' consumption data and the solar generation data is 15 minutes from 1pm to 8pm in all case

scenarios.

3.4.1 Decentralized RAS (local communications)

In decentralized mode, each building local controller (BMC) receives the appliances' consumption data and the solar generation of the building through the local communication layer and runs RAS for that building regardless of the available mutual resources in the community, i.e. energy stored in the CSF.

This scenario highlights the results for each individual building in DER-Maximization mode and priority based mode, both with decentralized communication fashion in the neighborhood, where there is no interaction with other buildings to exchange energy and information. The results of the decentralized RAS for the community under test is shown in Figure 3.6. Resources in decentralized fashion are grid and solar generation of each building.

Graphs in Figure 3.6 show resource allocation results for each building in the two operational modes at each time slot. The blue area represents the building power consumption supplied by the grid and the yellow area indicates the power consumption fed by the solar generation of the building at each time. It could be observed that in the Solar-max mode, the power consumption fed by solar generation in the building is higher compared to the Priority-based mode. As displayed in graphs, the solar generations around noon (until 15:00) are high enough to supply most of the appliances in each building and the grid demand in both operational modes is low. As time passes the solar generation decreases and the grid demand increases in the community until the solar generation does not suffice any appliance in the neighborhood. The main difference between the Solar-max mode and Priority-based mode is that the algorithm takes user-defined priorities for the appliances as additional inputs and ignores the maximum utilization of the solar generation. The aim of the latter mode is to supply the high-priority appliances continuously from the solar panels in the buildings to meet the comfort levels of the users. Summary of the results for the decentralized RAS is reported in Table 3.3 for each building at each mode.

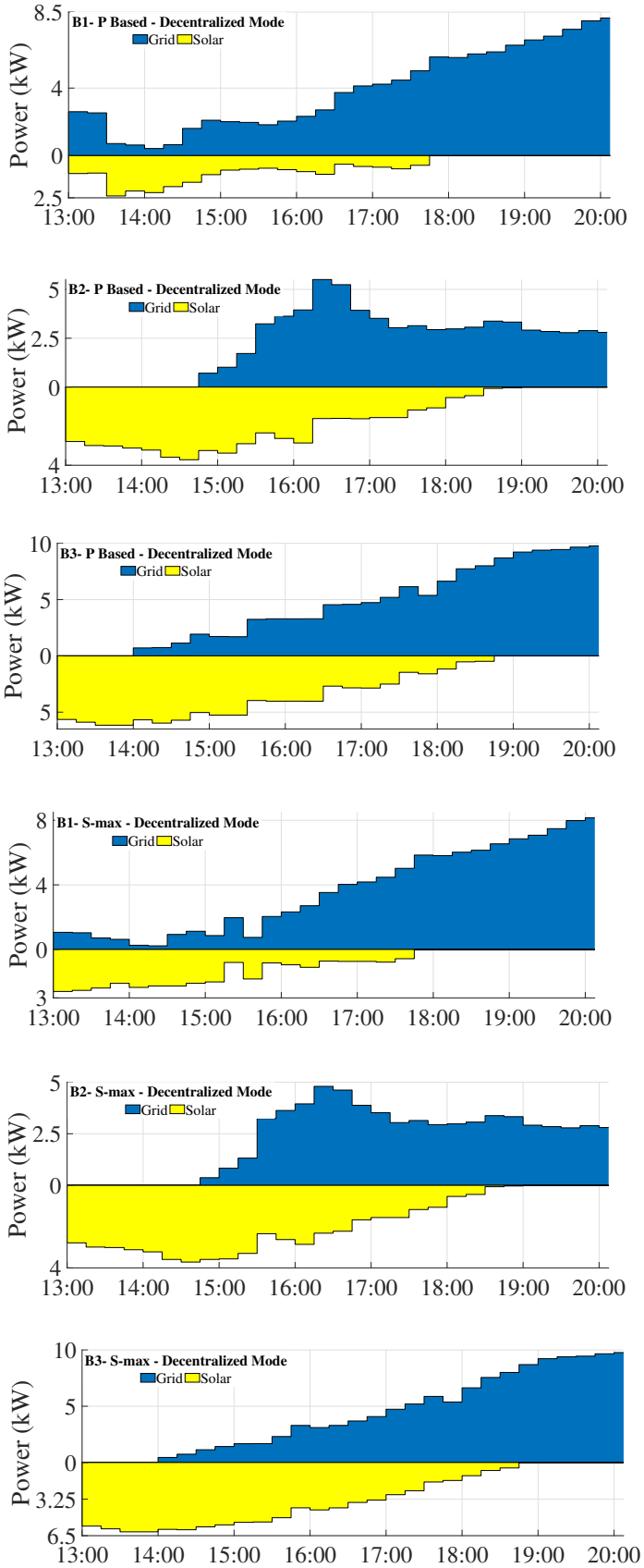

FIGURE 3.6: Decentralized RAS results for Solar-max and Priority-based modes.

TABLE 3.3: Summary of Results for Decentralized RAS

	Building	Grid (%)	Solar (%)
P_Based	B1	83.88	16.11
	B2	57.32	42.67
	B3	59.4	40.59
S_Max	B1	78.09	21.9
	B2	55.39	44.6
	B3	57.68	42.31

3.4.2 Centralized RAS (local and global communications)

Resources in centralized mode include both building self resources and mutual resources in the neighborhood. There is power flow from (a) grid, (b) solar generation of the buildings, and (c) the CSF in this case scenario. In centralized operation, local controller (BMC) at each building passes the published data from the local communication layer to the global communication layer and the data is processed via the cloud-based interface to MATLAB. The main difference between centralized and decentralized RAS is that in centralized mode, the algorithm considers the energy stored in the CSF and allocates that energy to the neighborhood appliances based on the collected bids. The CSF energy is not considered in the decentralized mode and there is no communication for exchanging energy with neighboring buildings through the CSF.

Once the data processing and algorithm results are accomplished, MATLAB scripts write the results in the configured channels to be received by the appliances MQTT subscribers and the CSF to be actuated. In order to exhibit successful implementation of the global communication layer, the graphical interface of the channel, dedicated to store the excess solar generation of each building captured directly from [3], is indicated in Figure 3.7. This figure shows the extra solar generation for each operational mode and each building at each time slot that is utilized to charge the CSF.

Results of the centralized RAS are illustrated in Figure 3.8 for each individual building. In addition to the blue and yellow areas, which represent power received from the grid and solar generations respectively, the green area indicates the power consumption of each building at each time supplied by the CSF. The results are provided for Solar-max and Priority-based mode with centralized communications including both local and global communications. In both operational modes, the stored energy in the CSF is returned back to the buildings

FIGURE 3.7: Graphical interface of the ThingSpeak channel representing excess solar generation of each building in each operational mode.

during the very-low-solar-generation period based on the collected bids in the local market. Bids are placed in the cloud according to the equations described in previous subsections of this chapter. The energy received from the CSF in each building is distributed between the appliances depending on the priorities and consumption levels of the appliances in Priority-based and Solar-max modes respectively.

Graphs in Figure 3.8 show that the solar generations around noon (13:00-15:00) suffice to supply most of the appliances in the neighborhood but around afternoon (16:00-18:00) the solar generations decrease. Consequently, less appliances are fed by the solar energy in the afternoon and bidding mechanism to trigger the CSF power flow starts when the solar generation in the building is below a pre-determined threshold (starting period between

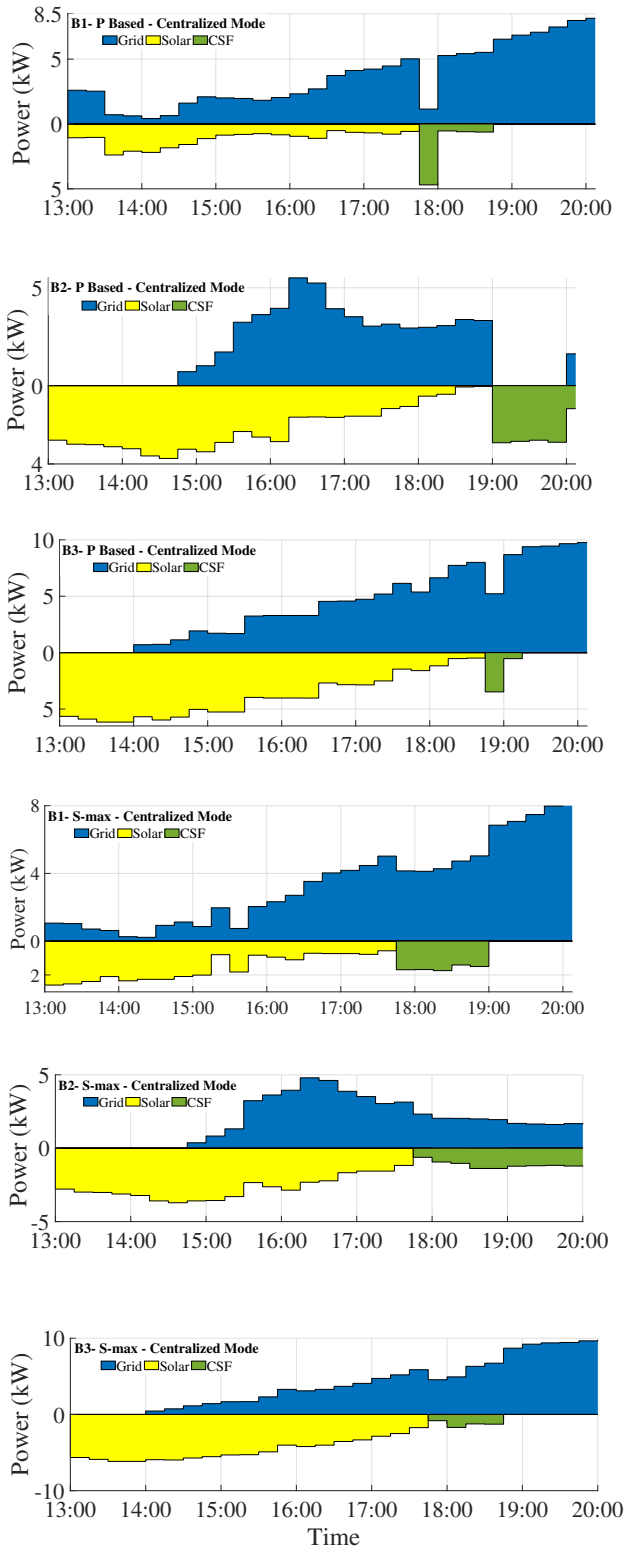

FIGURE 3.8: Centralized RAS results for Solar-max and Priority-based modes.

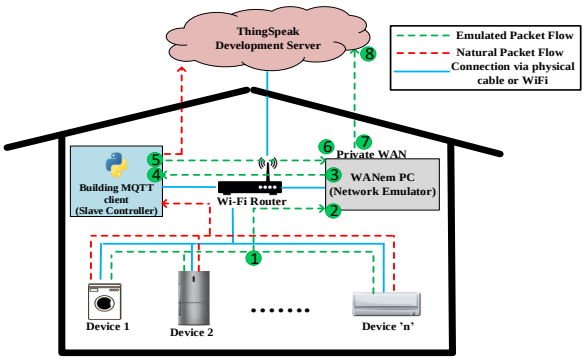

FIGURE 3.9: Normal packet flow vs emulated packet flow.

TABLE 3.4: Resource Allocation in Centralized Mode.

	Building	Grid (%)	Solar (%)	CSF (%)
P_Based	B1	79.12	16.11	4.76
	B2	46.77	42.67	10.54
	B3	57.57	40.59	1.83
S_Max	B1	72.15	21.9	5.93
	B2	45.91	44.6	9.47
	B3	55.39	42.31	2.29

17:00 and 19:00). In the Solar-max mode, buildings use the maximum of the building solar generation for the building itself and the amount which is shared with the community is minimum in this selfish mode. Consequently, the stored energy in the CSF in Priority-based mode is greater than the Solar-max mode. Due to this fact, green area in graphs related to the Priority-based mode is larger than the Solar-max mode for each building.

It must be noted that the energy flow indicated in the results is: (a) from the buildings to the CSF during the high-solar-generation period (until around 17:00) to store the excess generation of each building and (b) from the CSF to the buildings during the very-low-solar-generation period (generation below a pre-determined threshold). Case (a) and (b) does not occur simultaneously and consequently, the demand is supplied by a combination of the grid and the solar generation in case (a) and by a mixture of the grid and the CSF (global) in case (b). Hence, there is no simultaneous bidirectional energy flow between the buildings and the CSF. Summary of the results for the centralized RAS is reported in Table 3.4 for each building at each mode.

3.4.3 Communication failure in local layer

This scenario aims to exhibit resilience of the proposed RAS against possible local communication failures. To investigate the system performance with high-latency in the network, a virtual Wide Area Network Emulator (WANem) has been set up in the platform to emulate characteristics of a real network (e.g. packet loss and packet delay) [3], packets would reach to destination through the routing switch demonstrated in Figure 3.9 in red dotted lines.

WANem affects the packet flow in two separate layers as depicted in Figure 3.9 in green dotted lines: one is the communication inside each building between the appliances and the BMC (local). This affected route could be followed in Figure 3.9 by numbers from 1 to 4. The second affected route is the data exchange between the BMCs and the cloud (global). This could be followed by numbers from 5 to 8 in Figure 3.9.

Network emulation is the act of adding an extra device to a testing network in order to alter the packet flow path in the network in such a way that network characteristics such as delay, jitter, packet loss, and etc. could be set manually by WANem) to mimic the behavior of a real network [3]. A network analyzer software called Wireshark [3] is adopted to capture traffic in the network under test. Delay of 10000 ms, which represents extremely high latency or link failure [3], is emulated for the MQTT communication between Appliance 1 from Building 2 at Solar-max mode as a case study (could be any appliance in any building at any operational mode). Appliance static IP address is set to 10.37.19.25 and IP address of the online MQTT broker ("iot.eclipse.org") is 198.41.30.241. The hardware test setup for the implemented platform is indicated in Figure 3.10. The delayed data packet from Appliance 1 in Building 2 causes re-transmission in the local network as captured by Wireshark and indicated in Figure 3.12 (a).

The reason for re-transmission in the local network is to ensure that the lost packets would sustain reaching the destination that as MQTT messaging is on top of the TCP protocol. Re-transmission and the initial Round Trip Time (iRTT), after WANem is activated, are highlighted in Figure 11 (a) using Wireshark MQTT filtering option. By default, the appliances with communication failure would be connected to the grid during the faulty period but will be considered for neighborhood resource allocation once the failure is removed.

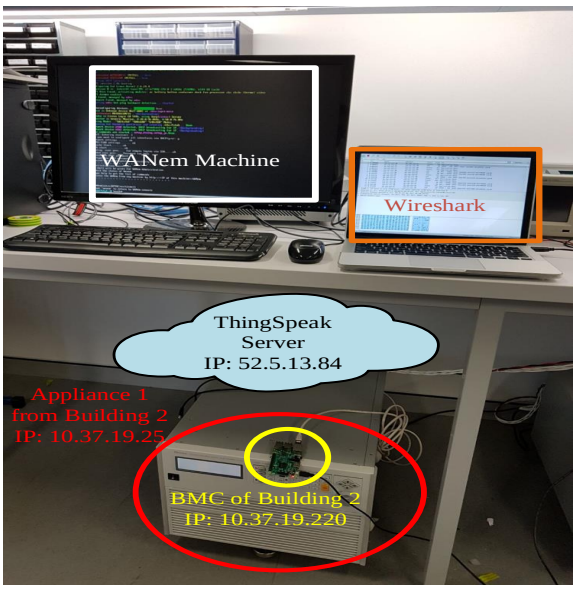

FIGURE 3.10: Hardware setup for the platform indicated in Figure 3.9.

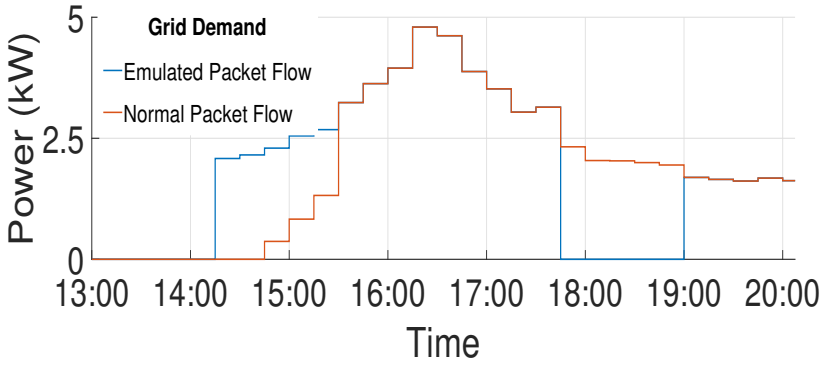

FIGURE 3.11: Proposed RAS under local communication failure.

Delay on MQTT data exchange inside Building 2 (local communication failure) is activated by running WANem during 14:15 to 15:30. In this period, appliance 1 (faulty appliance) is supplied by the grid and consequently the grid demand becomes higher for this building compared to the normal case with no communication failure as shown in Figure 3.11. The delay is removed after 15:30 and the extra solar generation, which was supposed to supply appliance 1 but is stored in the CSF due to the local communication failure, is used during the bidding mechanism to feed more appliances. Hence, the grid consumption during the bidding period in this case is less compared to the normal scenario with no communication failure.

3.4.4 Communication failure in global layer

This scenario investigates the RAS performance under global communication failure. WANem is activated on Route 5-6-7-8 in Figure 3.9 to realize packet delay in global communication layer. Delay of 1000ms [142] for extreme latency or or link failure between the BMC of Building 2 with a static IP address of 10.37.19.220 and the online ThingSpeak server with the IP address of 52.5.13.84 is emulated at Solar-max operational mode as case study (similar process could be emulated on any building at any operational mode).

Re-transmission and duplicate acknowledgement (Dup ACK) occur after the BMC sends an HTTP POST request to ThingSpeak server. This behavior proves the out of order reception of the data packets or a gap in the received sequence numbers or in other words, packet loss between the BMC and the cloud. This behavior is depicted in Figure 3.12 (b), wherein iRTT, Re-transmission, and Dup ACK are highlighted. The BMC is designed in such a way that if the expected messages (either data from the appliance MQTT publishers or results from the cloud) are not received within a pre-determined time range, it makes the decision for the faulty appliance or building as a local controller. In other words, in case of global communication failure, the centralized RAS switches to decentralized RAS and do not receive energy from the CSF during the faulty period.

In case of cloud communication failure (global failure), the faulty building would be isolated from the community and would not attend in the local market to receive energy from the CSF until the failure is removed. Once the cloud communication for the faulty building is back to the normal status, the BMC of that building participates in the bidding process and the building receives energy from the CSF. This behavior is illustrated in Figure 3.13.

Delay on cloud communication (global) is activated during 18:15 to 19:45. Hence, in this faulty period the building switches from centralized to decentralized operational mode and there is no energy flow from the CSF. Consequently, the grid demand for this building during the faulty period is higher compared to the normal case with the CSF supply. This could be followed by the blue curve in Figure 3.13. After 19:45, the WANem is stopped and the packet flow is back to normal. Therefore, after 19:45 this building switches back to centralized operation and participates in the local market to receive energy from the CSF.

[a]

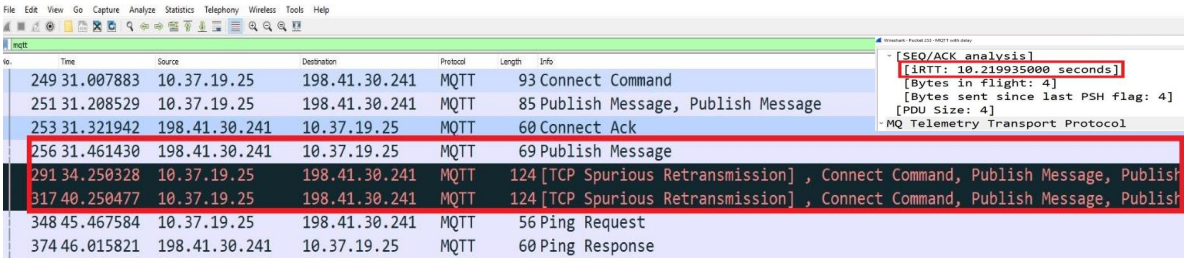

[b]

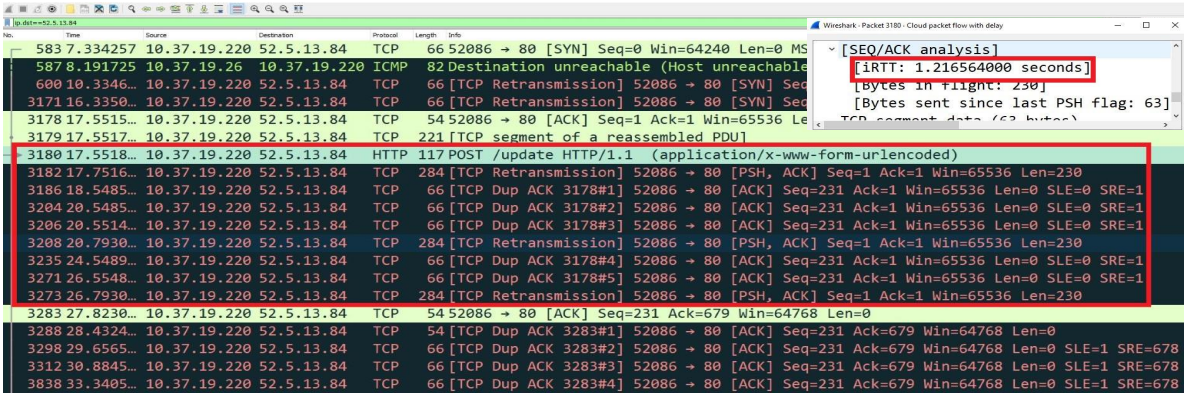

FIGURE 3.12: Network latency after using WANem captured by Wireshark for: a) Route 1-2-3-4 , b) Route 5-6-7-8 in Figure 3.9.

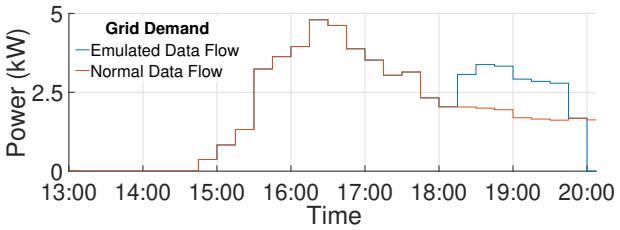

FIGURE 3.13: Proposed RAS under global communication failure.

The explained behavior is visible in Figure 3.13.

3.5 Chapter Summary

This section aims to compare the presented case scenarios by statistics for the entire neighborhood. Table 3.5 reports the resource allocation results for centralized (C) and decentralized (DC) operations at Solar-max and Priority-based modes. It must be noted that the proposed RAS functions similarly in centralized and decentralized operations to allocate solar energy in the neighborhood during the high-solar-generation period. The difference between centralized and decentralized operations becomes visible during the very-low-solar-generation

TABLE 3.5: Comparison of Neighborhood-level Results for RAS

Case Scenario	Operational Mode	Grid (%)	Solar (%)	CSF (%)
1	DC-P_based	65.87	34.13	N/A
2	DC-S_Max	62.93	37.07	N/A
3	C-P_based	61.02	34.12	4.86
4	C-S_Max	57.78	37.06	5.14

period. Hence, the amount of the solar energy allocated to the neighborhood appliances in centralized and decentralized operations is the same and equal to 34.12 % and 37.06 % of the total neighborhood power consumption for Priority-based and Solar-max modes respectively. Table 3.5 demonstrates higher utilization of the solar power by neighborhood appliances in Solar-max mode (37.06 % of the total load in the neighborhood) compared to the Priority-based one (34.12% of the total load). Another statement to be derived from the table is that the grid demand reduction of the entire neighborhood in centralized mode, with a relatively more complex architecture utilizing both local and global communications, is higher than the decentralized mode.

Based on the presented scenarios, there are cons and pros associated with each operational mode which could be selected depending on the user's desired comfort level. When Solar-max mode is selected, more self-resources are utilized for the buildings and less energy could be received from the mutual-resource (CSF) during the bidding time, as buildings bid for the CSF in the local market in proportion to the energy they shared with the community. According to the results, Scenario 4 with centralized Solar-max operational mode has achieved the highest grid demand reduction while Scenario 1 with decentralized Priority-based mode has the lowest grid demand reduction but meets the users comfort levels.

After covering the appliance-level load allocation algorithms in smart neighborhoods in this chapter, the next chapter will focus on load restoration frameworks in power networks to improve structural resilience. The following chapter will present a multi-objective decision making platform to optimally locate tie switches in power distribution networks to maximize resilience.

Chapter 4

Load Restoration Planning to Improve Resilience in Power Distribution Networks: A Multi-Objective Decision Support

This chapter is related to the second research objective introduced in Section 1.3 of Chapter 1 and focuses on planning for resilience in smart grids.

As the literature review in Chapter 2 suggested, power utilities require a comprehensive multi-objective decision making platform for resilience-oriented optimizations in the network. A major part of this section is to propose such a framework which could be utilized to solve optimization problems in order to maximize preparedness against extreme events in the network. The proposed framework in this chapter is used to optimally locate tie switches in the network in a way that resilience is maximized in the grid.

4.1 Components for Resilience-Oriented Analysis

The proposed multi-objective resilience-oriented framework is formed by adopting multiple resilience metrics and a state estimation technique. The components are introduced as follows:

State Estimation (SE) is a mathematical tool that is typically employed to evaluate the state of the system using real measurements, received from field devices, and are interpreted by measurement errors [143]. In other words, the SE algorithm estimates the operating

states and provides the confidence level of each estimate considering the uncertainty of the measurements, thus enabling the acquisition of accurate and real-time knowledge of the network operating condition [143]. SE is used for decades in power transmission systems, and is getting more attention to be utilized for control and management of power distribution grids as well [143]. The most common SE approach, which is based on the principle concepts of the WLS method, is adopted in this paper with measurements modeled as follows:

$$z = h(X) + e \tag{4.1}$$

where z is the measurement vector received from the field devices, X is the state variables vector, h is the non-linear function that maps the state variables to measurements, and e is the vector of the measurement errors. For WLS method, the mean of the measurement errors is assumed to be 0. Furthermore, the measurements are assumed to be independent, and hence, the covariance matrix of the measurement vector $\sum_z = diag(\sigma_z^2)$ is a diagonal matrix with σ_z as the standard deviation of the measurements. WLS-based SE aims to minimize the following objective function:

$$J(X) = [z - h(X)]^T W[z - h(X)] \tag{4.2}$$

where $W = \sum_z^{-1}$ prioritizes the measurements with higher accuracy in estimating the network operating states. To solve this optimization problem, the Gauss-Newton method is applied resulting in the following equation:

$$G.\Delta X = H^T W[z - h(X)] \tag{4.3}$$

where H is the Jakobian of $h(X)$, $G - H^T WH$ is the Gain matrix, and ΔX is the updated state vector. The state vector is updated after each iteration as follows:

$$X_{k+1} = X_k + \Delta X_k \tag{4.4}$$

The optimization process stops when the condition $max(|\Delta X|) < \epsilon$ is satisfied for a user-defined threshold. The input measurements to the SE algorithm in AC distribution grids are bus voltage magnitudes, branch current magnitudes, branch active and reactive power flows, nodal active and reactive power injections, and the pseudo measurements captured through historical data. The most common choice of the state variables are the voltage magnitude and voltage phase angles with the following state vector:

$$X_{AC} = [\theta_{AC}, V_{AC}] = [\theta_2, ..., \theta_{N_{AC}}, V_2, ..., V_{N_{AC}}] \tag{4.5}$$

where θ_i and V_i are the voltage phase angle and magnitude at node i, respectively. N_{AC} is the total number of nodes in the network. The proposed formulation and set of state variables are based on the polar voltages and the SE adopted here is generic enough to be applied in both transmission and distribution systems with any choice of the state vectors.

4.1.1 Proposed Resilience Measures and Metrics

An overview of the power system behavior in the face of a HILP incident is conceptually demonstrated in Figure 4.1. $P(t)$ is the time-variant system behavior function. At t_{NO}, an HILP event occurs and the system goes to a performance degradation phase until t_{PD}. From t_{PD} to t_{OU} is represented as the system downtime with minimum number of customers served. At t_{OU}, the system response and recovery starts and it takes multiple steps to realize a full restoration, where the system performance is migrated back to its normal operating condition. First partial recovery step leads to a temporary steady-state performance level indicated in Figure 4.1 from t_{ER_1} to t_{PR_1} and the last step ends in the pre-event system performance level corresponding to the time instant t_{FR}.

As described earlier, there are three main categories of metrics that are commonly used for resilience assessments in power distribution systems: (i) time-based metrics, (ii) energy-based metrics, and (iii) economy-based metrics. Since our focus here is on the pre-event planning for structural resilience (i.e., grid hardening), time-based measures (reflecting the rapidity of the system restoration) are not taken into account. This paper focuses on restoration

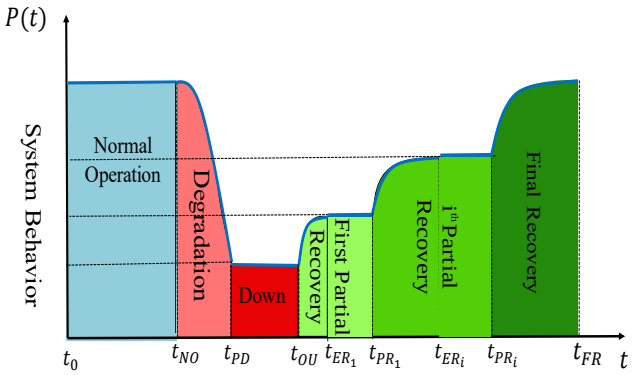

FIGURE 4.1: Overview of the system behavior subject to an HILP event.

of a faulty radial feeder by connecting a Tie switch between the best pair of nodes. Figure 2 demonstrates a generic view of a distribution system with a normally-open Tie switch in the network. The proposed resilience metrics are defined over a single-node and summed over the entire feeder to characterize the resilience objective functions. The suggested metrics are introduced as follows:

1) Nodal Restoration Criticality (NRC): which demonstrates the level of active power consumption and the type of the load (critical loads such as industry, hospitals, fire stations, etc.) served at each load point. This metric represents the proportion of the critical loads covered by the restoration process to the total loads restored. This index could be used to prioritize the nodes during the restoration process and is formulated for the node N in the network as indicated in (4.6).

$$NRC^N = \left(P^{inj,N} = \left| \sum_{j \in \Omega_G^N} P_j^{Gen,N} - \sum_{i \in \Omega_L^N} P_i^{L,N} \right| \right) \times \frac{Pr_N}{P^{Tot}} \tag{4.6}$$

where $P^{inj,N}$ is the injected power at each node. $P_i^{L,N}$ and $P_j^{Gen,N}$ are the level of consumed and generated active power at node N, respectively; Ω_L^N and Ω_G^N are the set of loads and generating units connected to node N, respectively; Pr_N is a utility-defined number assigned to node N depending on the type of the connected load, and P^{Tot} is the total amount of load restored by a restoration plan. Higher values of NRC reflect a higher degree of criticality covered by a given restoration plan and is more desired.

2) Nodal Robustness (NRS): is defined by the difference between the nodal voltage profile before and after the restoration plan, the number of connected generating units ($|\Omega_G^N|$) and the number of incoming branches to node N ($|\Omega_B^N|$). The higher the difference in the nodal voltage profile before and after a restoration plan and the lower k and G are, the less robust is the network to HILP incidents. Hence, NRS^N for node N is formulated as in (4.7).

$$NRS^N = \left(|V_{before}^{N^{th}} - V_{after}^{N^{th}}|\right) \times \frac{1}{|\Omega_B^N|} \times \frac{1}{|\Omega_G^N|} \tag{4.7}$$

3) Nodal Restorability (NRA): indicates the amount of load which would be restored by energizing a single node in the healthy section of a faulty feeder. This restored load for the N^{th} node in a radial feeder is equal to the summation over all loads served at node N to the furthest downstream node in the feeder. Additionally, the number of outgoing branches from the node ($|\Omega_U^N|$) is a critical factor when evaluating the NRA. The NRA^N for the Tie switch connected to node N is formulated in (4.8).

$$NRA^N = \Big(\sum_{i \in \Omega_L^N} P_i^{L,N} + \sum_{j \in \Omega_L^{N+1}} P_j^{L,N+1} + \ldots$$

$$\ldots + \sum_{q \in \Omega_L^{EOF}} P_q^{L,EOF} \Big) \times |\Omega_U^N| \tag{4.8}$$

where $P_q^{L,EOF}$ is the load served at the last node of the feeder.

4) Nodal Restoration Losses (NRL): aims to characterize the power losses related to the restoration path created by closing the Tie switch during the restoration process. NRL^N indicates the restoration losses in a radial feeder, where the Tie switch is connected to node N, as shown in (4.9)

$$NRL^N = P_N^{Loss} + P_{N+1}^{Loss} + \ldots + P_{EOF}^{Loss} + P_{Tie}^{Loss} \tag{4.9}$$

where P_N^{Loss} is the power losses at Segment N (between nodes N and $N+1$, P_{EOF}^{Loss} is the power losses in the last segment of the feeder, and P_{Tie}^{Loss} is the power losses corresponding

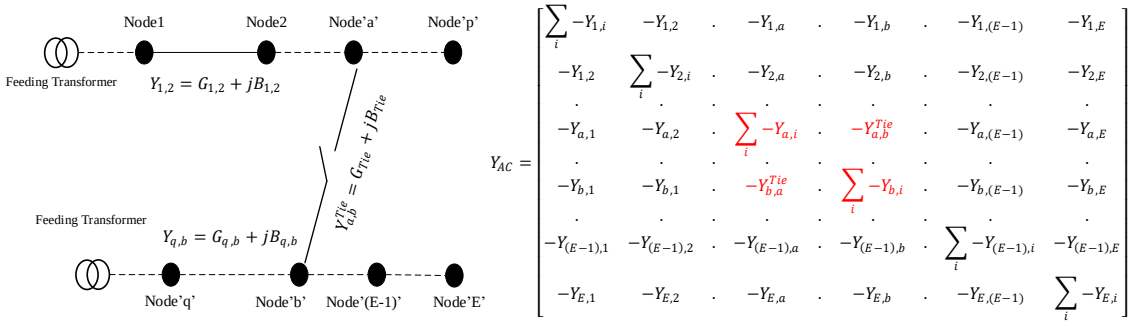

FIGURE 4.2: Generic view of a radial distribution network with Tie switches considered for formation of the Y_{AC} matrix.

to the path created by closing the Tie switch.

4.1.2 Objective Functions

The above metrics of resilience are here used to form the objective functions. The optimization engine embodies a mixed integer linear programming (MILP) formulation that aims to find the optimal location of the Tie switch in the network, primarily planned to enhance the network resilience against HILP disasters.

1) System-Wide Robustness: The first objective function utilizes the NRS^N metric to minimize the system-level performance degradation when subjected to an HILP event. NRS^N is defined over a single node in (4.7) and needs to be summed over the entire nodes in the network for a system-wide analysis. The objective function is formulated below subject to a set of system operational constraints:

$$\min \left(NRS^{Tot} = \sum_{N \in E} \alpha_N NRS^N \right) \qquad \alpha_N \in \{0, 1\} \tag{4.10}$$

$$NRS^N_{min} < \alpha_N . NRS^N \leq NRS^N_{max} \qquad \forall N \in \{E\} \tag{4.11}$$

$$P^{Gen,N}_{min} \leq \alpha_N . P^{Gen,N} \leq P^{Gen,N}_{max} \qquad \forall N \in \{E\} \tag{4.12}$$

$$P_{min}^{Flow,k} \leq \alpha_N . P^{Flow,k} \leq P_{max}^{Flow,k} \qquad \forall k \in \{\Omega_T\} \tag{4.13}$$

$$\sum_{q \in \Omega_U^N} P_q^{Flow,k} + \sum_{i \in \Omega_L^N} P_i^{L,N} = \sum_{j \in \Omega_G^N} P_j^{Gen,N} \tag{4.14}$$

$$\alpha_N \in \{0,1\} \qquad \forall N \in \{E\} \qquad \forall k \in \{\Omega_T\} \tag{4.15}$$

where $P^{Flow,k}$ is the power flow in branch k, Ω_T is the set of network branches, and α_N is a binary variable which indicates whether a node is involved in the restoration process. Constraint (4.11) ensures that the voltage difference in all nodes remains within a certain limit following the restoration process. The output power of generating units are limited to their physical capacities in (4.12). Constraint (4.13) enforces that the electricity flow in distribution lines, involved in the service restoration, are bounded by their capacities. The power balance constraint at each node is set in (4.14).

2) System-wide Restoreability: This objective function aims to maximize the amount of the restored load via connection of a Tie switch in a restoration plan and is built on the suggested NRA^N metric. As indicated in (4.8), the NRA^N represents the summation of all loads restored in the feeder by energizing the single-node N. The objective function is formulated in (4.16) subject to several operational constraints:

$$\max \left(NRA^{Tot} = \sum_{N \in E} \sum_{i \in \Omega_L^N} \beta_N P_i^{L,N} \right) \quad \beta_N \in \{0,1\} \tag{4.16}$$

$$NRA_{min}^N \leq \alpha_N . NRA^N \leq NRA_{max}^N \qquad \forall N \in \{E\} \tag{4.17}$$

$$P_{min}^{Gen,N} \leq \alpha_N . P^{Gen,N} \leq P_{max}^{Gen,N} \qquad \forall N \in \{E\} \tag{4.18}$$

$$P_{min}^{Flow,k} \leq \alpha_N . P^{Flow,k} \leq P_{max}^{Flow,k} \qquad \forall k \in \{\Omega_T\} \tag{4.19}$$

$$\beta_N \in \{0,1\} \qquad \forall N \in \{E\} \qquad \forall k \in \{\Omega_T\} \tag{4.20}$$

Constraint (4.17) ensures that the restored loads do not exceed a threshold, i.e., to avoid a possible overload in a neighboring feeder, and is set to be higher than a minimum expected value. NRA_{max}^{N} is determined by the capacity of a feeding transformer in the neighbor feeder which will export power to the faulty feeder when a Tie switch is connected. Constraints (4.18) to (4.20) are employed to avoid exceeding capacities of distribution lines and generation units. β_N is a binary variable indicating whether a node is involved in the restoration process.

3) Restoration of Critical Load Points: A higher load outage recovery through a restoration plan does not necessarily result in recovery of highly critical load points. This objective function maximizes the load criticality picked by a restoration plan and is formulated in (4.21):

$$\max \left(NRC^{Tot} = \sum_{N \in E} \gamma_N NRC^N \right) \qquad \gamma_N \in \{0,1\} \tag{4.21}$$

$$NRC_{min}^{N} \leq \gamma_N . NRC^N \leq NRC_{max}^{N} \qquad \forall N \in \{E\} \tag{4.22}$$

γ_N is a binary variable to select the nodes involved in the restoration plans. Constraint (4.22) summarizes various operational constraints and ensures a minimum recovery of critical loads via a restoration plan. Furthermore, the criticality picked by a restoration plan must not exceed a threshold, which otherwise violates the physical capacity of lines and generation units.

4) Restoration Losses: This objective function is characterized to minimize the active power losses in the network resulted by adoption of a restoration plan and connection of a Tie switch. The NRL^N, presented in Section 4.1.1, represents the network total power losses in the restoration path.

$$\min \left(NRL^{Tot} = \sum_{i \in \Omega_T} \zeta_i P_i^{Loss} \right) \qquad \zeta_N \in \{0,1\} \tag{4.23}$$

$$NRL_{min}^{N} \leq \zeta_N . NRL^{N} \leq NRL_{max}^{N} \qquad \forall N \in \{E\} \tag{4.24}$$

ζ_i is a binary variable to select distribution lines which are used during the service restoration process. Operational constraints (4.17) to (4.19) are aggregated in (4.24), which limit the amount of network losses in a restoration path. The thermal capacitance of the distribution lines and the physical capacity of generation units must not be violated via a restoration plan.

4.2 Decision-making Platform for Resilience-Oriented Placement of Tie Switches

This section describes the modular resilience-oriented framework developed to solve the optimization problem presented in Section 4.1.2.

The developed framework utilizes the WLS-based SE mechanism and tries to iteratively maximize the proposed R index of resilience. The key element in the proposed optimization platform is the dynamic admittance matrix (Y_{AC}), which determines the distribution network topology in each placement scenario of the Tie switch. The overall formation of Y_{AC} for a generic radial network with E number of nodes and a Tie switch connected between nodes a and b is illustrated in Figure 4.2.

The Y_{AC} shown in this figure is generic and the same approach could be applied to construct the Y_{AC} in radial networks with several Tie switches connecting multiple pairs of nodes. One needs to note that $Y_{i,j} = Y_{j,i} = G_{i,j} + j\ B_{i,j}$; where $G_{i,j}$ and $B_{i,j}$ are the conductance and the susceptance of the lines between nodes i and j, respectively. $Y_{a,b}^{Tie}$ is the admittance of of the tie-line that is set online when closing the normally-open Tie switch connecting nodes

FIGURE 4.3: The overall architecture of the proposed multi-objective decision platform for Tie switch placement in power distribution networks.

a and b in the network and is equal to $Y^{Tie}_{a,b} = Y^{Tie}_{b,a} = G_{Tie} + j\ B_{Tie}$; where G_{Tie} and B_{Tie} are the conductance and the susceptance of the tie-line, respectively. In a generic format, a Tie switch is connected between nodes a and b, which affects the elements on the corresponding rows and columns of the (Y_{AC}) matrix by $Y^{Tie}_{a,b}$ (admittance of the tie-line). The affected elements are highlighted in red in Figure 4.2. The size and the elements of the admittance matrix can change depending on the grid topology following a reconfiguration plan.

Figure 4.3 demonstrates the proposed multi-objective decision making framework for resilience-oriented placement of the Tie switches in radial power distribution networks. The proposed framework consists of four main stages as follows: (i) Scenario Generation, (ii) WLS-Based SE, (iii) Index Calculator, and (iv) Multi-Objective Optimization and Decision Making.

Stage 2: the WLS-based SE runs at this stage for each generated Y_{AC} at Stage 1 and

returns the estimated system operating profile in each scenario.

Stage 3: resilience metrics introduced earlier in (4.6) to (4.9) are evaluated system-wide. Stage 3 imports the estimated system profiles for each Tie switch location candidate and estimates the NRC, NRS, NRA, and NRL across the network. Such results are then used in a multi-objective decision platform to find the optimal solution.

Stage 4: among various multi-objective decision making techniques, Non-Dominated Sorting Genetic Algorithm II (NSGA-II), with demonstrated efficacy and usability [144], is employed. The main advantages of using NGSA-II for multi-objective optimization in this stage is as follows [144]: it uses non-dominated sorting techniques to provide the solution as close to the pareto-optimal solution as possible. In addition, it uses crowding distance techniques to provide diversity in solution. Finally, it uses elitist techniques to preserve the best solution of current population in the next generation.

Utilizing NSGA-II results in a set of non-dominant solutions (Pareto optimal sets) for all objective functions. The process starts with producing the first parent population followed by ranking them based on the concept of non-dominance. Classic operators (crossover and mutation) generate the children population to be used in combination with parent population for the next generation of Pareto solutions until a termination criterion is satisfied [144]. Fuzzy Satisfying Method (FSM) is next employed to chose between all optimal Pareto solutions (optimal Tie switch locations) [145, 146] considering a trade-off between all objectives introduced in Section 4.1.2.

The FSM approach is a mathematical expression tool that represents human judgments [146]. This approach is pursued as different user preferences and the decision maker (e.g., the utility) judgments may otherwise render the decision framework imprecise. User-defined targets for each objective (called satisfaction levels) are the inputs to the multi-objective decision making optimization module, the step-by-step procedure of which is introduced as follows:

1. Membership Function (MSF): which includes a set of attributes to each objective function indicating the significance level assigned to a given objective by a decision maker. MSF values are selected between zero and one, zero representing the lowest priority and one

the highest. For instance, in a minimization problem, the MSF equals to zero at the summit point of the objective and is equal to one at its minimum. The linear MSF utilized in here is expressed in (4.25).

2. Decision Maker: The final decision is made considering the user-defined satisfaction levels for each MSF as indicated in (26). This optimization minimizes the τ-norm deviations from the designated satisfaction levels considering the MSF of all solutions.

$$\min_{X \in SolutionSet} \Big(\sum_{i \in R} \mid \mu_{d_i} - \mu_{f_i}(X) \mid^{\tau} \Big) \quad \tau \in \{1, \infty\} \tag{4.25}$$

4.3 Case Study and Evaluation Results

In order to showcase the efficacy of the proposed multi-objective decision making framework, the IEEE 33-bus test system with network data (distribution line impedances, load profiles, and generation details) taken from [147] is selected as the test case. All the proposed metrics are evaluated in per-unit values (i.e., unit-less). A major HILP event is simulated as graphically illustrated in Figure 4.4. We aim to study such extreme scenarios to demonstrate how the system resilience can be improved by grid hardening planning solutions for optimal allocation of Tie switches across the network and with various customizable risk appetites.

4.3.1 Tie Switch Placement Candidates and Discussions

This sub-section describes details of the designed HILP event and the possible Tie switch placement candidates for effective restoration.

Figure 4.4 displays different zones in the network when facing a simulated HILP event. Nodes 7 to 10 highlighted in red (Zone 2) are affected by the HILP event and nodes 11 to 18 colored in blue (Zone 3) are the restorable section of the network. Zone 3 could be re-energized through a created path by closing a Tie switch to be installed in one of the candidate locations (green-dotted lines). While the presented decision making framework is generic enough to be applied to any HILP scenario with different spatiotemporal characteristics and

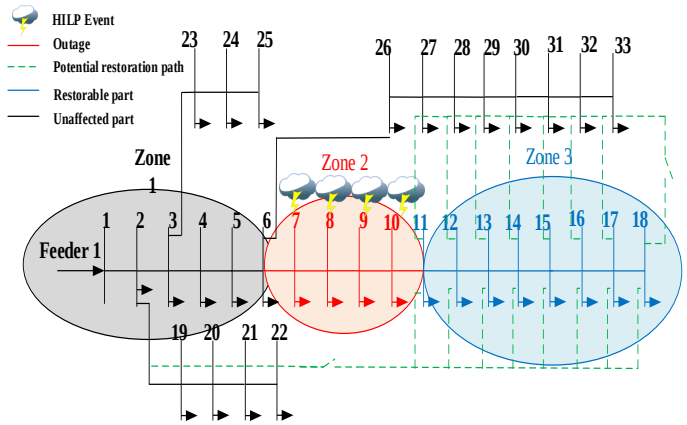

FIGURE 4.4: Single-feeder network affected by an HILP event.

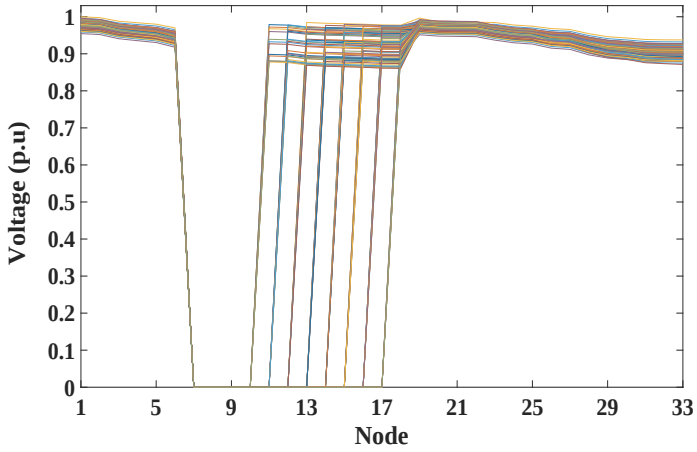

FIGURE 4.5: Voltage profile in the IEEE 33-bus system for 96 Tie switch locations during the restoration process.

severity levels, it finds 96 candidate locations for a Tie-switch placement. The gray zone in Figure 4.4 represents the unaffected section of the feeder, which would be used as the main restoration resource. The WLS-based SE runs for each Tie switch location to achieve the corresponding system profile following the implementation.

Figure 4.5 displays the voltage profile in the test system subject to black nodes (Node 7 to 10) for all possible restoration plans (i.e., the 96 Tie switch placements). It could be observed from Figure 4.5 that Nodes 7 to 10 remain black due to the HILP outage scenario while Nodes 11 to 18 are restored within various Tie switch connection plans. Note that the restoration process is here selective, in that either the entire healthy part of the faulty feeder or a portion of it are considered for restoration through the suggested reconfiguration plans.

Each resilience metric is evaluated at the nodal level for each Tie switch placement

TABLE 4.1: Statistical Comparison of Resilience Metrics

Performance Index	NRC	NRS	NRA	NRL
minimum	15.04	4.11	0.19	3.06
maximum	20.85	11.14	1.36	6.57
mean	17.69	7.71	0.42	5.28
standard deviation	1.91	2.12	0.21	0.82

scenario and summed over the entire feeder for system-wide performance analysis. The results in Figure 4.6(a) to 4.6(d) demonstrate the criticality covered by the restoration plans, system-wide robustness, restorability, and restoration losses, for each Tie switch placement candidate, respectively.

The statistical comparison of the above indices are tabulated in Table 4.1. It could be observed from Figure 4.6(a) that the NRC varies from 15.04 to 20.85 with some candidates providing acceptable demand criticality covered by the restoration process. Figures 4.6(b) and 4.6(c) illustrate the system robustness and restorability with multiple candidates capable of providing a reasonable solution for maximum amount of loads to be restored and minimum difference with the pre-event system profile. Figure 4.6(d) introduces the candidates with relatively low restoration losses with system-wide NRL ranging between 3-4 per unit.

4.3.2 FSM Application in Multi-Objective Decision Making

The proposed Objective functions are jointly taken into account in order to achieve a final optimal solution. As there is no unique solution for a multi-objective problem, the FSM fulfills an objective judgment within a set of optimal Pareto solutions to achieve a trade-off and differentiate the Tie switch placement candidates in the optimal Pareto front [148, 149]. The satisfaction levels (desired reference values) for each objective function should be determined by the decision maker (e.g., electric utility). The final results on the optimal allocation of the Tie switches are achieved following the FSM process with various satisfaction levels (see Table 4.2). From the numerical results presented in Table 4.2, it could be inferred that the final optimal solution relies heavily on the user-defined satisfaction levels (μ_{d1} to μ_{d4}) selected for each objective function.

There are two objective functions to be minimized: system-wide performance degradation

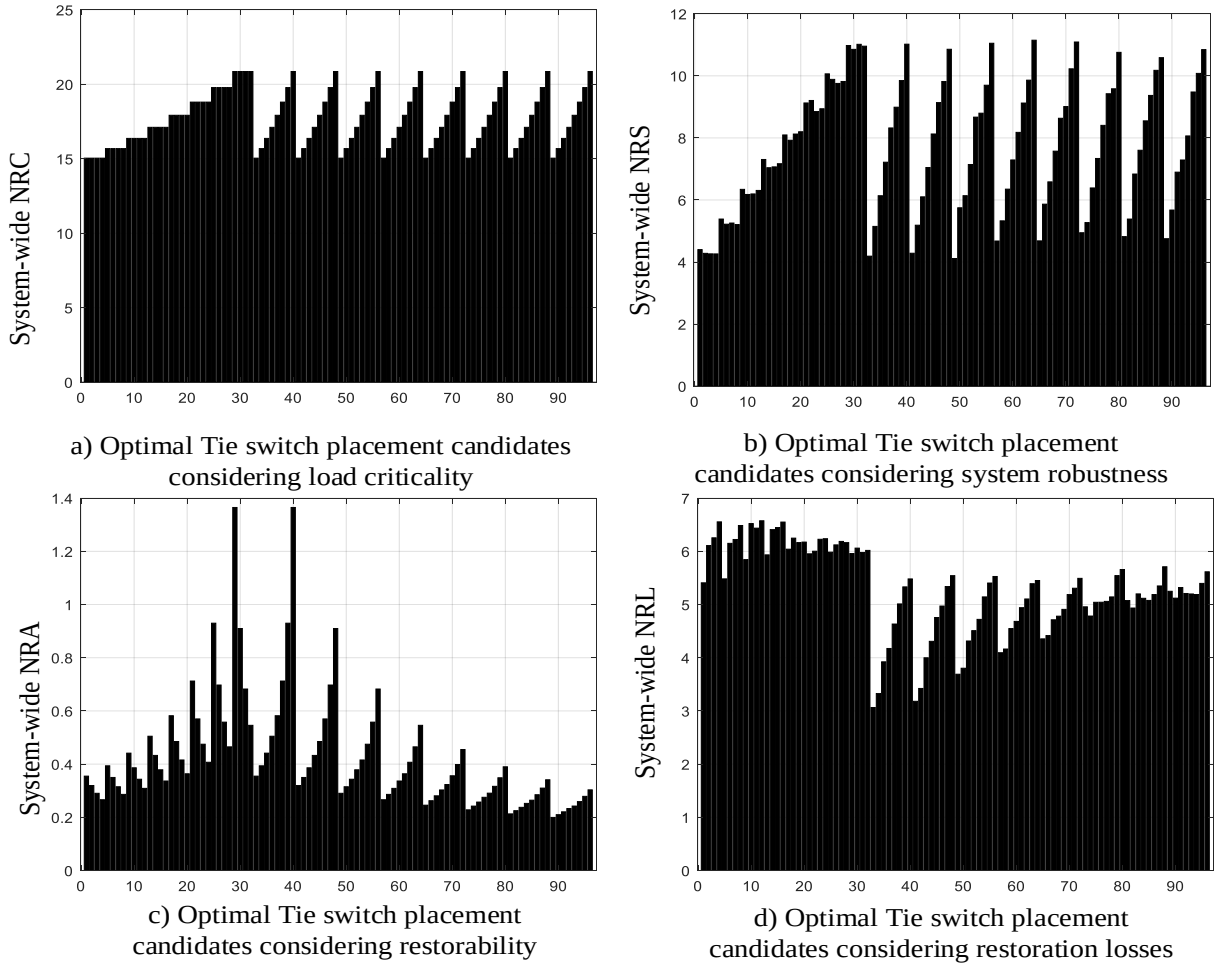

FIGURE 4.6: System-wide performance evaluation of the IEEE 33-bus test system for Tie switch placement candidates considering: (a) load criticality, (b) robustness, (c) restorability, and (d) restoration losses.

TABLE 4.2: Various Satisfaction Levels And the Final Resilience-Oriented Allocation of the Tie Switch

Satisfaction Levels				Objective Function Value				Final Tie Switch
μ_{d1}	μ_{d2}	μ_{d3}	μ_{d4}	f1	f2	f3	f4	Location
0.8	0.8	1	0.6	7.218	4.174	0.505	17.112	26-14
0.8	0.8	0.8	0.8	8.991	5.012	0.712	18.805	26-16
1	1	0.6	0.6	6.137	3.923	0.441	16.369	26-13
0.6	0.6	0.6	0.4	8.322	4.633	0.582	17.921	26-15

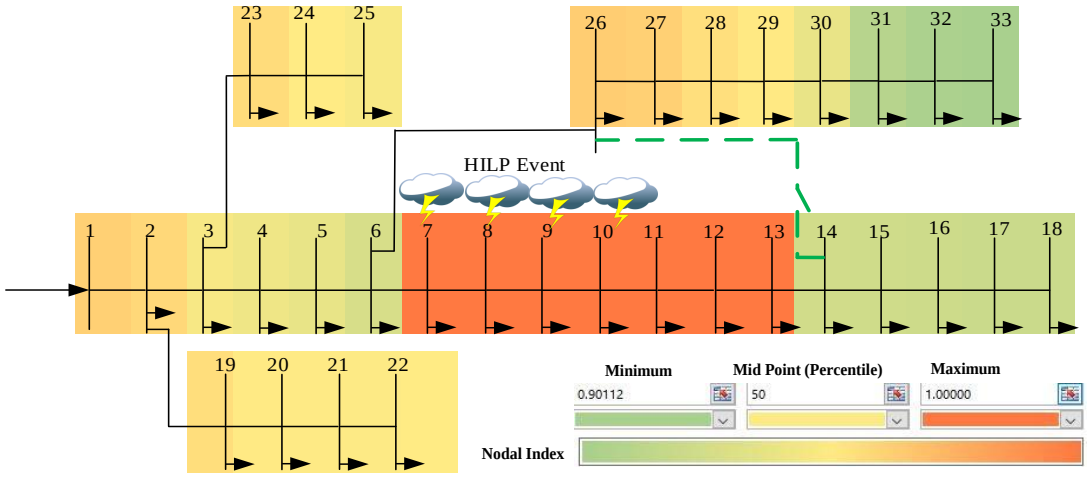

FIGURE 4.7: Nodal robustness for the optimal planning scenario with a Tie switch placed between Nodes 26 to 14.

NRS (f_1 associated with μ_{d1}) and restoration losses NRL (f_2 associated with μ_{d2}), and two objective functions to be maximized, system-wide restorability NRA (f_3 associated with μ_{d3}) and restoration criticality NRC (f_4 associated with μ_{d4}). As a consequence, higher satisfaction levels for f_1 and f_2 (μ_{d1} and μ_{d2}) results in these two objective functions to be more dominant and higher satisfaction levels for f_3 and f_4 (μ_{d3} and μ_{d4}) are desirable in the final decision. To provide the reader with a better understanding of the proposed decision making platform, the following example is presented: if the user decides on $\mu_{d3} = 1$ and $\mu_{d1}, \mu_{d2}, \mu_{d4} = 0$, the system wide restorability (NRA) is the only objective function reflected in the final decision. In this particular case, μ_{d3} is set to the highest value which is not desired for this objective function (NRA) and the decision would be to connect Nodes 26 to 18 with a Tie switch placement, which restores the lowest amount of loads. The user can tune the satisfaction levels and objective functions to meet the desired decision requirements.

Figure 4.7 demonstrates the nodal robustness in the network under test for the optimal solution with satisfaction levels of $\mu_{d1} = 0.8$, $\mu_{d2} = 0.8$, $\mu_{d3} = 1$, $\mu_{d4} = 0.6$. As reported in Table 4.2, such satisfaction levels result into a connection between Nodes 26–14 as the most optimal location for the Tie switch. The colors in Figure 4.7 depict the nodal robustness, where a lower nodal performance deviation reflects a higher robustness (dark green). The HILP-heavily-affected nodes have the highest performance deviations and are dressed by

colors in red.

4.4 Chapter Summary

In this chapter, a multi-objective decision making framework for resilience-oriented optimization and planning in power distribution grids is proposed. This framework employs a WLS-based state estimator and a fuzzy satisfying method to find out the desirable reconfiguration plan by optimally allocating the Tie switches across the network for maximized preparedness against HILP events.

In order to characterize the optimal restoration plan, several resilience features (such as system robustness, load criticality covered by a restoration plan, restoration losses, and recovered capacity) are introduced and quantified at both nodal and system levels. Effectiveness of the proposed framework, which aims to provide the distribution utilities with visions on network hardening planning against HILP events, is tested on the IEEE 33-bus test system and a detailed discussion on the numerical results was provided.

Following this chapter, which covered structural resilience and concentrated on planning phase, the next chapter would focus on operational resilience. A novel communication-based load restoration platform, which dispatches all modern components of smart grids during restoration, would be presented in the next chapter.

Chapter 5

Enhancing Power Grid Resilience through an IEC61850-based EV-assisted Load Restoration

This chapter is related to the third research objective introduced in Chapter 1.3 and concentrates on operational resilience and corrective actions after occurrence of an HILP event in the network.

As mentioned in the literature review provided in Chapter 2, unlike most of the previously developed restoration systems, the proposed service restoration in this chapter considers extreme events with multiple faults in the grid and dispatches all modern resources in the smart grids available for restoration during consecutive faults. The service restoration resources include aggregated Electric Vehicles (EVs), Distributed Energy Resources (DERs), and flexibilities in the adjacent feeders.

5.1 The Proposed Hierarchical Self-Healing System: Architecture, Components, And Models

The proposed self-reconfiguration system in this chapter focuses on radial distribution grids in the presence of DER units and EVs. The system architectural overview along with functional units are displayed in Figure 5.1 and described below:

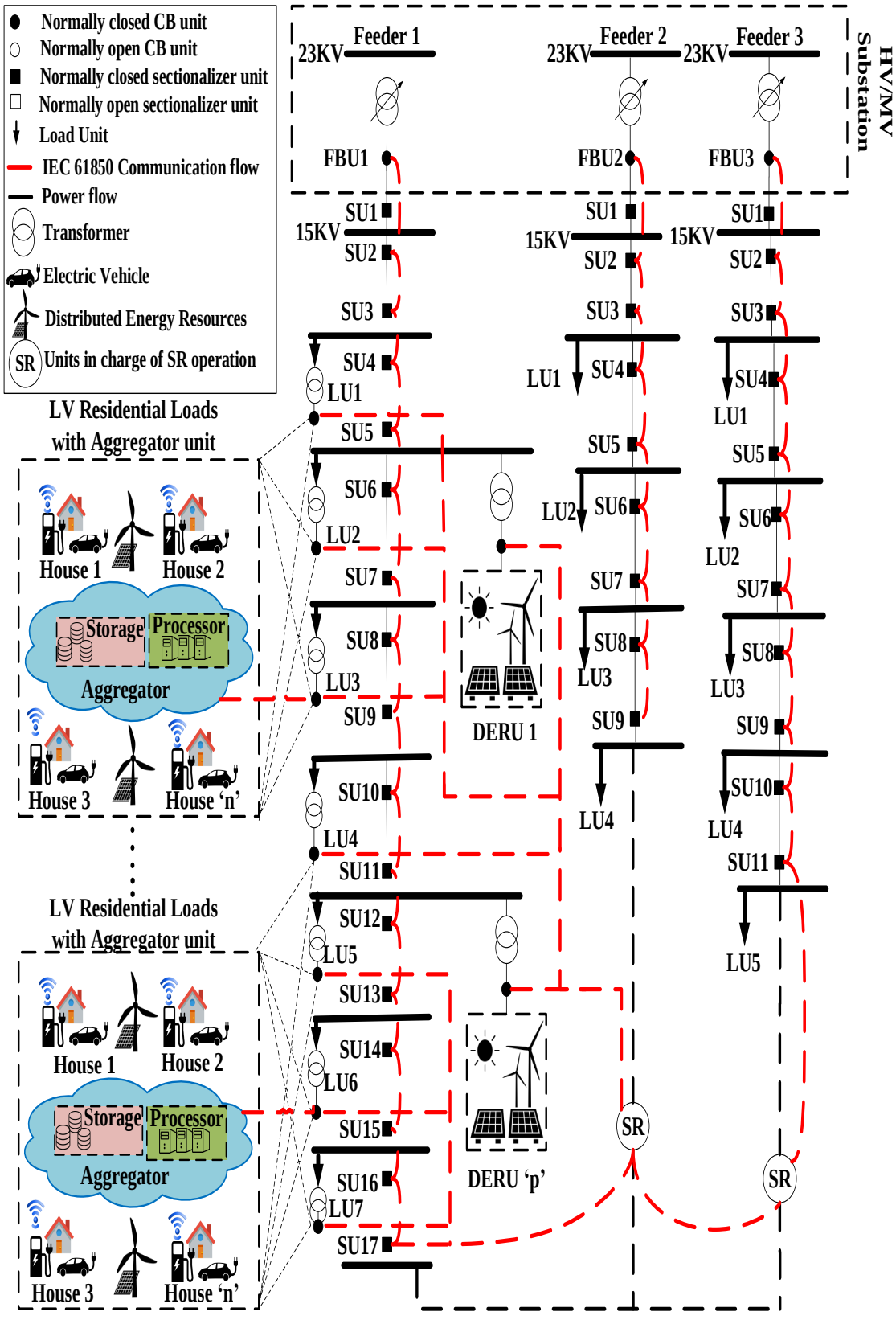

FIGURE 5.1: Generic view of the proposed hierarchical architecture.

1) **Feeder Breaker Units (FBUs)**: FBUs are located in the substations and include re-closing overcurrent relays, current transformers, and computational modules to frequently calculate and report the Reserve Current Capacity (RCC) of the feeder. In RCC calculations, the Feeding Transformer Capacity (FTC) and the current flow in the secondary side of the feeder transformer are characterized as follows:

$$RCC_{i,t} = (FTC_i / V_{s,i}^{TR}) - I_{s,i,t}^{TR} \tag{5.1}$$

2) **Sectionalizer Units (SUs)**: SUs are responsible to detect overcurrent conditions, report it to the relevant units, and oper- ate remotely to isolate a detected fault. Due to the bidirectional current flows in active radial distribution feeders, SUs typically consist of directional overcurrent relays and sectionalizing switches that are located at each terminal of the feeders in a double-ended protection fashion.

3) **Load Units (LUs)**: LUs are connected to each busbar covering the smart residential zone of the busbar. Smart residential loads include Electric Vehicles (EVs) capable of charging/discharging remotely. ZIP load modeling, presented in Refmanbachi2016impact, is adopted in (5.2) to characterize the load active and reactive power (with/without EVs):

$$P_{b,t} = P_{b,t}^0 \left(Z_p (V_{b,t}/V_{b,t}^0)^2 + I_p (V_{b,t}/V_{b,t}^0) + P_p \right) \tag{5.2}$$

$$Q_{b,t} = Q_{b,t}^0 \left(Z_q (V_{b,t}/V_{b,t}^0)^2 + I_q (V_{b,t}/V_{b,t}^0) + P_q \right) \tag{5.3}$$

where $(P_{b,t}, P_{b,t}^0)$ and $(Q_{b,t}, Q_{b,t}^0)$ represent the active and reactive power and their initial values for each busbar at each time interval t. (Z_p, I_p, P_p) and (Z_q, I_q, P_q) are the active and reactive ZIP load coefficients respectively. LUs include current transformers and computational modules to calculate and report the total current demand of their corresponding medium-voltage zones.

4) **DER Units (DERUs)**: DERUs are equipped with breakers that operate remotely, upon reception of certain published messages in the network, to isolate the DER in case of a fault

or to bring the DER unit back into the system operation during the SR process. Furthermore, DERUs publish their breakers current flows frequently and check the constraints on the active power injection of the DER units to the connected busbar as indicated in (5.4), where $P_{DER,t}$ is the active power injected by the DER unit to the connected busbar:

$$P_{DER,t}^{min} \leqslant P_{DER,t} \leqslant P_{DER,t}^{max} \tag{5.4}$$

5) **EV Aggregator Units (EVAUs)**: EVAUs are entities responsible for aggregation of EVs charging/discharging pro- files. These units communicate with other intelligent devices in the network to remotely control the EV chargers in their zone. Under fault scenarios, EVs are disconnected and those willing to participate in SR process would be effectively dispatched to inject power to the grid, once they receive the dispatch command from the EVAUs. The aggregated EV load profiles are reflected in the ZIP load models by changing the corresponding coefficients for aggregation of EVs. Among the different operational modes for EV chargers, the most common EV operating scenario for inverters is adopted here Refmanbachi2016novel, where $P > 0$, $Q = 0$ are set during charging and $P < 0$, $Q = 0$ are enforced during discharging operational modes. This reflects the fact that the EV fleet at each charging period consumes active power from the grid, while during the discharging (V2G) time interval, EVs which are plugged in and selected by the EVAUs would start injecting active power to the grid. It must be noted that EVAUs always ensure that there is enough energy remaining in each EV after the V2G time interval to meet the demanded mobility, which is the EVs primary function. The available energy by each EVAU and its corresponding constraints are formulated as follows:

$$E_t^{EVAU_j} = \sum_{i}^{\gamma_t} \left((E_i^0 + P_i^{G2V} \times \Delta t_i^{G2V}) - P_i^{V2G} \times \Delta t_i^{V2G} \right) \tag{5.5}$$

$$P_i^{G2V} = \left(\frac{1}{\Delta t_i^{G2V}} \int_0^{\Delta t_i^{G2V}} (p_{i,t}^C \times \lambda_{i,t}^C) dt \right) \times \eta_i^C \tag{5.6}$$

$$P_i^{V2G} = \left(\frac{1}{\Delta t_i^{V2G}} \int_0^{\Delta t_i^{V2G}} (p_{i,t}^D \times \lambda_{i,t}^D) dt \right) \times \eta_i^D \tag{5.7}$$

$$\lambda_{i,t}^C + \lambda_{i,t}^D = 1, \quad \lambda_{i,t}^C, \lambda_{i,t}^D \in \{0, 1\} \tag{5.8}$$

$$P_{V2G}^{Tot} = \sum_i^{\gamma_t} P_i^{V2G} \tag{5.9}$$

$$E_i^{min} \leqslant (E_i^0 + P_i^{G2V} \times \Delta t_i^{G2V}) - P_i^{V2G} \times \Delta t_i^{V2G} \tag{5.10}$$

$$0 \leqslant p_{i,t}^C \leqslant p_i^{C,max} \times \lambda_{i,t}^C \tag{5.11}$$

$$0 \leqslant p_{i,t}^D \leqslant p_i^{D,max} \times \lambda_{i,t}^D \tag{5.12}$$

Eq. (5.5) expresses the total available energy in the j^th EVAU at time t denoted by ($E_t^{EVAU_j}$) and is assessed by summation over the time-variant number of EVs in the fleet which are plugged in and ready to dispatch (γ_t). $E_t^{EVAU_j}$ is periodically published by each EVAU and subscribed by the units in charge of making decision for restoration in case of a fault or other prevailing conditions. The first term in (5.5) represents the energy in a single EV in the fleet after a charging interval (Δt_i^{G2V}) where E_i^0 is the initial energy in each EV battery determined by its initial State of Charge (SoC), and P_i^{G2V} is the average charging power of each EV. The second term in (5.5) represents the energy injected to the grid over a discharging interval (Δt_i^{V2G}), where P_i^{V2G} is the average discharging power of each EV. Eqs. (5.6) and (5.7) reflect the P_i^{G2V} and P_i^{V2G} assessment over the charging and discharging intervals, where η_i^C and η_i^D are the charging and discharging efficiency of each EV, respectively; $\lambda_{i,t}^C$ and $\lambda_{i,t}^D$ in (5.8) are binary variables to avoid charging and discharging at the same time.

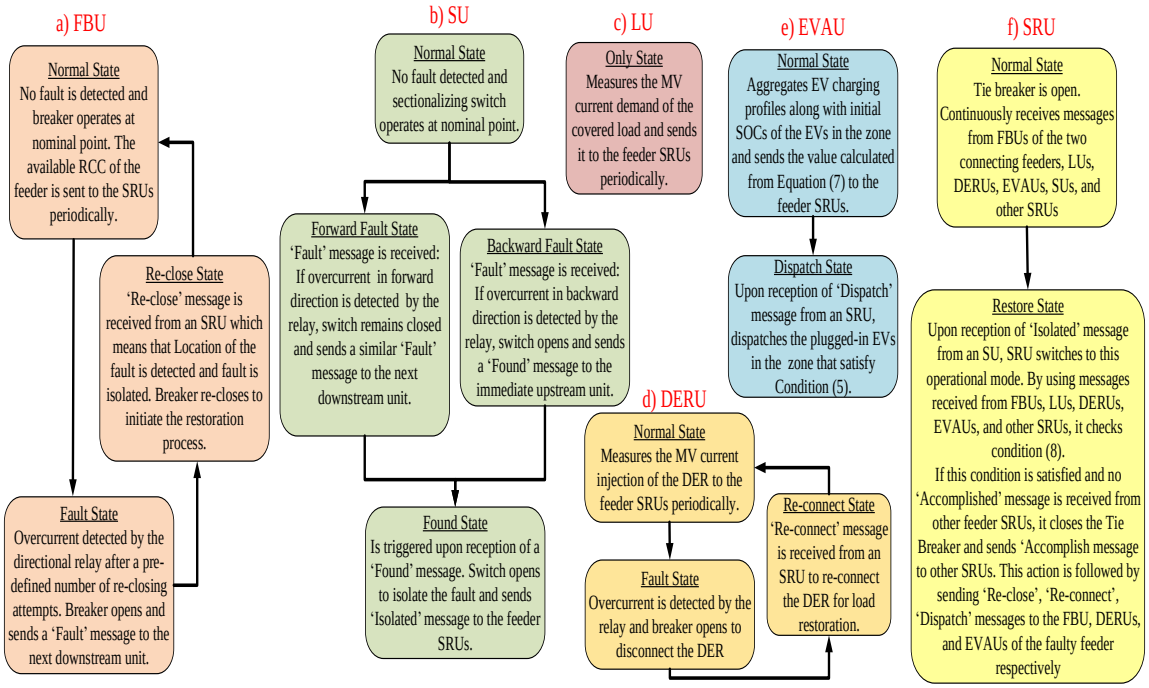

FIGURE 5.2: Proposed operational states for a) FBUs, b) SUs, c) LUs, d) DERUs, e) EVAUs, and f) SRUs.

The total injected power by each EVAU after a discharging interval (P_{V2G}^{Tot}) to be used during the SR process is assessed in (5.9). Constraint (5.10) limits the discharging energy at each EV to ensure there is sufficient energy after the V2G interval for its mobility; E_i^{min} is the minimum SoC of the EVs required for motion. Constraints on charging and discharging power of each EV are enforced in (5.9) and (5.10), where $p_{i,t}^{C}$ and $p_{i,t}^{D}$ are instantaneous charging and discharging power, respectively.

6) **SR Units (SRUs)**: SRUs play a key role in the SR process. They consist of normally-open circuit breakers which connect two radial feeders. SRUs are intelligent units that receive information (including measurements and statuses) from all other units, run the SR algorithm, and publish the results (re-configuration commands) to be subscribed and actuated by the corresponding units in the network. The SR algorithm runs in SRUs to restore the non-faulty loads of a feeder by utilizing all the available resources in the post-event interval. SRUs check the following criterion to make decisions on closing the Tie-breakers in their unit:

$$I_{demand}^{Tot} \leqslant (\alpha \times RCC) + (\beta \times I_{DER}^{Tot}) + (\zeta \times I_{V2G}^{Tot}) \tag{5.13}$$

where I_{demand}^{Tot} is the current representing the non-faulty loads to be restored; RCC is the reserve current capacity of the feeder that would be connected to the faulty feeder by closing the Tie-breaker in the SRU; I_{DER}^{Tot} is the current that could be injected by the DER units located in the non-faulty section of the feeder and is assessed via P_{DER} received from DERUs; and I_{V2G}^{Tot} is the potential current that could be injected by the EVs located in the non-faulty zone and is assessed by P_{V2G}^{Tot} received from EVAUs.

α, β, and ζ are auxiliary parameters designed to ensure that the decision on employing various resources (i.e., RCC, DER, and EVs) for SR do not heavily rely on EVs and DERs, where much higher capacity uncertainty can unfold than from resources in the adjacent feeders. Note that the main SR resource is the assisting capacity from the adjacent feeders, and DERUs and EVAUs are employed as the auxiliary resources for SR. These parameters could be tuned in such a way that even in the worst case scenario, where there is no contribution from DERUs and EVAUs, the SR algorithm converges and only certain pre-determined overload limits are violated. This could be achieved by checking condition (5.13), where β and ζ are set to zero.

5.2 Proposed EV-Assisted Load Restoration

The proposed units are deployed as finite-state machines and can switch between operational modes which are triggered upon reception of the external messages. The operational states for each unit are displayed in Figure 5.2 and the messages exchanged among the units are tabulated in Table 5.1. There are two main assumptions in this paper: (i) radial operation of the feeder is always ensured, and (ii) protection devices are fast and fully reliable.

All units operate in "Normal State" when there is no event in the grid. Measurements, including load current demands, available RCC, I_{DER}, and P_{V2G}^{Tot}, are continuously exchanged between the units. When an event occurs, FBU and DERUs are the first units to react. DERUs sense an overcurrent and, hence, transit into a "Fault State" by opening the DER breakers, and wait to receive a "Re- connect" message from the SRUs to contribute to the SR process. In such circumstances, FBU switches to "Fault State" by publishing a "Fault" message and

triggers the algorithm in the downstream units. In radial feeders, based on the direction of the overcurrent sensed by the relays in SUs, the event location could be detected and reported to the SRUs.

The SU which senses the overcurrent in the backward direction (i.e., from downstream to upstream unit), changes its status to the "Backward Fault State" and publishes a "Found" message to the upstream SU. Subsequently, its status changes to the "Found State" to isolate the faulty segment of the feeder and publishes an "Isolated" message to the SRUs, announcing that the fault location is identified and the fault is successfully isolated. Once the SRUs receive the "Isolated" message, they start the SR process by switching to "Restore State".

It must be noted that the publisher of the "Isolated" message is known to the SRUs, which assists to find out the location of the fault. By utilizing the pre-fault measurements received from all units in the feeder, the SRUs check the criterion in (5.13). If it is satisfied for an SRU and no other SRU in the faulty feeder has yet restored the loads, it closes its Tie- breaker and publishes an "Accomplished" message to other SRUs to terminate the SR process. The published "Accomplished" message by a particular SRU, subscribed by every other SRU, guarantees that only one SRU implements a restoration plan and the algorithm stops on other SRUs immediately. This action is followed by publishing "Dispatch", "Re-close", and "Re-connect" messages to be subscribed by the EVAUs, FBU, and DERUs of the faulty feeder, respectively, to complete the restoration process. These messages from the SRU would dispatch EVs, re-close the main feeder breaker, and re-connect DERs in the non-faulty segments of the feeder. Also, "Ready" message is published by this SRU after closing its Tie-breaker to be subscribed by all units and make them transit to "Normal State" and be prepared for the next emergency scenario. The system performance, described in this section, relies

heavily on functionality of the communication network and response time of the above-mentioned units (e.g. EV converters). Therefore, the performance of the designed system is significantly compromised under high latency or communication link failure scenarios. The system is designed to switch to the traditional SR mode, where no communication is required, if the Round Trip Time (RTT) of the messaging platform exceeds a pre-defined threshold. In

TABLE 5.1: Proposed Messages Exchanged Between the System Operational Units

Message	Publisher	Subscriber	Type
Fault	FBUs, SUs	adjacent downstream SU	Bool
Found	SUs	adjacent upstream SU	Bool
Isolated	SUs	SRUs	Bool
Dispatch	SRUs	EVAUs	Bool
Re-close	SRUs	FBUs	Bool
Re-connect	SRUs	DERUs	Bool
Accomplished	SRUs	SRUs	Bool
Ready	SRUs	All	Bool
Measurements	LUs, FBUs, EVAUs, DERUs	SRUs	Float

other words, if the SRUs do not receive the input information from all parties listed in Table 5.1 within a certain range of time, the traditional SR based on the information from the last energized counters and protection devices would react as a backup SR.

5.3 HIL Testing Platform and System Parameters

Real Time Digital Simulator (RTDS) with its specialized output boards, namely Giga-Transceiver Network Communication Card (GTNET), capable of publisher/subscriber IEC61850-8-1 GOOSE communication is utilized to verify the real-time performance of the proposed SR architecture.

GTNET cards are configured to publish/subscribe GOOSE messages over an ideal gigabit Ethernet communication infrastructure with a delay less than 3ms. Each GTNET card could be a publisher and a subscriber at the same time and it interacts with the grid model via an interface board, called Gigabit Processing Card (GPC). IEC61850-8-1 GOOSE messaging, which is generally used to transmit the time-critical event-driven information in the system, is adopted to exchange the messages proposed in Table 5.1 [150].

The testbed developed in this chapter offers provisions to test prototypes of protection devices (e.g. relays)capable of communications in IEC 61850 protocols. In Hardware-in-the-Loop (HIL) simulation fashion, the proposed GOOSE messages could be exchanged between RTDS and the relay prototypes. Adaptive control and protection schemes could be

characterized with the HIL platform from various aspects such as communications reliability. With utilization of network emulators, impact of communication delays could be investigated with the proposed platform as well. Furthermore, measurements required for implementation of the control and protection schemes, communicated from different nodes of the network, could be realized using IEC 61850 protocols supported by the platform. The platform has flexibility in terms of the number of nodes and the size of the grid under test due to distributed architecture of the processors. The other advantage of the testbed is capability to calculate reliability/resilience metrics online. This HIL platform setup is presented in Figure 5.3 with more details available in [2]. The main advantage of this setup is the automated record-and-replay facility in the RTDS environment using scripting features for online system performance evaluation. The system parameters corresponding to the developed modules in Figure 5.1 along with the connection points of each proposed unit are reported in Table 5.2. The load data and aggregated EV profiles have a 5-minute resolution, and data received by SRUs are updated every 15 minutes. Values reported in Table 5.2 are considered as the last updated information before the disruptive event (immediate pre-event measurements).

TABLE 5.2: Information on the Studied Grid and Simulation Parameters

Bus no.	Connected Unit	Parameters
1	FBU	Trans. 23kV/15kV, 150 MVA
2	LU, SU	P=63.1kW, Q=14.9kVAR, cust.no=19 ZIP= 0.418, 0.135, 0.447
3	LU, SU	P=42.3kW, Q=11.1kVAR, cust.no=13 ZIP= 0.418, 0.135, 0.447
4	LU, SU	P=140.2kW, Q=37.2kVAR, cust.no=38 ZIP= 0.418, 0.135, 0.447
5	DERU, LU, SU	P=140.1kW, Q=7.4kVAR, cust.no=41 ZIP= 0.418, 0.135, 0.447, P_{DER}^{normal}=5.1kW, P_{DER}^{high}=35.2kW
6	EVAU1, LU, SU	P=294.4kW, Q=74.5kVAR, cust.no=87 ZIP_{Normal}= 0.413, 0.138, 0.449, ZIP_{High}= 0.402, 0.143, 0.455 $P_{NormalInject}^{EVA}$=45.3kW,
7	LU, SU	P=140.3kW, Q=37.2kVAR, cust.no=44 ZIP= 0.418, 0.135, 0.447
8	EVAU2, LU, SU	P=294.1kW, Q=71.1kVAR, cust.no=102 ZIP_{Normal}= 0.413, 0.138, 0.449, ZIP_{High}= 0.402, 0.143, 0.455, $P_{NormalInject}^{EVA}$=26.4kW,
9	LU, SU	P=63.6kW, Q=18.7kVAR, cust.no=20 ZIP= 0.418, 0.135, 0.447
10	LU, SU	P=84.6kW, Q=29.8kVAR, cust.no=26 ZIP= 0.418, 0.135, 0.447
11	LU, SRUs	P=31.5kW, Q=11.6kVAR, cust.no=9 ZIP= 0.418, 0.135, 0.447 α = 0.9 , $\beta = \zeta$ = 0.75

The EV load profiles capture an aggregation of multiple EVs from various manufacturers, corresponding to EVs with the capacity up to 19.2 kW and $SoC^{min}_{mobility}$ = 30%, where additional information can be found in [151]. The constraints described in (5.5) to (5.13) are implemented through the built-in arithmetic modules, logic gates, and computational units in the RTDS environment. These arithmetic/computational modules, which are used to model the dispatched EVAUs, limit the output of the current source in such a way that constraints related to EV discharging, e.g., minimum energy left for mobility requirements in (5.10), are satisfied.

5.4 Test Case Scenarios and Evaluation Results

5.4.1 Evaluation Framework

Resilience assessments in power systems are centered on HILP events where most of the standard reliability metrics (based on outage frequency/duration) are not able to adequately address and quantify the restoration resources [101].

There are multiple dimensions involved in power grid resilience assessment such as energy-based, time-based, and cost-based improvements [101]. Assessment in this paper focuses on feeder-level energy-based improvements, i.e., Feeder Resourcefulness (FR) and Restoration Rapidity (RR). All the available resources involved in the SR process could be classified as: (i) Internal Backups (IB) and (ii) External Backups (EB).

IB refers to all resources *within the faulty feeder* which are employed to contribute to a swift restoration and, in this paper, include the DERs and EVs connected to the non-faulty segments of the faulty feeder.

EBs are any other resources in the network located *outside of the faulty feeder* which can be connected to the faulty feeder only during the SR process and is, in this paper, the assisting capacity from external feeders. Based on this classification, the ratio of the utilized IB and EB resources could represent the feeder resourcefulness (FR). The RR of the system is evaluated by restoration Plan Steps and Interruptions (PSI). This is indicated by summation of the ratios between interruption duration of each load and the Total Time to Restoration (TTR) in

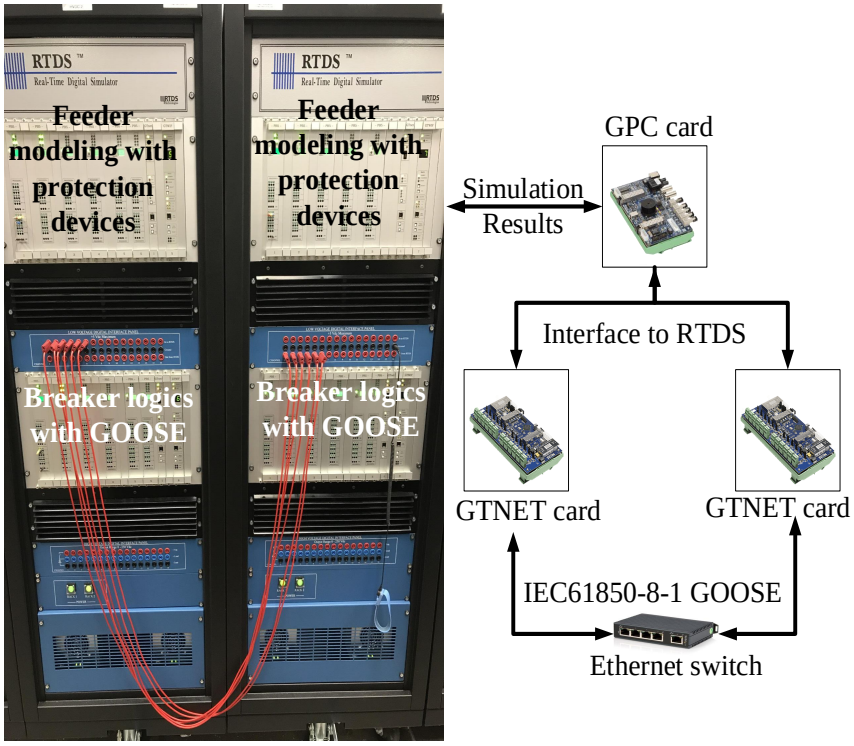

FIGURE 5.3: Hardware-in-the-loop simulation platform using RTDS.

a faulty feeder. TTR is the time interval from the moment an event occurs to that when its is entirely cleared. During the restoration process, different load interruption duration depends on the restoration algorithm and the number of steps taken to achieve a full restoration. This is reflected by multiplying the total number of steps taken for a full restoration (S) to the total interruption duration over TTR.

$$FR = \left(\frac{IB^{Tot}}{IB^{Tot} + EB^{Tot}}\right), RR = \underbrace{\frac{1}{S \times \left(\sum_i^S (\frac{\Delta t_i \times n_i}{TTR})\right)}}_{\text{Plan Steps and Interruptions (PSI)}} \tag{5.14}$$

Figure 5.4 conceptually visualizes the sensitivity of the feeder-level resilience with regards to the FR and PSI. It could be perceived from this figure that the grid resilience has a direct and reverse relation with FR and PSI, respectively, while swinging between maximum and minimum limits.The restoration process proposed in this paper includes three main steps

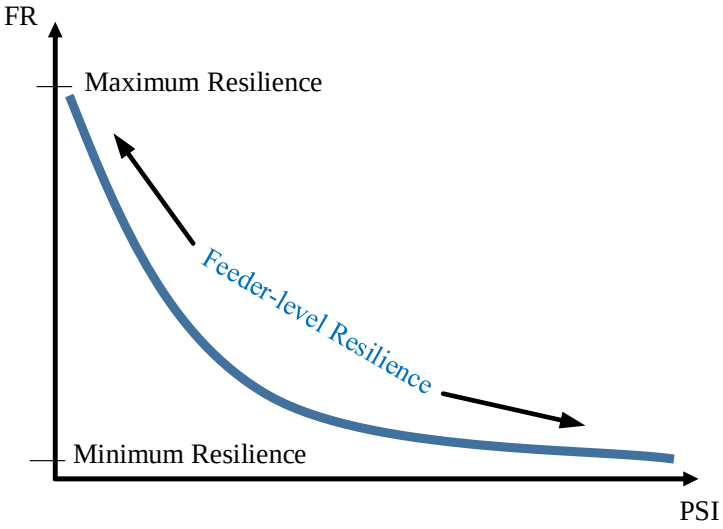

FIGURE 5.4: Conceptual sensitivity of the feeder-level resilience with regards to FR and PSI.

(S=3), and the interruption durations (Δt_i) are as follows: Δt_1: time interval between opening and re-closing FBU; Δt_2: time interval between opening FBU and closing SRUs; Δt_3: time for human intervention to clear the fault and close the open SUs manually.

5.4.2 Test Case Scenarios

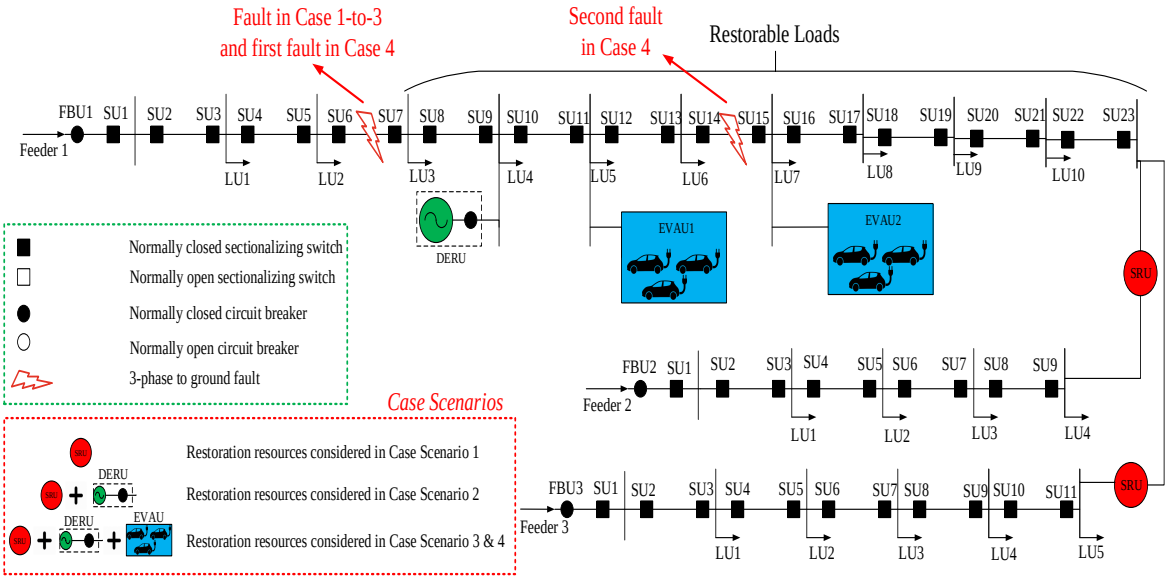

FIGURE 5.5: Detailed demonstration of the grid under test related to Table 5.2 along with the case scenarios.

Figure 5.5 demonstrates details of the case scenarios which are tested and presented from

the simplest to the most advanced one. In order to compare various feasible scenarios, a disastrous fault event is simulated at a fixed location between Bus 3 and Bus 4 (SU6 and SU7) in Feeder 1 and a given outage duration. The fault events can, however, occur at any time and location in the system. Pre-fault values of the system parameters, which are used by SRUs, are presented in Table 5.2. In order to capture the entire behavior of the system from pre-event to post-event operating state, values are taken in kA and zoomed several orders of magnitudes for better comparisons.

Case I: Original System (Base Scenario):

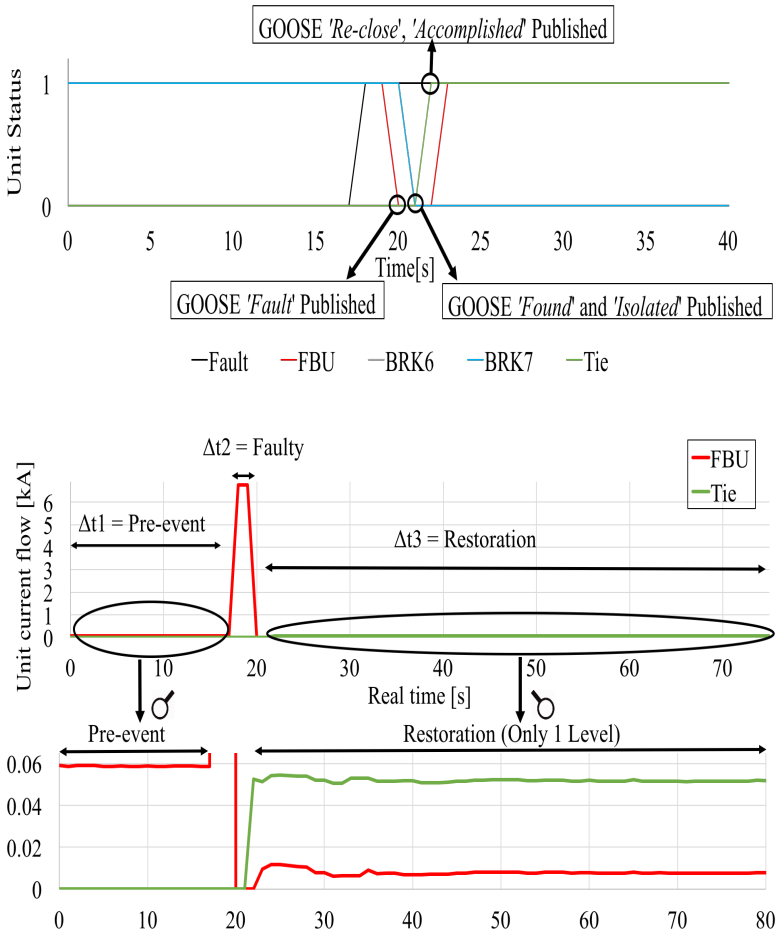

FIGURE 5.6: HIL results for operational units in Case I.

As the reference test case, the original system without DER units and EV aggregators is investigated in Case I. The faulty feeder is restored solely through imported power from an external feeder. The self-reconfiguration and real-time current flows of the critical units

TABLE 5.3: Summary of the Results in Case I

Total restorable [A]	**FBU covered** [A]	**SRU covered** [A]	**RR Inx.**	**FR Inx.** %
59.96	7.73	52.23	0.75	12.89

are displayed in Figure 5.6, where different stages of the entire process including the pre-event, faulty, and restoration are highlighted. The first display in Figure 5.6 illustrates the moment when each unit publishes its event-driven GOOSE message (see Table 5.1). It can be observed from curves in Figure 5.6 that, once the event is activated, the feeder-level current captured by the FBU (red curve) reaches a peak and the protection units are triggered to operate and exchange messages to isolate the fault. The total load to be restored, restoration rapidity, and the load eventually restored by FBU and SRU are reported in Table 5.3. Based on the event location between Buses 3 and 4 and the information on the number of customers connected to each Bus, 32 customers experience Δt_1 and 367 customers go through Δt_2. According to [117], 45 minutes is considered for Δt_3 in order to evaluate the restoration rapidity. Fewer number of units involved in the SR process leads to lower complexity of the restoration mechanism, lower number of messages exchanged between the units, and a lower computational burden, and hence, the units can react fast to contribute to the SR process. However, the tension on the external backup is high due to low utilization of internal backups and available resources.

Case II: Original System with DERU:

In this test case, DERU located in the non-faulty segment of the faulty feeder is involved in the restoration process in addition to the external backup. The first display in Figure 5.7 demonstrates the self-reconfiguration actions based on the GOOSE messages along with the current flows in critical units. Color-coded curves in Figure 5.7 illustrate the contribution of the DERU and the moment when it is re-connected for SR. Purple line represents the DERU contribution which makes the green line (current flow in SRU representing imported power) remain at a lower level compared to Case I.

The total restorable load along with contributions from FBU, SRU, DERU, and the Reduced Imported Power (RIP) are reported in Table 5.4. In order to highlight the DERs

TABLE 5.4: Summary of the Results in Case II

Total restorable [A]	**FBU covered** [A]	**SRU covered** [A]	**DERU covered** [A]	**RIP** %	**RR Inx.**	**FR Inx.** %
59.62	7.56	50.59	1.473	3.13	0.67	15.15

role and contribution in the SR, the high power injection rate of the DERU in Table 5.2 is employed in this test scenario. Due to the fixed fault location in all scenarios, the number of affected customers by each interruption duration (Δt_i) is considered the same as that in Case I. The number of messages and the computational burden of SRUs increase in this case by taking DERU into account (α and β), while the imported power is reduced by 3.13%.

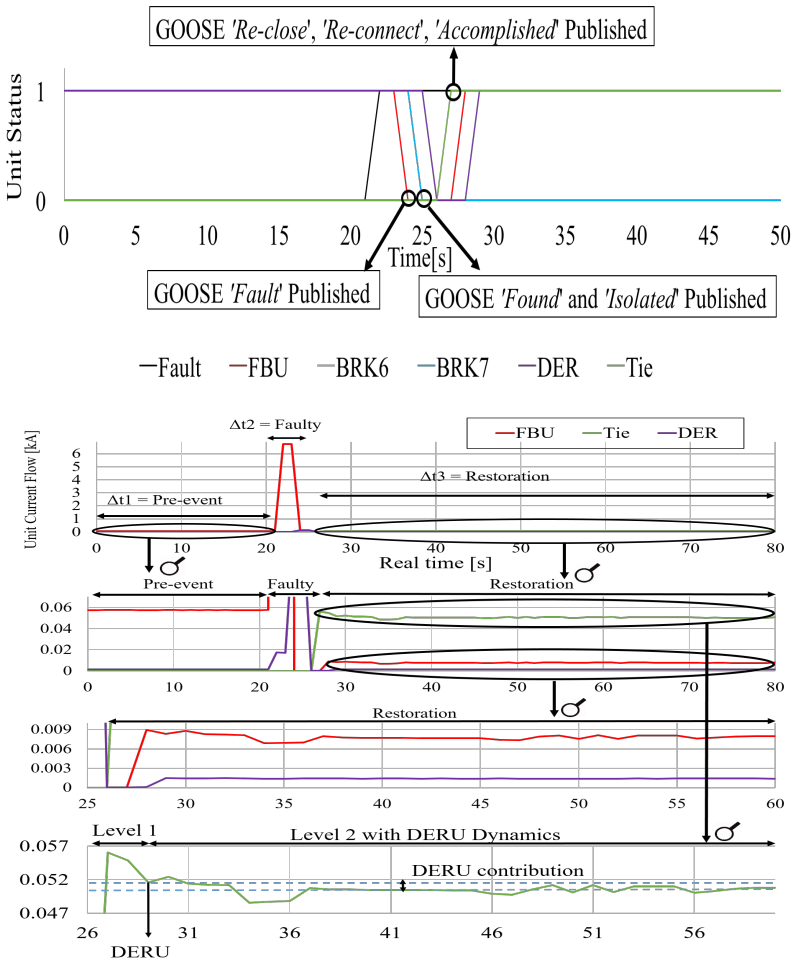

FIGURE 5.7: HIL results for operational units in Case II.

Case III: Original System with DERU + EVAUs:

This scenario aims at demonstrating the contributions of the internal backups to further

improvement of the feeder-level resourcefulness and resilience through EVs in addition to the available resources considered in Case II. In the pre-event stage, the EVAUs publish the potential V2G capacity by the EVs in their zone based on the conditions described in Section 5.2. Once the fault is detected and isolation is accomplished by responsible units, GOOSE messages are exchanged between SRUs and EVAUs to trigger utilizing the V2G capacity for restoration.

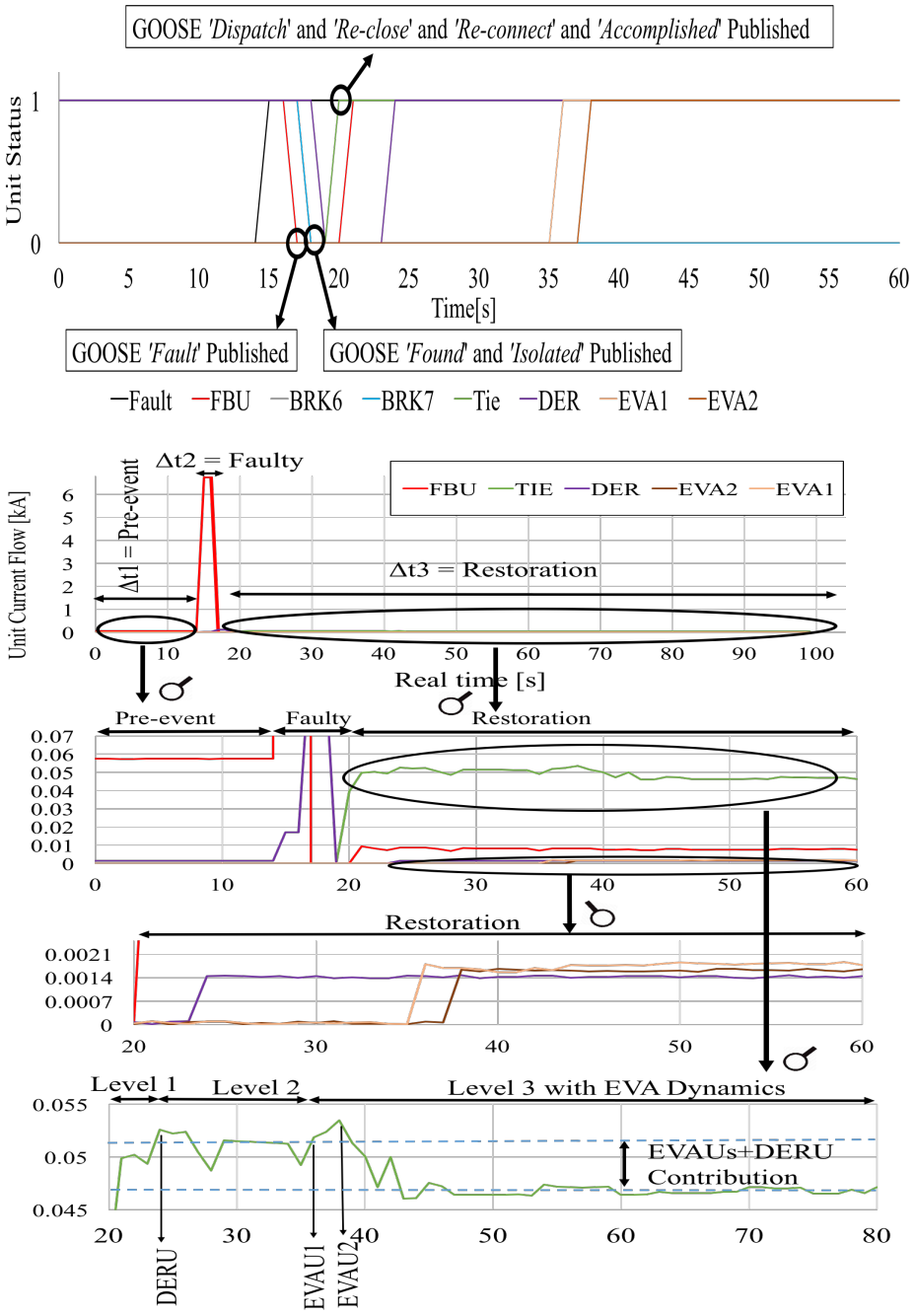

FIGURE 5.8: HIL results for operational units in Case III.

TABLE 5.5: Summary of the Results in Case III

Total restorable [A]	**FBU covered** [A]	**SRU covered** [A]	**DERU covered** [A]	**EVAUs covered** [A]	**RIP Inx.** %	**RR Inx.**	**FR Inx.** %
59.50	7.94	46.70	1.40	3.46	10.59	0.57	21.39

The penetration rate of EVAUs and DERU are reported in Table 5.2. The total power injection of the EVAUs is 85.2 kW with 75% availability, with the potential to increase with more prevalent deployment of EVs in the near future. Similar to the previous test cases, a summary of results are displayed in Table 5.5. The colored curves in Figure 5.8 highlight the joint contribution of EVAUs and DERU in the SR. The safety margin via α, β and ζ in Table 5.2 accounts for the uncertainties in the injected power by V2G capacity (due to drivers' behavior) and DER units. Hence, the restoration does not heavily rely on DERU and the EVAUs. The main advantage of employing such auxiliary internal backups is to reduce the stress on the external feeder through local resources.

The most magnified display on the green line, which represents the EBs, shows the contribution of EBs in this case compared to previous scenarios. The number of published GOOSE messages and SR computational burden in this case has increased. However, higher penetration of EVAUs and DERU results in a drastic reduction in the imported power from the external backup. Specifically, the imported power in this scenario has reduced by 10.59% compared to the base case condition which highlights a higher cost-effective feeder-level resilience in the post-contingency interval.

Case IV: Subsequent Events (Multiple Faults):

This test case extends the previous Case III to showcase the functionality of the designed resilience-focused load restoration in response to extreme events with subsequent impacts on the grid (e.g. cascading failure or multiple faults).

Critical moments are marked in the first display of Figure 5.9 from t_1 to t_{17}. The first fault occurs at t_1 and the corresponding SR process is accomplished at t_9 through the procedure described in Case III. A GOOSE message named "Ready" has been published by the SRU after the first restoration and subscribed by all non-faulty units to be switched back to the

TABLE 5.6: Sequence of Events Related to the Top Curve in Figure 5.9

t_1	t_2	t_3	t_4	t_5	t_6
First fault occurs, 59.5 [A] to be restored	'Fault' GOOSE published	'Found' 'Isolated' GOOSEs published	Restoration triggered SRU closes 46.70 [A] restored	'Dispatch', 'Re-close', 'Re-connect', 'Accomplished' 'Ready' GOOSEs published	FBU1 recloses 7.94 [A] restored
t_7	t_8	t_9	t_{10}	t_{11}	t_{12}
DERU reconnects 1.94 [A] restored	EVAU1 dispatches 1.81 [A] restored	EVAU2 dispatches 1.65 [A] restored	Second fault occurs	'Fault' GOOSE published	'Found' 'Isolated' GOOSEs published
t_{13}	t_{14}	t_{15}	t_{16}	t_{17}	$t \geqslant t_{17}$
Restoration triggered	EVAU1 isolated 'Re-close' 'Dispatch' GOOSEs published	EVAU2 isolated	FBU2 recloses 21.16 [A] restored	EVAU2 dispatches 1.77 [A] restored 'Ready'GOOSE Published	Ready for the next fault

normal operating state (pre- fault state). This ensures the system preparedness for the next fault.

At t_{10}, the next fault occurs located between SU14 and SU15 (see Figure 5.5) while the first fault is not yet fully cleared. This could be followed in the second display in Figure 5.9, where there are two over-currents detected. Once the second fault occurs, the proposed SR solution, which runs in the external feeder connected temporarily to the main faulty feeder after the first fault, initiates a self-reconfiguration action by opening FBU2, SU14, and SU15 to isolate the fault. Also, EVAUs and DERUs are isolated by the corresponding reconfiguration action.

Once the second fault is isolated, the FBU2 in the external feeder recloses to restore the non-faulty loads in the external feeder and SRU dispatches the local generations and the EVAUs located in the non-faulty areas. Considering the location of the first fault (between Bus 3 and Bus 4) and the second fault (between Bus 7 and Bus 8), only EVAU2, located at Bus 8 (non-faulty segment and energized by FBU2), re-dispatches for restoration of the

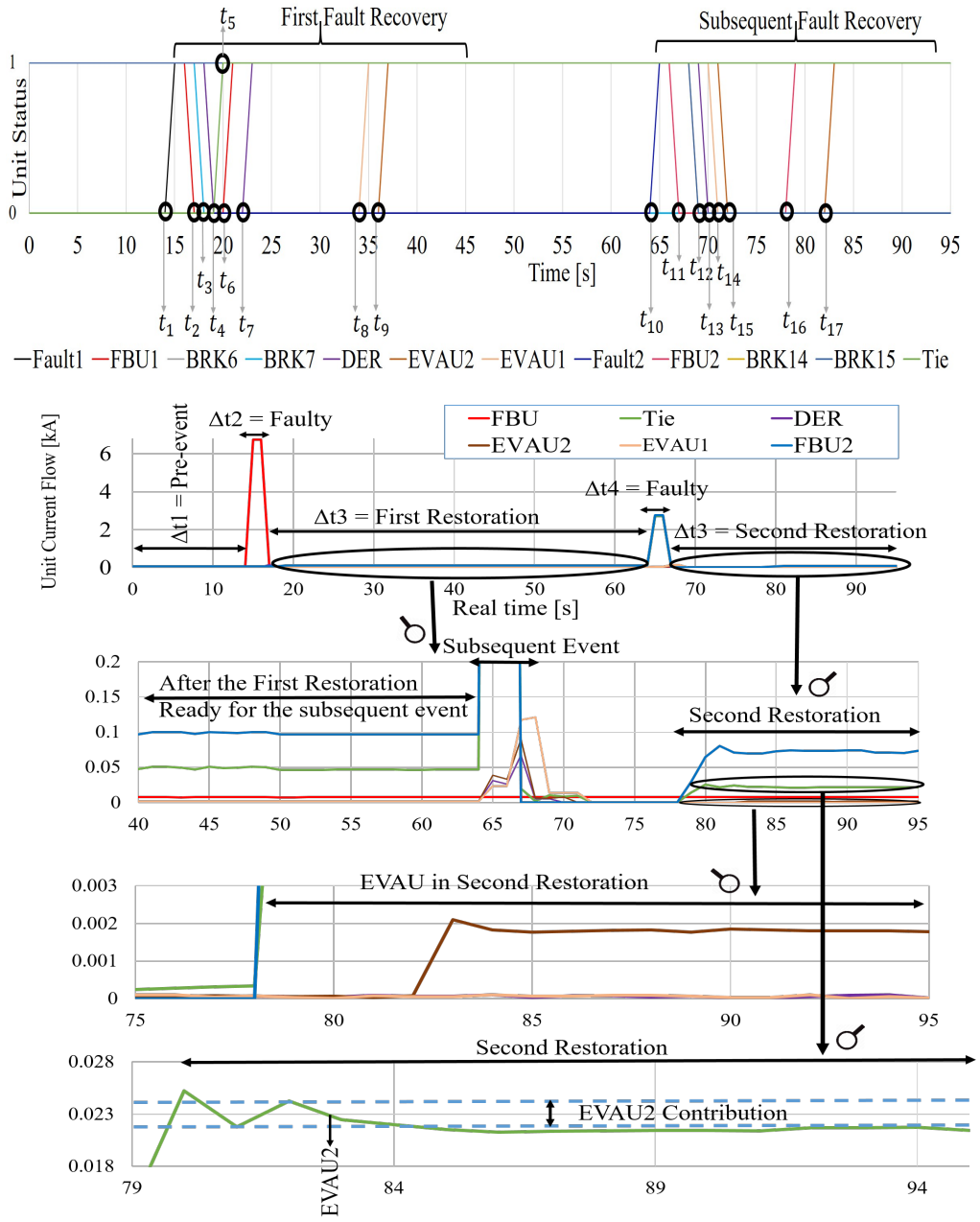

FIGURE 5.9: HIL results for operational units in Case IV.

second fault (EVAU1 and DERU remain isolated). This behavior is observed in the most bottom display in Figure 5.9, where the contribution of EVAU2 is magnified.

Sequence of events in real time along with the load restoration achievements are reported in Table 5.6 and Figure 5.9. At t_{17}, the "Ready" GOOSE message is published again to make the system prepared for the next possible faults.

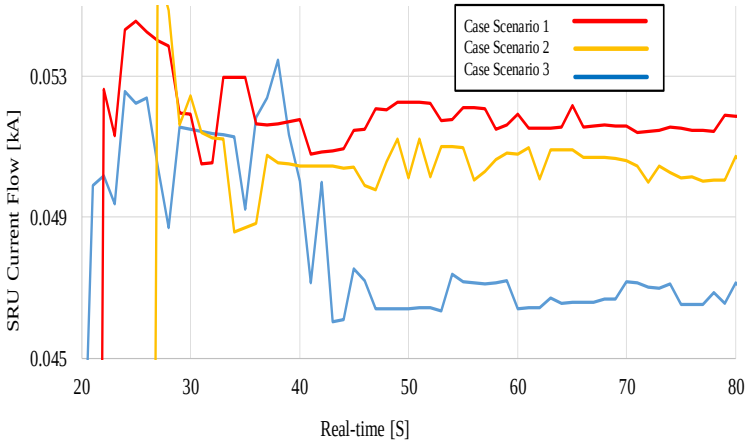

FIGURE 5.10: Real-time HIL results for comparison of the current flow in SRU unit, EB utilization, in different case scenarios.

5.4.3 Discussion

Among all dimensions (energy, cost, and time) involved in resilience improvement, this paper focused on energy restoration and feeder-level resilience improvements. Test Cases I to III demonstrated that more investments on peer-to-peer communications in distribution grids enable implementation of advanced SR algorithms that are able to best utilize the feeder-level internal backups. Consequently, with a relatively faster restoration process, resourcefulness and resilience in the system will be enhanced. While the restoration rapidity of all scenarios are similar, Case I, with the simplest SR mechanism and the lowest number of published GOOSE messages, has the highest restorative rapidity but the lowest feeder-level resourcefulness during the post-contingency operating state. By utilizing the DERU in Case II and a joint DERU and EVAUs in Case III, deployment of available external backups is statistically presented in Table 5.7. Figure 5.10 provides a comparison overview of the real-time utilization of EBs in the studied test case scenarios. The lowest EB utilization belongs to Case 3 (blue curve) and the red curve sits on top of others, representing the EB utilization in Case 1. The higher utilization of the modern grid services results in a heightened feeder-level resilience when tested on the same event in all test case scenarios. Case IV is designed to highlight the functionality of the proposed SR architecture to best respond to extreme HILP scenarios with multiple faults in a feeder in presence of DERs and

TABLE 5.7: Comparison of the Test Case Scenarios

Case no.	Internal Backup (FR) [%]	External Backup [%]	RR Index	RIP [%]
1	12.89	87.10	0.75	N/A
2	15.15	84.84	0.67	3.13
3	18.27	81.72	0.57	10.59

EV aggregators. With increased number of EVs in the near future, the numerical results in this paper proved the efficacy of the V2G technologies as a modern auxiliary SR resource to improve the feeder-level resourcefulness during HILP events.

5.5 Chapter Summary

In this chapter, a resilient service restoration architecture was designed utilizing the IEC 61850-8-1 GOOSE communication principles. Unlike the past studies, the proposed solution harnesses (a) the imported power and flexibility from the neighboring networks, (b) Distributed Energy Resources (DERs), and (c) aggregated vehicle to grid (V2G) capacity in all steps of restoration when facing an extreme HILP incident with multiple faults. The proposed real-time SR mechanism was implemented using the RTDS HIL platform and the contribution of each SR resource was numerically quantified by a developed resilience evaluation framework. The proposed solution ensures an enhanced feeder-level resourcefulness that can contribute to agile response and efficient recovery. This is primarily achieved by a strategic deployment of major modern resources (with focus on EVs contribution) during a sequence of multiple faults. Four test case scenarios were tested and presented, through which a 10.59% stress reduction on external SR resources compared to the base case condition was realized.

Chapter 6

Conclusion and Future Work

This thesis has proposed a communication based load allocation and load restoration system for higher efficiency and resilience in smart grids. There are different aspects of the proposed system, which are presented in this thesis. This includes communication side of the platform, mathematics behind the load allocation and restoration algorithms, and optimization techniques utilized in this thesis. The PhD work in this thesis considers both operational and structural resilience in power grids.

6.1 Thesis Conclusion

The thesis has investigated the prospect and challenges of design and implementation of communication-based load allocation and load restoration in smart grids. An appliance-level load allocation algorithm for smart neighborhoods is designed and implemented with MQTT protocol in this thesis. An IEC-61850 based load restoration algorithm is presented to improve resilience of smart grids by strategic dispatch of all modern resources such as aggregated Electric Vehicles (EVs). A novel multi-objective decision making platform has been introduced in this PhD work to be adopted by power utilities to plan for a more resilient network. In detail, the performed tasks and contributions of this research are outlined as follows:

6.1.1 Conclusion for Chapter 2

An extensive literature review has been carried out on communication-based load allocation and restoration systems in Chapter 2.

- The first part of literature review was composed of a comprehensive review on smart grid communication protocols, standards, and technologies. This part offers provisions on cons and pros of each communication architecture used in smart grids to justify the communication protocols adopted in this PhD work.

- The next part of this chapter focuses on previous studies on communication-based load allocation algorithms in smart neighborhoods. This sub-section aims to highlight limitations in previous studies and to provide the reader with a background on load allocation systems in smart neighborhoods.

- The rest of this chapter concentrates on a review of communication-based load restoration in resilient smart grids. The concept of resilience in smart grids is discussed in details and multi-objective optimization approach to boost resilience is presented. Various resources utilized during the restoration in previous studies have been discussed in details.

6.1.2 Conclusion for Chapter 3

A novel appliance-level MQTT-based load allocation algorithm has been designed and implemented in Chapter 3. The proposed architecture considers unreliable communication links in the smart neighborhood and switches from centralized control to decentralized depending on the latency in the network. The case scenarios in this chapter are built based on real-world load profiles of a residential community in Australia. A virtual Wide Area Network emulator (WANem Machine) has been adopted in this work to mimic realistic behavior of the network under various traffic conditions to justify efficacy of the proposed platform. MQTT topics, which convey Metadata of the payload of the MQTT messages, are proposed to reflect source and destination of the messages from the appliance to the controller.

The implemented platform utilizes a cloud-based services to facilitate data exchange among controllers of the smart buildings in the residential community. Three main resources are considered in the community under test which are: 1) local generation in the community, 2) Community Storage Facility, 3) Main grid.

6.1.3 Conclusion for Chapter 4

A multi-objective decision making framework to maximize resilience in restoration of smart grids is proposed in Chapter 4. A multi-dimensional resilience-oriented objective function has been defined in this chapter to be utilized by power utilities to quantify resilience in networks and run resilience-oriented optimization.

This chapter focuses on structural resilience and planning of power networks to maximize resilience by optimally locating the tie switches between the feeders in the network.The developed framework utilizes a WLS-based state estimator, which considers dynamic admittance matrix to evaluate the network operating condition at each reconfiguration plan. This will result in higher preparedness against High Impact Low Probability (HILP) events in the network.

A diverse set of HILP scenarios is generated, followed by a detailed analysis of the results to demonstrate the efficacy of the proposed framework in boosting the network resilience against HILP disasters.

6.1.4 Conclusion for Chapter 5

An IEC-61850-based EV-assisted Load restoration system is designed and implemented in Chapter 5 of this Thesis. The proposed load Restoration scheme offers provisions to respond to disastrous events with subsequent impacts on the grid (multiple faults).

In addition to the imported flexibility from neighboring feeders, the proposed autonomous load restoration in this chapter dispatches all modern resources including DERs, and especially the aggregated non-faulty V2G capacity in a faulty feeder as a new restoration resource. The developed solution continues dispatching these modern services even during the successive events, which in turn, relaxes the stress on the external resources and enhances feeder-level resourcefulness and resilience.

The real-time performance and scalability of the proposed load restoration approach are verified on a real-world Medium Voltage (MV) distribution grid in a practical setting. This includes Hardware-in-the-Loop (HIL) simulations using specialized output boards of Real Time Digital Simulator (RTDS), which are capable of standardized publisher/subscriber IEC

61850-8-1 GOOSE communication.

6.2 Future Research Direction

The proposed load allocation and restoration systems in this thesis could be expanded as follows:

6.2.1 Extension for Chapter 3

Energy stored in the Community Storage Facility (CSF) in Chapter 3 is distributed amongst the smart community members through a simplified local market mechanism. The focus of the chapter was on the communication aspect of the platform and the transactive management of the energy sharing among the community could be extended in future works.

6.2.2 Extension for Chapter 4

Power system resilience is a complex concept with multi dimensions involved in the system behavior, such as time-based, cost-based, energy-based factors. The proposed resilience indices in Chapter 4 could be expanded to encompass more dimensions of the system behavior. In particular, the cost-based aspect of the optimization in this chapter can be developed further to reflect restoration costs in great details.

6.2.3 Extension for Chapter 5

The proposed EV-assisted load restoration system in Chapter 5 is implemented by communications between utilities and the proposed EV aggregator units. This implementation could be expanded further to become more realistic by extending the communications from utilities all the way down to single EV-owners. In other words, a two-layer nested communication platform is required to fully implement the proposed system: 1) Communications between power utilities and the EV aggregator units via industrial protocols, 2) Communications between EV aggregator units and the EV owners via Internet of Things (IoT) protocols. This

requires a hybrid communication platform which links industrial communication platforms to modern IoT platforms.

List of Symbols

$RCC_{i,t}$ ..... Reserve Current Capacity of the i^{th} feeder at time t

FTC_i ..... Feeding Transformer Capacity of the i^{th} feeder. operators

$V_{s,i}^{TR}$ ..... Rated voltage level at the secondary side of the transformer in the the i^{th} feeder.

$I_{s,i,t}^{TR}$ ..... Current flow at the secondary side of the transformer in the i^{th} feeder at time t.

$P_{b,t}$,$P_{b,t}^{0}$ ..... Active power at each bus at time t and its initial value.

$Q_{b,t}$,$Q_{b,t}^{0}$ ..... Reactive power at each bus at time t and its initial value.

$V_{b,t}$,$V_{b,t}^{0}$ ..... Voltage at each bus at time t and its initial value.

Z_p, I_p, P_p.... Active ZIP load coefficients.

Z_q, I_q, P_q.... Reactive ZIP load coefficients.

$P_{DER,t}$ ..... Active power injected by DER unit at time interval t.

P_i^{G2V} ..... Average charging power of the i^{th} EV.

P_i^{V2G} ..... Average discharging power of the i^{th} EV.

$p_{i,t}^{C}$, $p_{i,t}^{D}$ ..... Instantaneous charging and discharging power of the i^{th} EV.

P_{V2G}^{Tot} ..... Total injected power by each EVAU during the restoration period.

$E_t^{EVAU_i}$ ..... Total available energy in the i^{th} EVAU at time interval t.

E_i^{min} ..... Minimum energy required for the i^{th} EV battery serving its mobility.

E_i^0 ..... Initial energy in the i^{th} EV battery determined by its initial State of Charge (SoC).

I_{demand}^{Tot} ..... Total current of the restorable demand.

I_{DER}^{Tot} ..... Total current injected by DERs during the restoration period.

I_{V2G}^{Tot} ..... Total current injected by EVs during the restoration.

Δt_i^{G2V} ..... Charging time interval of the i^{th}EV.

Δt_i^{V2G} ..... Discharging time interval of the i^{th}EV.

Δt_i ..... Minutes of interruption related to the i^{th} restoration step.

S ..... Total number of steps in a restoration plan.

n_i ..... Number of customers involved in the i^{th} restoration step.

IB^Tot ..... Total current injected by internal backups for restoration.

EB^Tot ..... Total current injected by external backups for restoration.

TTR ..... Total time to restoration in a restoration plan.

η_i^C, η_i^D ..... Charging and discharging efficiency of the i^{th} EV in the fleet.

$\lambda_{i,t}^C, \lambda_{i,t}^D$ ..... Binary variables indicating charging and discharging status of the i^{th} EV battery.

γ_t ..... Time-variant number of ready-to-dispatch EVs in the fleet.

α ..... Contribution factor of the RCC in restoration.

β ..... Contribution factor of the DERs in restoration.

ζ . . . . . Contribution factor of the EVs in restoration.

P_R . . . . . Requested power from the Community Storage Facility.

P_S . . . . . the power shared with the community by a community member.

NRC . . . . . Nodal Restoration Criticality.

NRS . . . . . Nodal Robustness.

NRA . . . . . Nodal Restorability.

NRL . . . . . Nodal Restoration Losses.

$P^{inj,N}$ . . . . . injected power at each node.

$P_i^{L,N}$, $P_j^{Gen,N}$. The level of consumed and generated active power at node N respectively.

Ω_L^N, Ω_G^N . . . . . The set of loads and generating units connected to node N respectively

Pr_N . . . . . A utility-defined number assigned to node N depending on the type of the connected load.

P^{Tot} . . . . . The total amount of load restored by a restoration plan.

P_N^{Loss} . . . . . Power losses at Segment N, between nodes N and $N + 1$.

P_{EOF}^{Loss} . . . . . The power losses in the last segment of the feeder.

P_{Tie}^{Loss} . . . . . The power losses corresponding to the path created by closing the Tie switch.

$P^{Flow,k}$ . . . . . The power flow in branch k.

Ω_T . . . . . The set of network branches.

References

[1] B. Celik, R. Roche, D. Bouquain, and A. Miraoui. *Decentralized neighborhood energy management with coordinated smart home energy sharing*. IEEE Transactions on Smart Grid (2017).

[2] P. Jamborsalamati, A. Sadu, F. Ponci, and A. Monti. *A flexible HIL testing platform for performance evaluation of IEC 61850-based protection schemes*. In *Power and Energy Society General Meeting (PESGM), 2016*, pp. 1–5 (IEEE, 2016).

[3] P. Jamborsalamati, E. Fernandez, M. Moghimi, M. J. Hossain, A. Heidari, and J. Lu. *Mqtt-based resource allocation of smart buildings for grid demand reduction considering unreliable communication links*. IEEE Systems Journal (2018).

[4] P. Jamborsalamati, J. Hossain, S. Taghizadeh, G. Konstantinou, M. Manbachi, and P. Dehghanian. *Enhancing power grid resilience through an iec61850-based ev-assisted load restoration*. IEEE Transactions on Industrial Informatics (2019).

[5] P. Dehghanian, S. Aslan, and P. Dehghanian. *Quantifying power system resiliency improvement using network reconfiguration*. In *IEEE 60th International Midwest Symposium on Circuits and Systems (MWSCAS)*, pp. 1–4 (2017).

[6] B. Zhang, P. Dehghanian, and M. Kezunovic. *Optimal allocation of pv generation and battery storage for enhanced resilience*. IEEE Transactions on Smart Grid (2017).

[7] P. Dehghanian. *Power system topology control for enhanced resilience of smart electricity grids*. Ph.D. Dissertation (2017).

[8] M. Panteli and P. Mancarella. *The grid: Stronger, bigger, smarter?: Presenting a conceptual framework of power system resilience*. IEEE Power and Energy Magazine **13**(3), 58 (2015).

[9] P. Jamborsalamati, M. Moghimi, M. Hossain, S. Taghizadeh, J. Lu, and G. Konstantinou. *A framework for evaluation of power grid resilience case study: 2016 south australian blackout*. In *2018 IEEE International Conference on Environment and Electrical Engineering and 2018 IEEE Industrial and Commercial Power Systems Europe (EEEIC/I&CPS Europe)*, pp. 1–6 (IEEE, 2018).

[10] K. Moslehi, R. Kumar, *et al. A reliability perspective of the smart grid.* IEEE Trans. Smart Grid **1**(1), 57 (2010).

[11] P. P. Parikh, M. G. Kanabar, and T. S. Sidhu. *Opportunities and challenges of wireless communication technologies for smart grid applications*. In *IEEE PES General Meeting*, pp. 1–7 (IEEE, 2010).

[12] L. Chhaya, P. Sharma, G. Bhagwatikar, and A. Kumar. *Wireless sensor network based smart grid communications: cyber attacks, intrusion detection system and topology control*. Electronics **6**(1), 5 (2017).

[13] M. Kuzlu, M. Pipattanasomporn, and S. Rahman. *Communication network requirements for major smart grid applications in han, nan and wan*. Computer Networks **67**, 74 (2014).

[14] H. Farooq and L. T. Jung. *Choices available for implementing smart grid communication network*. In *2014 International Conference on Computer and Information Sciences (ICCOINS)*, pp. 1–5 (IEEE, 2014).

[15] L. Chhaya, P. Sharma, A. Kumar, and G. Bhagwatikar. *Iot-based implementation of*

field area network using smart grid communication infrastructure. Smart Cities **1**(1), 176 (2018).

[16] S. Xu, Y. Qian, and R. Q. Hu. *On reliability of smart grid neighborhood area networks*. IEEE Access **3**, 2352 (2015).

[17] B. Alohali, K. Kifayat, Q. Shi, and W. Hurst. *Group authentication scheme for neighbourhood area networks (nans) in smart grids*. Journal of Sensor and Actuator Networks **5**(2), 9 (2016).

[18] Y. Zhang, L. Wang, W. Sun, R. C. Green II, and M. Alam. *Distributed intrusion detection system in a multi-layer network architecture of smart grids*. IEEE Transactions on Smart Grid **2**(4), 796 (2011).

[19] C. Kalalas, L. Thrybom, and J. Alonso-Zarate. *Cellular communications for smart grid neighborhood area networks: A survey*. IEEE access **4**, 1469 (2016).

[20] C. Greer, D. A. Wollman, D. E. Prochaska, P. A. Boynton, J. A. Mazer, C. T. Nguyen, G. J. FitzPatrick, T. L. Nelson, G. H. Koepke, A. R. Hefner Jr, *et al. Nist framework and roadmap for smart grid interoperability standards, release 3.0*. Tech. rep. (2014).

[21] M. Kuzlu and M. Pipattanasomporn. *Assessment of communication technologies and network requirements for different smart grid applications*. In *2013 IEEE PES innovative smart grid technologies conference (ISGT)*, pp. 1–6 (IEEE, 2013).

[22] O. Starynets. *Communication in microgrids and virtual power plants*. Master's thesis, UiT Norges arktiske universitet (2016).

[23] S. Safdar, B. Hamdaoui, E. Cotilla-Sanchez, and M. Guizani. *A survey on communication infrastructure for micro-grids*. In *2013 9th international wireless communications and mobile computing conference (IWCMC)*, pp. 545–550 (IEEE, 2013).

[24] R. Daryapurkar and R. Karandikar. *Wimax for data aggregation in smart grid communication network—a review*. In *2017 International Conference on Wireless Communications, Signal Processing and Networking (WiSPNET)*, pp. 97–100 (IEEE, 2017).

[25] V. C. Gungor, D. Sahin, T. Kocak, S. Ergut, C. Buccella, C. Cecati, and G. P. Hancke. *Smart grid technologies: Communication technologies and standards*. IEEE transactions on Industrial informatics **7**(4), 529 (2011).

[26] I. Parvez, M. Jamei, A. Sundararajan, and A. I. Sarwat. *Rss based loop-free compass routing protocol for data communication in advanced metering infrastructure (ami) of smart grid*. In *2014 IEEE Symposium on Computational Intelligence Applications in Smart Grid (CIASG)*, pp. 1–6 (IEEE, 2014).

[27] M. Erol-Kantarci and H. T. Mouftah. *Energy-efficient information and communication infrastructures in the smart grid: A survey on interactions and open issues*. IEEE Communications Surveys & Tutorials **17**(1), 179 (2014).

[28] A. Bani-Ahmed, L. Weber, A. Nasiri, and H. Hosseini. *Microgrid communications: State of the art and future trends*. In *2014 International Conference on Renewable Energy Research and Application (ICRERA)*, pp. 780–785 (IEEE, 2014).

[29] B. Leiner, R. Cole, J. Postel, and D. Mills. *The darpa internet protocol suite*. IEEE Communications Magazine **23**(3), 29 (1985).

[30] S. Mohagheghi, J. Stoupis, and Z. Wang. *Communication protocols and networks for power systems-current status and future trends*. In *2009 IEEE/PES Power Systems Conference and Exposition*, pp. 1–9 (IEEE, 2009).

[31] X. Lu, W. Wang, and J. Ma. *An empirical study of communication infrastructures towards the smart grid: Design, implementation, and evaluation*. IEEE Transactions on Smart Grid **4**(1), 170 (2013).

[32] F. Costa, A. Monti, F. Lopes, K. Silva, P. Jamborsalamati, and A. Sadu. *Two-terminal traveling-wave-based transmission-line protection*. IEEE Transactions on Power Delivery **32**(3), 1382 (2016).

[33] P. CODE and C. PRIX. *Communication networks and systems for power utility automation–part 8-1: Specific communication service mapping (scsm)–mappings*

to mms (iso 9506-1 and iso 9506-2) and to iso/iec 8802-3 réseaux et systèmes de communication pour l'automatisation des systèmes électriques– (2011).

[34] P. Jamborsalamati, E. Fernandez, M. J. Hossain, and F. H. M. Rafi. *Design and implementation of a cloud-based iot platform for data acquisition and device supply management in smart buildings*. In *2017 Australasian Universities Power Engineering Conference (AUPEC)*, pp. 1–6 (2017).

[35] J. Dizdarević, F. Carpio, A. Jukan, and X. Masip-Bruin. *A survey of communication protocols for internet of things and related challenges of fog and cloud computing integration*. ACM Computing Surveys (CSUR) **51**(6), 116 (2019).

[36] D. Dragomir, L. Gheorghe, S. Costea, and A. Radovici. *A survey on secure communication protocols for iot systems*. In *2016 International Workshop on Secure Internet of Things (SIoT)*, pp. 47–62 (IEEE, 2016).

[37] L. Daniel, M. Kojo, and M. Latvala. *Experimental evaluation of the coap, http and spdy transport services for internet of things*. In *International conference on internet and distributed computing systems*, pp. 111–123 (Springer, 2014).

[38] E. Dijk, A. Rahman, T. Fossati, S. Loreto, and A. Castellani. *Advanced guidelines for http-coap mapping implementations* (2015).

[39] A. Antonić, M. Marjanović, P. Skočir, and I. P. Žarko. *Comparison of the cupus middleware and mqtt protocol for smart city services*. In *2015 13th International Conference on Telecommunications (ConTEL)*, pp. 1–8 (IEEE, 2015).

[40] M. Laine and K. Säilä. *Performance evaluation of xmpp on the web*. Aalto Univ. Tech. Rep. (2012).

[41] J. L. Fernandes, I. C. Lopes, J. J. Rodrigues, and S. Ullah. *Performance evaluation of restful web services and amqp protocol*. In *2013 Fifth International Conference on Ubiquitous and Future Networks (ICUFN)*, pp. 810–815 (IEEE, 2013).

[42] F. Bonomi, R. Milito, J. Zhu, and S. Addepalli. *Fog computing and its role in the internet of things*. In *Proceedings of the first edition of the MCC workshop on Mobile cloud computing*, pp. 13–16 (ACM, 2012).

[43] J. Dizdarevic, F. Carpio, A. Jukan, and X. Masip-Bruin. *Survey of communication protocols for internet-of-things and related challenges of fog and cloud computing integration*. arXiv preprint arXiv:1804.01747 (2018).

[44] M. Moghimi, P. Jamborsalamati, J. Hossain, S. Stegen, and J. Lu. *A hybrid communication platform for multi-microgrid energy management system optimization*. In *2018 IEEE 27th International Symposium on Industrial Electronics (ISIE)*, pp. 1215–1220 (IEEE, 2018).

[45] S. Taghizadeh, P. Jamborsalamati, M. Hossain, and J. Lu. *Design and implementation of an advanced vehicle-to-vehicle (v2v) power transfer operation using communications*. In *2018 IEEE International Conference on Environment and Electrical Engineering and 2018 IEEE Industrial and Commercial Power Systems Europe (EEEIC/I&CPS Europe)*, pp. 1–6 (IEEE, 2018).

[46] E. Lindén. *A latency comparison of iot protocols in mes* (2017).

[47] A. Hornsby and R. Walsh. *From instant messaging to cloud computing, an xmpp review*. In *IEEE International Symposium on Consumer Electronics (ISCE 2010)*, pp. 1–6 (IEEE, 2010).

[48] D. Mønster. *Studying complex interactions in real time: an xmpp-based framework for behavioral experiments.* In *COMPLEXIS*, pp. 130–138 (2017).

[49] N. Naik. *Choice of effective messaging protocols for iot systems: Mqtt, coap, amqp and http*. In *2017 IEEE international systems engineering symposium (ISSE)*, pp. 1–7 (IEEE, 2017).

[50] M. Moghimi, J. Liu, P. Jamborsalamati, F. Rafi, S. Rahman, J. Hossain, S. Stegen, and

J. Lu. *Internet of things platform for energy management in multi-microgrid system to improve neutral current compensation*. Energies **11**(11), 3102 (2018).

[51] P. Jamborsalamati, E. Fernandez, M. Hossain, and F. Rafi. *Design and implementation of a cloud-based iot platform for data acquisition and device supply management in smart buildings*. In *2017 Australasian Universities Power Engineering Conference (AUPEC)*, pp. 1–6 (IEEE, 2017).

[52] C. Bormann, S. Lemay, H. Tschofenig, K. Hartke, B. Silverajan, and B. Raymor. *Coap (constrained application protocol) over tcp, tls, and websockets*. Internet Requests for Comments, RFC Editor, RFC **8323** (2018).

[53] N. J. Al Fardan and K. G. Paterson. *Lucky thirteen: Breaking the tls and dtls record protocols*. In *2013 IEEE Symposium on Security and Privacy*, pp. 526–540 (IEEE, 2013).

[54] D. Baimel, S. Tapuchi, and N. Baimel. *Smart grid communication technologies-overview, research challenges and opportunities*. In *2016 International Symposium on Power Electronics, Electrical Drives, Automation and Motion (SPEEDAM)*, pp. 116–120 (IEEE, 2016).

[55] I. S. Association *et al. Ieee standard for broadband over power line networks: Medium access control and physical layer specifications*. IEEE Std **2010**(2010), 1 (1901).

[56] M. Chafii, Y. J. Harbi, and A. G. Burr. *Wavelet-ofdm vs. ofdm: Performance comparison*. In *2016 23rd International Conference on Telecommunications (ICT)*, pp. 1–5 (IEEE, 2016).

[57] V. Oksman and S. Galli. *G. hn: The new itu-t home networking standard*. IEEE Communications Magazine **47**(10), 138 (2009).

[58] A. Mengi, S. Ponzelar, and M. Koch. *The itu-t g. 9960 broadband plc communication concept for smartgrid applications*. In *2017 IEEE International Conference on Smart Grid Communications (SmartGridComm)*, pp. 492–496 (IEEE, 2017).

[59] D. G. Photovoltaics and E. Storage. *Ieee guide for smart grid interoperability of energy technology and information technology operation with the electric power system (eps), end-use applications, and loads* (2011).

[60] D. Goodin. *Buggy smart meters open door to power-grid botnet*. Register, June **12** (2009).

[61] T. Otani. *A primary evaluation for applicability of iec 62056 to a next-generation power grid*. In *2010 First IEEE International Conference on Smart Grid Communications*, pp. 67–72 (IEEE, 2010).

[62] S. Fries, H. J. Hof, and M. Seewald. *Enhancing iec 62351 to improve security for energy automation in smart grid environments*. In *2010 Fifth International Conference on Internet and Web Applications and Services*, pp. 135–142 (IEEE, 2010).

[63] R. Schlegel, S. Obermeier, and J. Schneider. *A security evaluation of iec 62351*. Journal of Information Security and Applications **34**, 197 (2017).

[64] A. Chattopadhyay, A. Ukil, D. Jap, and S. Bhasin. *Toward threat of implementation attacks on substation security: Case study on fault detection and isolation*. IEEE Transactions on Industrial Informatics **14**(6), 2442 (2017).

[65] A. Mahmood, I. Khan, S. Razzaq, Z. Najam, N. A. Khan, M. Rehman, and N. Javaid. *Home appliances coordination scheme for energy management (HACS4EM) using wireless sensor networks in smart grids*. Procedia Computer Science **32**, 469 (2014).

[66] F. Shrouf and G. Miragliotta. *Energy management based on internet of things: practices and framework for adoption in production management*. Journal of Cleaner Production **100**, 235 (2015).

[67] N. Blaauwbroek, P. H. Nguyen, M. J. Konsman, H. Shi, R. I. Kamphuis, and W. L. Kling. *Decentralized resource allocation and load scheduling for multicommodity smart energy systems*. IEEE Trans. on Sustainable Energy **6**(4), 1506 (2015).

[68] S. Javaid and T. Kato. *Real-time power supply and demand mediation algorithm for energy on demand system*. In *Consumer Electronics-Taiwan (ICCE-TW), 2017 IEEE International Conference on*, pp. 191–192 (IEEE, 2017).

[69] M. Rastegar, M. Fotuhi-Firuzabad, and H. Zareipour. *Centralized home energy management in multi-carrier energy frameworks*. In *2015 IEEE 15th International Conference on Environment and Electrical Engineering (EEEIC)*, pp. 1562–1566 (2015).

[70] M. Tasdighi, P. J. Salamati, A. Rahimikian, and H. Ghasemi. *Energy management in a smart residential building*. In *Environment and Electrical Engineering (EEEIC), 2012 11th International Conference on*, pp. 128–133 (IEEE, 2012).

[71] Y. Guo, M. Pan, Y. Fang, and P. P. Khargonekar. *Decentralized coordination of energy utilization for residential households in the smart grid.* IEEE Trans. Smart Grid **4**(3), 1341 (2013).

[72] A. C. Luna, N. L. Diaz, M. Graells, J. C. Vasquez, and J. M. Guerrero. *Cooperative energy management for a cluster of households prosumers*. IEEE Trans. on Consumer Electronics **62**(3), 235 (2016).

[73] R. Carli and M. Dotoli. *A decentralized resource allocation approach for sharing renewable energy among interconnected smart homes*. In *Decision and Control (CDC), 2015 IEEE 54th Annual Conference on*, pp. 5903–5908 (IEEE, 2015).

[74] M. Moghimi, C. Bennett, D. Leskarac, S. Stegen, and J. Lu. *Communication architecture and data acquisition for experimental microgrid installations*. In *Power and Energy Engineering Conference (APPEEC), 2015 IEEE PES Asia-Pacific*, pp. 1–5 (IEEE, 2015).

[75] R. K. Kodali and S. Soratkal. *MQTT based home automation system using ESP8266*. In *Humanitarian Technology Conference (R10-HTC), 2016 IEEE Region 10*, pp. 1–5 (IEEE, 2016).

[76] M. Singh, M. Rajan, V. Shivraj, and P. Balamuralidhar. *Secure MQTT for internet of things (IOT)*. In *Communication systems and network technologies (CSNT), 2015 fifth international conference on*, pp. 746–751 (IEEE, 2015).

[77] N. Tantitharanukul, K. Osathanunkul, K. Hantrakul, P. Pramokchon, and P. Khoenkaw. *MQTT-topics management system for sharing of open data*. In *Digital Arts, Media and Technology (ICDAMT), International Conference on*, pp. 62–65 (IEEE, 2017).

[78] G. Suciu, O. Fratu, L. Necula, A. Pasat, and V. Suciu. *Machine-to-machine communications for cloud-based energy management systems within SMEs*. In *Design and Technology in Electronic Packaging (SIITME), 2016 IEEE 22nd International Symposium for*, pp. 114–117 (IEEE, 2016).

[79] J. Byun, Y. Kim, Z. Hwang, and S. Park. *An intelligent cloud-based energy management system using machine to machine communications in future energy environments*. In *Consumer Electronics (ICCE), 2012 IEEE International Conference on*, pp. 664–665 (IEEE, 2012).

[80] Y.-W. Chen and J. M. Chang. *Emaas: Cloud-based energy management service for distributed renewable energy integration*. IEEE Trans. on Smart Grid **6**(6), 2816 (2015).

[81] Y.-T. Lee, W.-H. Hsiao, C.-M. Huang, and T. C. Seng-cho. *An integrated cloud-based smart home management system with community hierarchy*. IEEE Trans. on Consumer Electronics **62**(1), 1 (2016).

[82] Z. Zhu, Z. Chu, N. Wang, S. Huang, Z. Wang, and I. Lee. *Beamforming and power splitting designs for an-aided secure multi-user mimo swipt systems*. IEEE Transactions on Information Forensics and Security **12**(12), 2861 (2017).

[83] Z. Zhu, Z. Chu, Z. Wang, and I. Lee. *Outage constrained robust beamforming for secure broadcasting systems with energy harvesting*. IEEE Transactions on Wireless Communications **15**(11), 7610 (2016).

[84] P. Dehghanian, B. Zhang, T. Dokic, and M. Kezunovic. *Predictive risk analytics for weather-resilient operation of electric power systems*. IEEE Transactions on Sustainable Energy **10**(1), 3 (2019).

[85] P. Jamborsalamati, M. Moghimi, M. Hossain, S. Taghizadeh, J. Lu, and G. Konstantinou. *A framework for evaluation of power grid resilience case study: 2016 south australian blackout*. In *2018 IEEE International Conference on Environment and Electrical Engineering and 2018 IEEE Industrial and Commercial Power Systems Europe (EEEIC/I&CPS Europe)*, pp. 1–6 (IEEE, 2018).

[86] H. Haes Alhelou, M. E. Hamedani-Golshan, T. C. Njenda, and P. Siano. *A survey on power system blackout and cascading events: Research motivations and challenges*. Energies **12**(4), 682 (2019).

[87] P. Dehghanian. *Power System Topology Control for Enhanced Resilience of Smart Electricity Grids*. Ph.D. thesis, Texas A&M University (2017).

[88] P. Bajpai, S. Chanda, and A. K. Srivastava. *A novel metric to quantify and enable resilient distribution system using graph theory and choquet integral*. IEEE Transactions on Smart Grid **9**(4), 2918 (2018).

[89] H. Farzin, M. Fotuhi-Firuzabad, and M. Moeini-Aghtaie. *Enhancing power system resilience through hierarchical outage management in multi-microgrids*. IEEE Transactions on Smart Grid **7**(6), 2869 (2016).

[90] H. Gao, Y. Chen, Y. Xu, and C.-C. Liu. *Resilience-oriented critical load restoration using microgrids in distribution systems*. IEEE Transactions on Smart Grid **7**(6), 2837 (2016).

[91] S. Mousavizadeh, M.-R. Haghifam, and M.-H. Shariatkhah. *A linear two-stage method for resiliency analysis in distribution systems considering renewable energy and demand response resources*. Applied Energy **211**, 443 (2018).

[92] A. Khodaei. *Resiliency-oriented microgrid optimal scheduling*. IEEE Transactions on Smart Grid **5**(4), 1584 (2014).

[93] Y. Wei, C. Ji, F. Galvan, S. Couvillon, and G. Orellana. *Dynamic modeling and resilience for power distribution.* In *SmartGridComm*, pp. 85–90 (2013).

[94] C. Ji and Y. Wei. *Dynamic resilience for power distribution and customers*. In *Smart Grid Communications (SmartGridComm), 2015 IEEE International Conference on*, pp. 822–827 (IEEE, 2015).

[95] J.-P. Watson, R. Guttromson, C. Silva-Monroy, R. Jeffers, K. Jones, J. Ellison, C. Rath, J. Gearhart, D. Jones, T. Corbet, *et al. Conceptual framework for developing resilience metrics for the electricity, oil, and gas sectors in the united states*. Sandia National Laboratories, Albuquerque, NM (United States), Tech. Rep (2014).

[96] H. Zhang, H. Yuan, G. Li, and Y. Lin. *Quantitative resilience assessment under a tri-stage framework for power systems*. Energies **11**(6), 1427 (2018).

[97] A. Kwasinski. *Quantitative model and metrics of electrical grids' resilience evaluated at a power distribution level*. Energies **9**(2), 93 (2016).

[98] H. Gao, Y. Chen, S. Mei, S. Huang, and Y. Xu. *Resilience-oriented pre-hurricane resource allocation in distribution systems considering electric buses*. Proceedings of the IEEE **105**(7), 1214 (2017).

[99] C. Chen, J. Wang, and D. Ton. *Modernizing distribution system restoration to achieve grid resiliency against extreme weather events: an integrated solution*. Proceedings of the IEEE **105**(7), 1267 (2017).

[100] C. Wang, Y. Hou, F. Qiu, S. Lei, and K. Liu. *Resilience enhancement with sequentially proactive operation strategies*. IEEE Transactions on Power Systems **32**(4), 2847 (2017).

[101] P. Bajpai, S. Chanda, and A. K. Srivastava. *A novel metric to quantify and enable resilient distribution system using graph theory and choquet integral*. IEEE Transactions on Smart Grid (2016).

[102] H. Farzin, M. Fotuhi-Firuzabad, and M. Moeini-Aghtaie. *Enhancing power system resilience through hierarchical outage management in multi-microgrids*. IEEE Transactions on Smart Grid **7**(6), 2869 (2016).

[103] Z. Li and M. Shahidehpour. *Security-constrained unit commitment for simultaneous clearing of energy and ancillary services markets*. IEEE transactions on power systems **20**(2), 1079 (2005).

[104] W. Ling, D. Liu, Y. Lu, P. Du, and F. Pan. *IEC 61850 model expansion toward distributed fault localization, isolation, and supply restoration*. IEEE Transactions on Power Delivery **29**(3), 977 (2014).

[105] M. Manbachi, A. Sadu, H. Farhangi, A. Monti, A. Palizban, F. Ponci, and S. Arzanpour. *Impact of EV penetration on volt–var optimization of distribution networks using real-time co-simulation monitoring platform*. Applied Energy **169**, 28 (2016).

[106] Y. Xu, C.-C. Liu, K. Schneider, F. Tuffner, and D. Ton. *Microgrids for service restoration to critical load in a resilient distribution system*. IEEE Transactions on Smart Grid (2016).

[107] V. Kumar, I. Gupta, and H. O. Gupta. *DG integrated approach for service restoration under cold load pickup*. IEEE Transactions on power delivery **25**(1), 398 (2010).

[108] Y.-L. Ke. *Distribution feeder reconfiguration for load balancing and service restoration by using G-nets inference mechanism*. IEEE Transactions on Power Delivery **19**(3), 1426 (2004).

[109] M. AlOwaifeer, M. AlMuhaini, and A. AlSaggaf. *The impact of load management and renewable DG on the service restoration of future power distribution systems*.

In *Environment and Electrical Engineering (EEEIC), 2015 IEEE 15th International Conference on*, pp. 1789–1794 (IEEE, 2015).

[110] A. Gholami, F. Aminifar, and M. Shahidehpour. *Front lines against the darkness: Enhancing the resilience of the electricity grid through microgrid facilities*. IEEE Electrification Magazine **4**(1), 18 (2016).

[111] X. Liu, M. Shahidehpour, Z. Li, X. Liu, Y. Cao, and Z. Bie. *Microgrids for enhancing the power grid resilience in extreme conditions*. IEEE Transactions on Smart Grid **8**(2), 589 (2017).

[112] B. Zhang, P. Dehghanian, and M. Kezunovic. *Optimal allocation of pv generation and battery storage for enhanced resilience*. IEEE Transactions on Smart Grid (2017).

[113] H. Hosseinirad and M. R. Haghifam. *An agent-based control system for outage management in distribution network in presence of distributed generation* (2012).

[114] T. Zheng and H. Jia. *Application of multi-agent and impedance-based algorithm for fault location in power distribution systems with DG*. In *Advanced Power System Automation and Protection (APAP), 2011 International Conference on*, vol. 2, pp. 1044–1049 (IEEE, 2011).

[115] A. Farraj, E. Hammad, and D. Kundur. *A storage-based multiagent regulation framework for smart grid resilience*. IEEE Transactions on Industrial Informatics **14**(9), 3859 (2018).

[116] P. Parikh, I. Voloh, and M. Mahony. *Fault location, isolation, and service restoration (FLISR) technique using IEC 61850 GOOSE*. In *Power and Energy Society General Meeting (PES), 2013 IEEE*, pp. 1–6 (IEEE, 2013).

[117] P. Jamborsalamati, A. Sadu, F. Ponci, and A. Monti. *Design, implementation and real-time testing of an IEC 61850 based FLISR algorithm for smart distribution grids*. In *Applied Measurements for Power Systems (AMPS), 2015 IEEE International Workshop on*, pp. 114–119 (IEEE, 2015).

[118] A. Ahmadi, A. Tavakoli, P. Jamborsalamati, N. Rezaei, M. R. Miveh, F. H. Gandoman, A. Heidari, and A. E. Nezhad. *Power quality improvement in smart grids using electric vehicles: a review*. IET Electrical Systems in Transportation (2019).

[119] J. A. P. Lopes, F. J. Soares, and P. M. R. Almeida. *Integration of electric vehicles in the electric power system*. Proceedings of the IEEE **99**(1), 168 (2011).

[120] K. Knezović, S. Martinenas, P. B. Andersen, A. Zecchino, and M. Marinelli. *Enhancing the role of electric vehicles in the power grid: field validation of multiple ancillary services*. IEEE Transactions on Transportation Electrification **3**(1), 201 (2017).

[121] N. Xu and C. Chung. *Reliability evaluation of distribution systems including vehicle-to-home and vehicle-to-grid*. IEEE Transactions on Power Systems **31**(1), 759 (2016).

[122] W. Kempton and J. Tomić. *Vehicle-to-grid power implementation: From stabilizing the grid to supporting large-scale renewable energy*. Journal of power sources **144**(1), 280 (2005).

[123] K. Clement-Nyns, E. Haesen, and J. Driesen. *The impact of vehicle-to-grid on the distribution grid*. Electric Power Systems Research **81**(1), 185 (2011).

[124] M. Yilmaz and P. T. Krein. *Review of the impact of vehicle-to-grid technologies on distribution systems and utility interfaces*. IEEE Transactions on power electronics **28**(12), 5673 (2013).

[125] M. Shaaban, M. Ahmed, T. EL-Fouly, and M. Salama. *Impact of integrating PEV and renewable sources on power system reliability assessment*. In *Electric Power and Energy Conversion Systems (EPECS), 2015 4th International Conference on*, pp. 1–6 (IEEE, 2015).

[126] H. Farzin, M. Fotuhi-Firuzabad, and M. Moeini-Aghtaie. *Reliability studies of modern distribution systems integrated with renewable generation and parking lots*. IEEE Transactions on Sustainable Energy **8**(1), 431 (2017).

[127] R. Francis and B. Bekera. *A metric and frameworks for resilience analysis of engineered and infrastructure systems*. Reliability Engineering & System Safety **121**, 90 (2014).

[128] C. Chen, J. Wang, and D. Ton. *Modernizing distribution system restoration to achieve grid resiliency against extreme weather events: an integrated solution*. Proceedings of the IEEE **105**(7), 1267 (2017).

[129] Y. Wei, C. Ji, F. Galvan, S. Couvillon, and G. Orellana. *Dynamic modeling and resilience for power distribution*. In *2013 IEEE International Conference on Smart Grid Communications (SmartGridComm)*, pp. 85–90 (IEEE, 2013).

[130] C. Ji and Y. Wei. *Dynamic resilience for power distribution and customers*. In *2015 IEEE International Conference on Smart Grid Communications (SmartGridComm)*, pp. 822–827 (IEEE, 2015).

[131] M. Bruneau, S. E. Chang, R. T. Eguchi, G. C. Lee, T. D. O'Rourke, A. M. Reinhorn, M. Shinozuka, K. Tierney, W. A. Wallace, and D. Von Winterfeldt. *A framework to quantitatively assess and enhance the seismic resilience of communities*. Earthquake spectra **19**(4), 733 (2003).

[132] S. Chanda and A. K. Srivastava. *Quantifying resiliency of smart power distribution systems with distributed energy resources*. In *2015 IEEE 24th International Symposium on Industrial Electronics (ISIE)*, pp. 766–771 (IEEE, 2015).

[133] Z. Bie, Y. Lin, G. Li, and F. Li. *Battling the extreme: A study on the power system resilience*. Proceedings of the IEEE **105**(7), 1253 (2017).

[134] H. Gao, Y. Chen, S. Mei, S. Huang, and Y. Xu. *Resilience-oriented pre-hurricane resource allocation in distribution systems considering electric buses*. Proceedings of the IEEE **105**(7), 1214 (2017).

[135] E. Global. *outlook 2017*. International Energy Agency pp. 1–71 (2017).

[136] W. Yang, J. Wang, Z. Zhang, and Y. Gao. *Simulation of electric vehicle charging*

station and harmonic treatment. In *2012 International Conference on Systems and Informatics (ICSAI2012)*, pp. 609–613 (IEEE, 2012).

[137] H. Farzin, M. Fotuhi-Firuzabad, and M. Moeini-Aghtaie. *Reliability studies of modern distribution systems integrated with renewable generation and parking lots*. IEEE Transactions on Sustainable Energy **8**(1), 431 (2016).

[138] N. Xu and C. Chung. *Reliability evaluation of distribution systems including vehicle-to-home and vehicle-to-grid*. IEEE transactions on power systems **31**(1), 759 (2015).

[139] *Energy Efficiency and Conservation Authority, Department of Environment and Energy, Australia, Energy Rating*. http://reg.energyrating.gov.au/comparator/product_types/.

[140] *Laplace systems*. URL http://www.laplacesolar.com/.

[141] S. van der Kooij, P. Kempker, J. van den Berg, and S. Bhulai. *Optimal charging/discharging strategies for batteries in smart energy grids*. Ph.D. thesis, Master's thesis, VU Amsterdam (2016).

[142] M. Manbachi, A. Sadu, H. Farhangi, A. Monti, A. Palizban, F. Ponci, and S. Arzanpour. *Real-time communication platform for smart grid adaptive volt-var optimization of distribution networks*. In *Smart Energy Grid Engineering (SEGE), 2015 IEEE International Conference on*, pp. 1–7 (IEEE, 2015).

[143] M. Pau, A. Sadu, S. Pillai, F. Ponci, and A. Monti. *A state estimation algorithm for hybrid ac/dc networks with multi-terminal dc grid*. In *PES Innovative Smart Grid Technologies Conference Europe (ISGT-Europe), 2016 IEEE*, pp. 1–6 (IEEE, 2016).

[144] N. Srinivas and K. Deb. *Muiltiobjective optimization using nondominated sorting in genetic algorithms*. Evolutionary computation **2**(3), 221 (1994).

[145] S. Bath, J. Dhillon, and D. Kothari. *Fuzzy satisfying stochastic multi-objective generation scheduling by weightage pattern search methods*. Electric Power Systems Research **69**(2-3), 311 (2004).

[146] Y.-L. Chen and C.-C. Liu. *Interactive fuzzy satisfying method for optimal multi-objective var planning in power systems*. IET Generation, Transmission and Distribution **141**(6), 554 (1994).

[147] A. Wazir and N. Arbab. *Analysis and optimization of ieee 33 bus radial distributed system using optimization algorithm*. Journal of Emerging Trends in Applied Engineering **1**(2), 17 (2016).

[148] R. T. Marler and J. S. Arora. *Survey of multi-objective optimization methods for engineering*. Structural and multidisciplinary optimization **26**(6), 369 (2004).

[149] N. Srinivas and K. Deb. *Muiltiobjective optimization using nondominated sorting in genetic algorithms*. Evolutionary computation **2**(3), 221 (1994).

[150] F. Costa, A. Monti, F. Lopes, K. Silva, P. Jamborsalamati, and A. Sadu. *Two-terminal traveling-wave-based transmission-line protection*. IEEE Transactions on Power Delivery **32**(3), 1382 (2017).

[151] M. Manbachi, H. Farhangi, A. Palizban, and S. Arzanpour. *A novel volt-var optimization engine for smart distribution networks utilizing vehicle to grid dispatch*. International Journal of Electrical Power & Energy Systems **74**, 238 (2016).

Appendix: Miscellaneous applications of the proposed IOT platform in Chapter 3

With minor modifications, the proposed platform in Chapter 3 can be used in energy management of Multi Microgrid (MMG) environments and for coordination of Multi MicroGrid components.

In this application, the platform contains two main layers. The first layer focuses on a single MicroGrid and the connections between the devices within the MG. The second layer represents the communications between the MicroGridss. These two layers are explained in details as follows:

.0.4 Intra-MG Communications

This part describes the intra-MG data exchange among the devices within a MG. An overview of a typical campus MG is indicated in Figure 1. HTTP TCP/IP is used as a backup intra-MG communication protocol between the installed local controllers and the MGCC. Messages are triggered by clients (not server) in Modbus and are transmitted over Ethernet with the default port of 502. With this architecture, the interconnection between the communication network and power systems could be monitored in the MG.

This figure demonstrates an overview of a single-MG communication architecture. All inverters connected to PV cells are connected via a local controller to the Micro Grid Central Controller (MGCC). There are data loggers in the architecture connected to smart meters

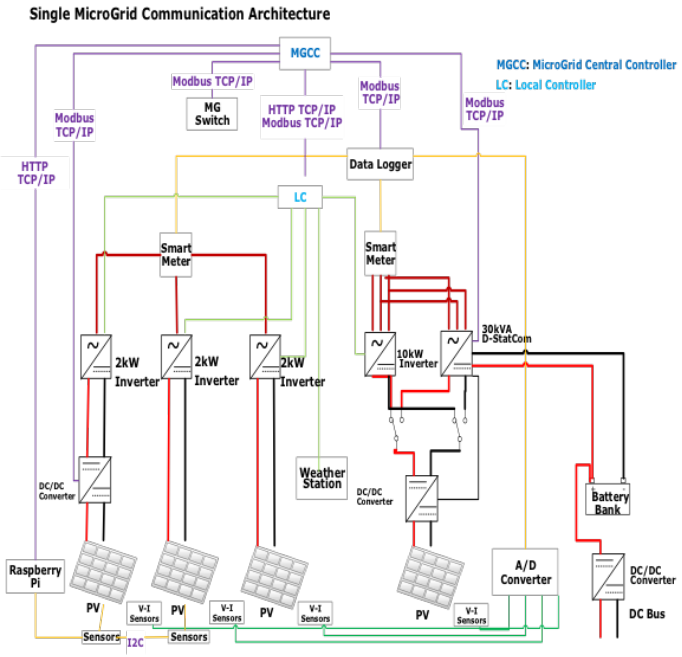

FIGURE 1: Overview of Inter-MG communications.

to collect measured data and provide an interface to the MGCC. The purple lines show the flow of communications through Modbus TCP/IP and the red and black lines show the power flow. Other colored lines show the physical connections among the devices within the MG. As a backup system, sensors are connected to a Raspberry Pi interfaced to the MGCC. Furthermore, the local controller can provide the MGCC with HTTP TCP/IP connections as well.

.0.5 Inter-MG Communications

This sub-section presents the communication architecture proposed for MMG management applications. The MGCC in each MG is connected to an IoT gateway to communicate with peer MGCCs through a cloud-server. As there is no Metadata in MQTT communications, the topics could carry meaningful characters to be used for message identifications. An example of a proposed topic string for MMG environment could be: *DataTypeName/DeviceName/MicroGridName/*

Further coding is done in the subscriber scripts to define the desired reactions when a message is received and for the publisher scripts to prepare the payload format desirably, to define the time rate according to the application, and to determine the topics with routing

information.

.0.6 Cloud Communications

Hypertext Transfer Protocol (HTTP), which is an application-level protocol with default port of 80, is used over TCP/IP connections to interact with a cloud server.

Because of a number of distinguished specifications listed below, ThingSpeak is the favored IoT platform for the proposed MMG platform:

First. Easy-to-use interface to MATLAB: the main advantage of using ThingSpeak platform, over the others, is the MATLAB ThingSpeak Toolbox and the detailed documentation of this toolbox, which makes the implementation of the big data analytics and algorithms very easy through this interface. This feature is not provided by other two platforms in the table. *Second*. Representational State Transfer (REST) Services: ThingSpeak provides REST services, which make the hardware-integrated communications straightforward through Application Programming Interface (API) functions. Hardware integration in other platforms require protocol buffers and third-party programming tool such as Node-Red. *Third*. Easy Integration with Arduino, Raspberry Pi, and ESP8266 Wi-Fi module: another significant privilege of ThingSpeak is that software installation and device configuration are not required unlike other platforms. This makes the system expansion with less effort when additional hardware is required to be joined to the ongoing system. *Fourth*. Provisions for real-time data collection: The data rate is customizable in all three platforms mentioned in the table above. This feature offers flexibilities to make the platform compatible with various applications in different time scales.

The built-in functional blocks of the ThingSpeak platform are explained below: Channel feed manager block. The core element of ThingSpeak activity is the channel. A channel stores the data that is sent by the smart appliances to ThingSpeak. Each channel comprises of the following items: *Item 1*. Fields for storing any type of data: these can be used to store the data from a sensor or from an embedded device.

Item 2. Location fields: that can be used to store the latitude, longitude, and the elevation in case of tracking a moving device. *Item 3*. Status field: this is a short message to describe

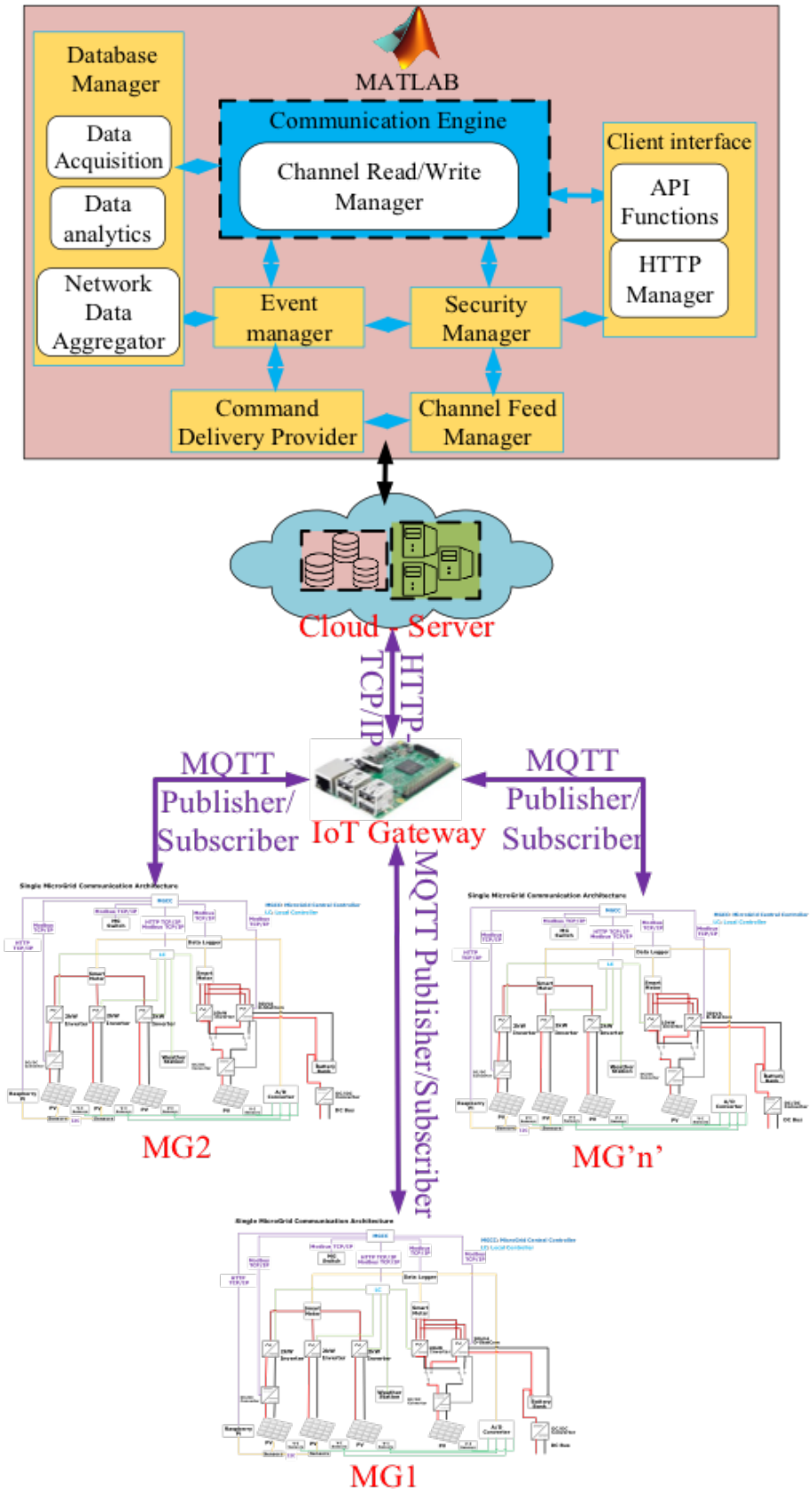

FIGURE 2: Overview of Intra-MG communications.

the data stored in the channel. Security manager block. Channels could be configured as private or public. In this work, secure private channels are configured to collect data. Security manager block assigns a unique ID to each private channel, which is required by the MQTT client to interact with ThingSpeak platform. Client interface block. For each channel, there is a private write API key and a read API key. The unique read/write API keys are required to send data to the channel and to retrieve the collected data later in MATLAB. This block includes ThingHTTP library, which manages the HTTP services to any client.

Database manager block. ThingSpeak has a cloud-based data storage and retrieval services. This database manager block has a Graphical User Interface (GUI) that visualizes the channel fields in customizable plots. Furthermore, from the GUI the channel field data could be exported in various formats including JSON, XML, and CSV. Event manager and command delivery provider. Inside any event-driven command-and-query architecture there must be an event-sourcing block and a command provider unit. These units interact with the database manager block to update it every time that a new data or command is published. The interactions between the IoT gateway and the cloud server (ThingSpeak in this work) are implemented by HTTP POST and HTTP GET requests in Python scripts.

The IoT gateway subscribes to all of the topics defined by the MGCCs and updates the corresponding channel feed to its MicroGrid by sending an HTTP POST request to https://api.thingspeak.com/channel/channelID. Therefore, MGCCs communicate with each other through the ThingSpeak platform. In addition, this gateway receives the outputs of the MATLAB post-processing, which are written in a separate private channel, using HTTP GET requests to the aforementioned URL. In other words, the IoT gateway executes HTTP Get requests and publishes the MATLAB results to the corresponding topics, which are subscribed by the relevant MGCCs to be actuated by them. Two Python codes, one MQTT publisher and one MQTT subscriber represent each MGCC for implementation purposes.